UNOBTRUSIVE VITAL SIGN DETECTION THROUGH AMBIENT PHYSICAL VIBRATIONS

by

ZHENHUA JIA

A dissertation submitted to the

School of Graduate Studies

Rutgers, The State University of New Jersey

In partial fulfillment of the requirements

For the degree of

Doctor of Philosophy

Graduate Program in Electrical and Computer Engineering

Written under the direction of

Yanyong Zhang

And approved by

_____

_____

_____

_____

New Brunswick, New Jersey

January, 2019

ABSTRACT OF THE DISSERTATION

Unobtrusive Vital Sign Detection Through Ambient Physical Vibrations

by Zhenhua Jia

Dissertation Director: Yanyong Zhang

Vital sign monitoring is critically important to ensuring the well-being of many people, ranging from patients to the elderly. Technologies that support vital sign monitoring should be unobtrusive, and solutions that are accurate and can be easily applied to existing beds is an important need that has been unfulfilled. In this dissertation, we aim at tackling the challenge of accurate, low-cost and easy to deploy vital sign monitoring. We focus on two scenarios ones everyday life – sleeping during the night and sitting during the daytime, considering that a person spends a large portion of time on both activities.

In the first part of this dissertation, we investigate whether off-the-shelf analog geophone sensors can be used to detect heartbeats when installed under a bed. Geophones have the desirable property of being insensitive to lower-frequency movements, which lends itself to heartbeat monitoring as the heartbeat signal has harmonic frequencies that are easily captured by the geophone. With carefully-designed signal processing algorithms, we show it is possible to detect and extract heartbeats in the presence of environmental noise and other body movements a person may have during sleep. We built a prototype sensor and conducted detailed experiments involving 43 subjects, which demonstrate that the geophone sensor is a compelling solution to long-term, at-home heartbeat monitoring. We compared the average heartbeat rate estimated by our prototype and that reported by a pulse oximeter. The results revealed that the average

error rate is around 1.30% over 500 data samples when the subjects were still on the bed, and 3.87% over 300 data samples when the subjects had different types of body movements while lying on the bed. We also deployed the prototype in the homes of 9 subjects for a total of 25 nights, and found that the average estimation error rate was 8.25% over more than 181 hours' data.

In the second part of this dissertation, we greatly extend our previous system towards a more realistic scenario. We develop a system, called VitalMon, aiming to monitor a person's respiratory rate as well as heart rate, even when she is sharing a bed with another person. In such situations, the vibrations from both persons are mixed together. VitalMon first separates the two heartbeat signals, and then distinguishes the respiration signal from the heartbeat signal for each person. Our heartbeat separation algorithm relies on the spatial difference between two signal sources with respect to each vibration sensor, and our respiration extraction algorithm deciphers the breathing rate embedded in the amplitude fluctuation of the heartbeat signal. We have developed a prototype bed to evaluate the proposed algorithms. A total of 86 subjects participated in our study, and we collected 5084 geophone samples, totaling 56 hours of data. We show that our technique is accurate – its breathing rate estimation error for a single person is 0.38 breaths per minute (median error is 0.22 breaths per minute), heart rate estimation error when two persons share a bed is 1.90 beats per minute (median error is 0.72 beats per minute), and breathing rate estimation error when two persons share a bed is 2.62 breaths per minute (median error is 1.95 breaths per minute). By varying the sleeping posture and mattress type, we show that our system can work in many different scenarios.

In the third part of this dissertation, we introduce a system, called Touch-Chair, which unobtrusively monitors a user's respiration and learns a user's identity through capacitive sensing. Touch-Chair consists of 16 capacitive sensors mounted on the surface of a chair. The system can easily detect any occupancy event and extract the unique micro details about the user's respiration and sitting behavior patterns, through signal processing and supervised machine learning techniques. Our system can provide fine-grained information towards better understanding a user's health state.

Acknowledgements

I am deeply indebted to my adviser, Prof. Yanyong Zhang, for her fundamental role in my doctoral work. Yanyong provided me with a tremendous amount of patience, guidance, and expertise throughout my entire Ph.D. study. During my first year at WINLAB, she was extremely patient and allowed me to explore the related research field. Then, when I was ready for new research topics and new challenges, Yanyong provided me with insightful advice and great encouragement. Yanyong also guided me through academic thinking and writing. Without her help, I would never achieve so much. In addition to our research collaboration, she also taught me how to treat people with kindness and respect. I am very lucky to have her as my advisor.

I would like to thank Prof. Rich E. Howard for his enormous effort over my entire Ph.D. study. He taught me to think from a physicist's perspective and traced down to the fundamental problems. Rich showed me multiple ways of solving the same problem. All the knowledge I learned from him turned to be important problem-solving skills and significantly benefited my research. He has been a great mentor and a great friend to me.

I greatly appreciate Prof. Pei Zhang from Carnegie Mellon University (CMU) for his advice and support. He guided through my research with his erudition, patience and preciseness. His insightful questions and suggestions made my research complete, repeatable and more deliberate. I wish to thank my collaborator, Ms. Amelie Bonde from CMU, for her help in solving research problems and writing papers. Also, I would like to thank Dr. Musaab Alaziz for his extensive help through my research. Specifically, he helped me with experiment design and validation and also provided me the view of research with his unique expertise and perspective.

Besides my advisor, I gratefully acknowledge the members of my Ph.D. committee,

including Prof. Janne Lindqvist, Prof. Richard P. Martin and Prof. Richard E. Howard, for their precious time and valuable feedback on my dissertation. Especially, I am grateful to Prof. Janne Lindqvist for his insightful comments and for sharing with me his tremendous experience in the Human-Computer Interaction field. I am also thankful to Prof. Richard P. Martin for his crucial remarks that shaped my research and dissertation.

I also want to thank Prof. Dipankar Raychaudhuri, Prof. Wade Trappe, and the members of WINLAB for their selfless support. Last but not the least, I am grateful to many of my friends, including Dr. Sugang Li, Prof. Chenren Xu, Dr. Ben Firner, Dr. Rob Moore, Mr. Michael Sherman, Mr. Jakub Kolodziejski, Mr. Wuyang Zhang, Mr. Xiaoran Fan, etc., for the tremendous help in the last 6 years.

Table of Contents

Abstract ii

Acknowledgements iv

1. Introduction 1

1.1. Overview 1

1.2. Proposed Solutions for vital sign monitoring 2

1.2.1. A Geophone-based Bed-mounted Heart Rate Monitoring System for a Single User 2

1.2.2. A Heart Rate and Respiratory Rate Monitoring System on a Shared Bed Using Geophones 3

1.2.3. A Capacitive-based Chair-mounted Respiratory Rate Monitoring and User Identification System 4

1.3. Organization 4

2. HB-Phone: a Bed-Mounted Geophone-Based Heartbeat Monitoring System 5

2.1. Introduction 5

2.2. HB-Phone System Design 8

2.2.1. HB-Phone Hardware Design and Prototype 9

2.2.2. Unique Challenges of the HB-Phone System 12

Insensitive to Heartbeats at the Fundamental Frequency 12

Highly Sensitive to Noise Caused by Motion 14

2.3. Extracting Heartbeats from Geophone Signals 16

2.3.1. FFT and Low-pass filtering 16

2.3.2. Calculating Sample ACF 18

2.3.3. Sample ACF Peak Finding and Measurement 18
2.3.4. Extracting Heartbeats from Original Geophone Signals 19
2.4. Evaluation Results 20
2.4.1. Evaluation Phase I: Controlled Experiments 20
2.4.2. Evaluation Phase II: Long-Term At-Home Deployment for Heartbeat Monitoring During Sleep 24
2.5. Related Work 29
2.5.1. Overview of Existing Bed-Mounted Heartbeat Sensors 29
2.5.2. Overview of Signal Processing for Heartbeat Detection 31
2.6. Concluding Remarks and Future Direction 33

3. VitalMon: Geophone Based Heart Rate and Respiratory Rate Monitoring 34
3.1. Introduction 34
3.2. Background and Overview 38
3.2.1. BCG Based Heart Rate and Respiratory Rate Monitoring . . . 39
3.2.2. VitalMon Overview 40
3.3. Monitoring Respiratory Rate Using Geophone 41
3.3.1. Formulating Respiration Signals as Amplitude Modulation 42
3.3.2. Respiratory Rate Estimation 44
3.4. Monitoring Target Heart Rate When Multiple Subjects are Present . . . 45
3.4.1. Modeling Mixture Signals 46
3.4.2. Background on Blind Source Separation and the DUET Algorithm 47
3.4.3. Heartbeat Signal Separation and Heart Rate Estimation 48
FFT and Low-pass Filtering for Noise Reduction 50
Time-Frequency Representation for Locating Spatial Information 50
Calculating Symmetric Attenuation and Relative Delay 52
Finding Cluster Peaks and Applying Binary Masking in 3D Space 53
Estimating Target Heart Rate 53

3.5. VitalMon Testbed 54
3.6. Evaluation 57
3.6.1. Monitoring a Single Subject's Respiratory Rate 57
3.6.2. Monitoring Target Heart Rate when Multiple Subjects are Available 59
Mean Heart Rate Estimation Error 59
The Impact of Lying Posture 61
The Impact of Different Mattress Type 61
3.6.3. Monitoring Target Respiratory Rate When Multiple Subjects are Present 62
3.6.4. Discussion on Real World Deployment 63
3.7. Related Work 64
3.7.1. Vital Sign Monitoring of a Single Person 64
3.7.2. Vital Sign Monitoring of Multiple People 66
3.8. Concluding Remarks and Future Direction 67

4. Touch-Chair: Learning a User's respiratory rate and identity through Capacitive Sensing 68
4.1. Introduction 68
4.2. Motivation: Chair Occupancy Detection Using a Single Capacitive Sensor 70
4.2.1. Chair Occupancy Detection 70
4.2.2. Capacitance Measurement 71
4.3. Touch-Chair Prototype 72
4.4. User Identification 75
4.4.1. Classification Algorithms 76
4.4.2. Experiment Design 77
4.4.3. User Identification Evaluation Results 78
4.5. Respiratory Rate Monitoring 82
4.5.1. Respiration Monitoring Algorithms 83
4.5.2. Experiment Design 85

4.5.3. Respiration Evaluation Results 87
4.6. Touch-Chair App Implementation 89
4.7. Related Work 89
4.7.1. User Identification 89
4.7.2. Posture and Activity Detection 91
4.7.3. Respiratory Rate Measurement 92
4.7.4. Comparison with Other Types of Sensors 92
4.8. Concluding Remarks and Future Direction 93

5. Conclusion 94

References 96

Chapter 1

Introduction

1.1 Overview

Continuous vital sign monitoring systems have been proposed in both industry and academia, promising to provide rich information about a person's well-being. Potentially, these systems can be used to detect emotional state [1–3], monitor sleep quality [4], detect obstructive sleep apnea [5], evaluate the risk of heart failure under certain situations [6, 7], and even monitor patients with Parkinson's disease [8], etc.

Due to the importance of vital sign monitoring, many systems have been proposed in the literature. We category these systems into three groups: wearable devices [9–11], remote radio frequency (RF) sensors [12–15] and carrier-mounted sensors [16–31]. Wearable devices can continuously monitor the heart rate, but they fail to monitor respiration, have to be bundled to other mobile devices and require frequent battery charging. Also, they are rather cumbersome and inconvenient to many users, especially children, patients or the elderly. RF sensors can monitor vital signs without direct contact of the skin but suffer from the RF multipath situation in the background environment. Carrier-mounted systems, such as bed-mounted and chair-mounted systems, are usually difficult to deploy and obtrusive to use as they introduce additional special designed components, such as seat mats, mattresses, bed posts, etc.

In this study, we aim to develop such sensors that are able to provide continuous vital sign monitoring, regardless that a user is sleeping or work. Towards building accurate and robust systems for such a purpose, we believe a better approach is to develop sensors that can be easily mounted on target objects (such as beds and chairs) and monitor users in a completely unobtrusive manner. In this dissertation, we demonstrate our bed-mounted systems that monitor users' vital signs during sleep and a chair-mounted

system that monitors users' respiratory rate and sitting behavior in the daytime.

1.2 Proposed Solutions for vital sign monitoring

Unobtrusively monitoring a person's vital signs provides rich information about a person's well being. Our propose systems which continuously monitor a person's vital sign through ambient vibrations. We developed a bed-mounted system which is accurate and easy to install. To be specific, we investigated building a geophone-based bed-mounted heart rate monitoring system for a single user, have extended the system towards monitoring a target user's heart rate and respiratory rate, while at the same time the target user shares the bed with another user. Further, we propose a capacitive-based chair-mounted system which can unobtrusively monitor a user's respiratory rate and identity.

1.2.1 A Geophone-based Bed-mounted Heart Rate Monitoring System for a Single User

Compared to existing sensor systems mentioned in Section 1.1, geophone sensors [32,33], which measure the vibration velocity caused by ballistic force within each heartbeat, provides a viable alternative in detecting both the heart rate on a bed without having the problems of the existing systems. A geophone sensor consists of a magnet mass surrounded by a coil. When a geophone sensor gets excited by the weak vibration from the environment, the magnet mass and the coil may have relative motion leading to an alternating current (AC) due to the electromagnetic field effect. As such, geophone sensors are sensitive to weak vibrations and offer accurate monitoring.

We have built our system prototype, called HB-Phone, which consists of a geophone sensor, an AC amplifier and an Arduino Duemilanove board [34], all mounted on a non-magnetic wood board. Our prototype can be installed anywhere on the bed frame and accurately detects the weak vibrations caused by heartbeats. Also, we designed our heart rate detection algorithm in three steps: we first apply a low-pass filter to reduce noise caused by body motions during sleep, ambient vibrations from the environment,

etc.; we compute the signal power and apply a Sample autocorrelation function [35] in order to extract the periodicity of the signal; then, we adopt a peak finding algorithm [36] to count the number of heartbeats and convert it to a heart rate. Through extensive controlled experiments and a real-world deployments, we show it is possible to detect and extract heartbeats in the presence of environmental noise and other body movements a person may have during sleep – even in real-world deployment, the average estimation error rate of our system is as low as 8.25% over 181 hours' data.

1.2.2 A Heart Rate and Respiratory Rate Monitoring System on a Shared Bed Using Geophones

Continuously monitoring a single user's heart rate enables quite a few applications. However, we still miss some crucial information, towards a much more practical system – the previous system only works for a single user and cannot monitor the user's respiratory rate. Thus, we extended our work towards a more complex scenario – tracking the heart rate and respiratory rate of a target user when he/she shares the bed with another user. The challenges are two-fold. First, a geophone sensor is naturally a second-order high-pass filter and is insensitive to low-frequency motion such as respiration (around 0.25 Hz). We find the vibration caused by respiration is buried under noise from the environment. We address this challenge by observing that the respiration signal is amplitude modulated with the heartbeat signal and used a square-law amplitude demodulation algorithm [37] to recover the respiration signal. The second challenge is that the heartbeat signals from two users are mixed together and hard to separate. We addressed this challenge by installing two geophones on the left and right side of the bed and designed a series of signal processing algorithms to separate the signals from the two users. Our algorithm is centered around a blind source separation algorithm, called Degenerate Unmixing Estimation Technique (DUET) [38, 39], and takes advantages of the embedded vibration source (heartbeats) location within the geophone signals to separate the signals apart.

We have built our prototype system, VitalMon, and show that VitalMon can successfully monitor the target person's respiration and heart rate, even when he/she

shares the bed with others. The overall absolute estimation error for heart rate and respiratory rate is at 1.90 beats per minutes and 2.62 breaths per minute, respectively, and the median is 0.72 beats per minutes and 1.95 breaths per minute.

1.2.3 A Capacitive-based Chair-mounted Respiratory Rate Monitoring and User Identification System

Our previous systems showed that we can accurately monitor users' heart rate and respiratory rate during sleep. However, continuous monitoring during the daytime is still missing. Here, we developed a smart chair system, called Touch-Chair, which unobtrusively learns a user's sitting behaviors, including his/her identity and respiration rate, all through capacitive sensing. Our Touch-Chair prototype consists of 16 capacitive sensors that are mounted on the chair surface. The system can accurately detect when a user sits on the chair and extracts unique micro details about a user's sitting patterns. Touch-Chair collects the sensor signals through ultra-low power wireless tags, and processes the signals on a Raspberry Pi. The system identifies a user using Extreme Gradient Boosting and Random Forests algorithms, and extracts the respiratory rate using an autocorrelation-based algorithm. We conducted more than 5,000 experiments involving 29 subjects for user identification and more than 800 experiments involving 19 subjects for respiratory rate monitoring. In total, we collected 77.3 hours of data over a period of 7 months. The system can accurately recognize the user and extract the respiratory rate, with an error of 1.23% and 1.05 breaths per minute (bpm), respectively.

1.3 Organization

The dissertation is organized as follows. In Chapter 2, we present our HB-Phone system which can monitor a single user's heart rate during sleep without additional constraints. In Chapter 3, we discuss our VitalMon system which tracks a target user's heart rate and respiratory rate simultaneously on a shared bed. In Chapter 4, we propose our Touch-Chair capacitive sensing system for respiratory rate monitoring and sitting behavior detection. Finally, we conclude the dissertation in Chapter 5.

Chapter 2

HB-Phone: a Bed-Mounted Geophone-Based Heartbeat Monitoring System

2.1 Introduction

When we consider a person's well-being, it is important to focus on the time when he/she is resting and sleeping. We spend a large fraction of our time in sleeping, and yet, reliable mechanisms that can monitor our sleep and heartbeats during sleep are still missing. In the last few years, we have seen an increasing number of wearable devices that can be used for this purpose, but they usually need to be bundled to other mobile devices and require frequent battery charging, which is rather cumbersome to many users, especially patients or elderly. As a result, we believe a better approach is to develop bed-mounted sensors that can monitor users in a completely unobtrusive manner. In this study, we aim to develop such sensors that are able to detect and monitor heartbeats during sleep. Detecting heartbeats and monitoring the heartbeat rate, is an important part of ensuring our well-being.

Due to the importance of heartbeat monitoring during sleep, many bed-mounted heartbeat sensing and monitoring systems have been proposed in the literature. However, few solutions have managed simultaneously to achieve ease of use, low cost, high accuracy, and robustness. Firstly, many systems, such as those proposed in [16, 17, 30], require custom-made sheets or mattresses. For example, an air cushion is required in [16, 17]; sensors need to be embedded in the mattress in [30]. Some systems require the user to place (film) sensors under a certain part of the sheet [24]. These requirements are rather cumbersome, which may greatly hinder the widespread adoption of the proposed systems, particularly amongst demographics that are adverse to noticeable changes in their routines. Secondly, many systems, such as those proposed

in [25, 26], require special sensors that yield accurate heartbeat sensing, but can be quite costly. Thirdly, some systems are hard to install; for example, the system proposed in [13] needs to install a plywood board and an aluminum guide rail on the bed surface. Because of these limitations, even though a number of systems have been proposed, at-home heartbeat monitoring during sleep still remains a problem for which there are no completely suitable solutions.

In this study, we seek to fill this void by proposing a system that is accurate, robust, low cost, and easy to use. Our solution involves the use of a commercial off-the-shelf analog geophone under the mattress to detect and monitor the user's heartbeats during sleep. Just like a geophone can detect pressure waves (i.e. "sounds) in the earth (e.g., [40, 41]), our system can detect the sounds of heartbeats that are propagated through a mattress. Therefore, we refer to our system as heartbeat-phone, or HB-Phone in short. Compared to other sensors, the geophone sensor has several advantages, which make it a suitable choice for heartbeat detection[1]. Firstly, it is highly sensitive to tiny motions – geophones are often used to detect distant motions (such as earthquakes), and can generate a noticeable response to minute movements such as heartbeats (after going through a normal mattress). Secondly, it is commercially available and rather affordable. Thirdly, deploying a geophone-based system can be very conveniently done, without interfering with the bed or how it is used. As a result, we believe that HB-Phone offers a very practical solution to at-home heartbeat monitoring during sleep, and in this study, we show that such a solution is also accurate and robust against environmental noise or other body movements a person may have during sleep.

Extracting heartbeats from geophone signals, poses serious challenges to the underlying system design, which we have addressed in our study. The first challenge stems from the fact that the geophone is naturally a second-order high-pass filter, hence insensitive to low-frequency motions. Specifically, when a movement's frequency increases from 1Hz to 10Hz, the geophone's response may become 100 times stronger. Considering that the fundamental frequency range of the heartbeat signal falls between 0.45Hz

[1]In this chapter, we use the term geophone to refer to the analog geophone.

and 3.33Hz (corresponding to a heartbeat rate range from 27 beats to 200 beats per minute), it is difficult to detect geophone responses at their fundamental frequency. In this study, we address this challenge by considering harmonic frequencies of the heartbeat signal, i.e., integral multiples of its fundamental frequency, that are caused by a high-frequency component in a heartbeat.

The second challenge is that geophones are highly sensitive to noise in the environment. During sleep, a person may have various body movements including arm swings, leg kicks, or snoring [2]. At the same time, another person may be walking in the bedroom, or opening/closing the bedroom door. All of these movements will be picked up by a geophone that is installed under the bed mattress. Therefore, it is a daunting task to extract heartbeats from all types of the noise, requiring very careful design of both hardware and software components to mitigate such harmful interference. In hardware design, the key is to control the amplification to ensure heartbeat responses are detectable and distinguishable from noise while maximizing the amplitude of noise that we can cope with. In software design, the key is to carefully devise signal processing algorithms that can effectively filter out both environmental noise and noise caused by a person's body movements while in sleep.

To summarize, we have made the following contributions in this study:

1. We have developed an accurate, robust, low-cost, and easy-to-use bed-mounted heartbeat monitoring system HB-Phone, which is centered around a commercial off-the-shelf analog geophone. The HB-Phone system consists of both hardware and software components. Its hardware components include a geophone, an amplifier and an A/D converter; software components involve filtering, sample auto-correlation calculation, peak finding, and heartbeat extraction. Though geophones were suggested for detecting the presence of heartbeats in [42, 43], to our knowledge, this is the first geophone-based system that can accurately monitor the heartbeat rate in realistic settings.

[2]Our system has an upper bound on the amplitude of the movements it can handle, which is dependent on the configuration of the hardware; in our prototype, we chose to use lower-end hardware components and can cope with body movements whose amplitude is 14 times of that of heartbeats.

2. We have built a HB-Phone prototype and used it to instrument an experimental bed. We have used the experimental bed to collect 502 30-second geophone signals from 34 subjects while they lay still on the bed; 301 30-second geophone signals from these subjects when they had various types of gentle body movements while lying on the bed. We have compared the calculated heart rate with the results measured by a pulse oximeter, and found that the average error rate is 1.30% in the former case, and 3.87% in the latter case.

3. We have deployed the HB-Phone prototype in 9 homes for a total of 25 nights, along with a pulse oximeter and video camera. We observe that the average error rate is 8.25%, even though the subjects had various body movements and environmental noise during the experiments.

The remainder of the chapter is organized as follows. In Section 2.2, we present the hardware system design of HB-Phone, and in Section 2.3, we present the software design that we have built to support heartbeat monitoring. We present our evaluation setup and experimental results in Section 2.4. In Section 2.5, we summarize the existing bed-mounted heartbeat monitoring systems, and compare their pros and cons. Finally, we provide concluding remarks in Section 2.6.

2.2 HB-Phone System Design

We show the overview of HB-Phone in Figure 2.1. In HB-Phone, we place an analog geophone under a mattress to capture movements in the environment, including the user's heartbeats. We first amplify the raw geophone response, and then convert it to a digital signal. Next, we feed the digital geophone signal to a series of signal processing functions, which extract heartbeats and other relevant movements from the signal. The outcome from the HB-Phone system includes estimation of the average heartbeat rate, estimation of the instant heartbeat rate, detection of snoring during sleep, and detection of body movements during sleep, etc.

In this section, we first present the hardware design of HB-Phone. Then we discuss the unique challenges we have faced in designing the HB-Phone system.

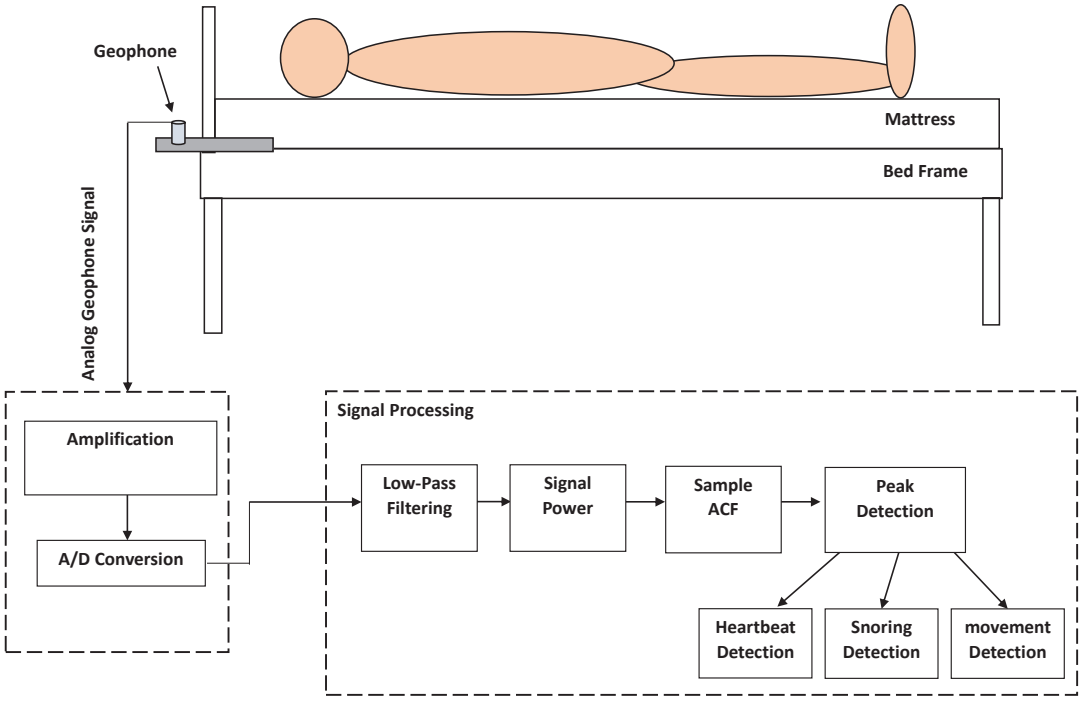

Figure 2.1: Overview of the HB-Phone system. An analog geophone is placed under a mattress. The raw geophone signal goes through amplification and A/D conversion to generate a digital signal that is suitable for subsequent signal processing. A series of signal processing methods will then be applied to detect heartbeats in the signal.

2.2.1 HB-Phone Hardware Design and Prototype

The HB-Phone system is centered around the use of a geophone sensor. As shown in Figure 2.2, a geophone consists of a spring-mounted magnet that moves within a wire coil to generate a voltage, which can thus measure the speed of a movement at different frequencies. The use of a powerful magnet and a differentially wound coil gives it low noise and high sensitivity at frequencies 7Hz and above, while being less sensitive to movements with lower frequencies. In our HB-Phone prototype, we use the SM-24 Geophone Element [44], whose natural frequency is at 10Hz.

The raw geophone signal is first filtered by a hardware bandpass filter in the range from 0.25 to 10kHz, which is then fed to a TI LMV358 amplifier circuit [45]. We have carefully configured the amplifier circuit to ensure the HB-Phone is robust against other types of body movements during sleep (such as snoring, hand/arm swings, or leg kicks). For this purpose, we first need to make sure signals caused by such body movements

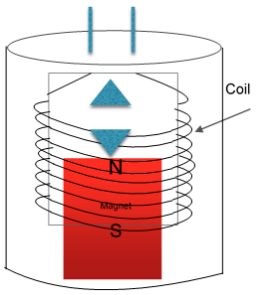

Figure 2.2: The geophone consists of a spring-mounted magnet that is moving within a wire coil to generate electrical signals that measure movements in the environment.

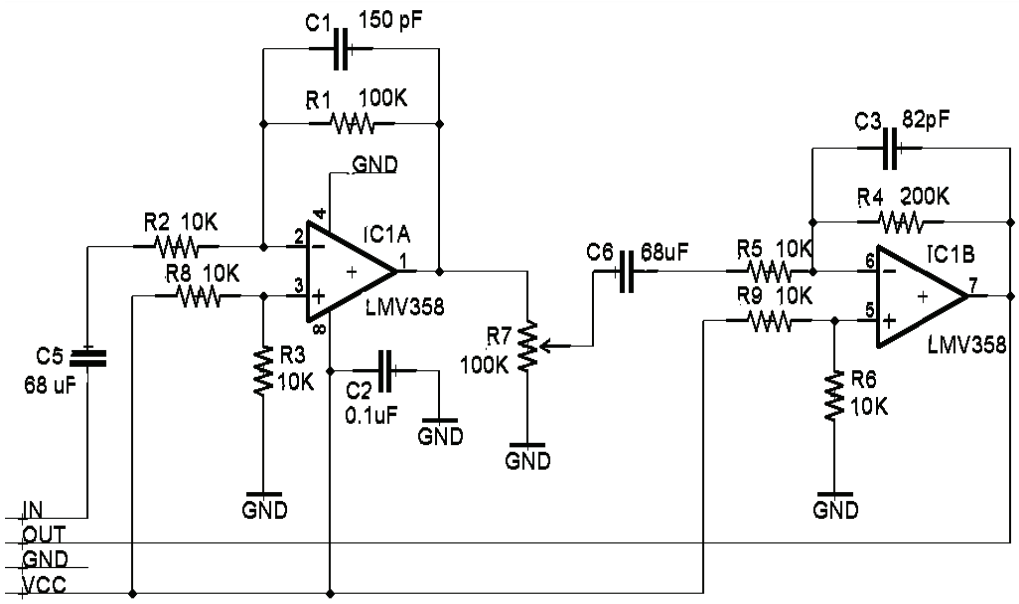

Figure 2.3: The AC amplifier circuit design.

stay within the range of the amplification circuit output after amplification, i.e., 0-3V in our case; once this range is reached, no information can be extracted from the resulting geophone signal. That is, if we desire to extract heartbeats in the presence of noise caused by body movements (whose amplitude is usually much larger than that of heartbeats), then the amplification should be kept sufficiently small to avoid the above-mentioned situation. On the other hand, we are limited by the ADC unit's resolution, especially that of a low-cost ADC unit: if the amplification is too small, then it is hard to correctly detect heartbeats due to a combination of low signal amplitude and low ADC resolution (i.e. quantization error becomes dominant). In this study, our

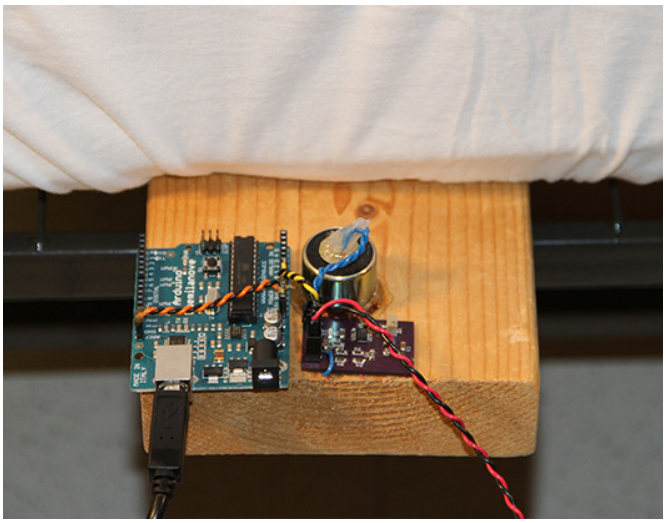

Figure 2.4: The picture of our HB-Phone prototype, where the geophone and the amplifier are glued to a wooden board that is inserted between the memory foam mattress and bed frame.

objective is to maximize the amplitude of body movements that we can handle in the system while still being able to detect heartbeats. For this purpose, we configured the amplification circuit such that the heartbeat signal's amplitude falls within 0-200mV, which is a range determined by the resolution of our ADC. Given that the amplification circuit's output range is 0-3V, we leave 2.8V as the maximum amplitude for detectable body movements, which is roughly 14 times of the amplitude of a heartbeat motion.

Figure 2.3 shows the resulting double-stage amplification circuit. Both the first-stage and second-stage amplifying circuit have a RC bandpass filter in the range from 0.25Hz to 10kHz. The gain of the first-stage amplifier is 10 so that we can reduce some noise from the circuit itself. The maximum gain of the second-stage amplifier circuit is 20 and the gain is adjustable by tuning the adjustable resistor R_7 shown in Figure 2.3. In total, the maximum gain of this circuit is 200. The amplified signal is based on 3.3V and quantized to 1024 levels (10 bits) using an Arduino Duemilanove A/D converter [34]. The ADC output signal is thus ready for subsequent signal processing and heartbeat extraction. In the rest of this chapter, we use the term "geophone signal" to denote the signal after amplification and ADC.

In Figure 2.4, we show the picture of our prototype HB-Phone system. We attached the geophone to a piece of wooden lumber and insert the wood under a memory-foam

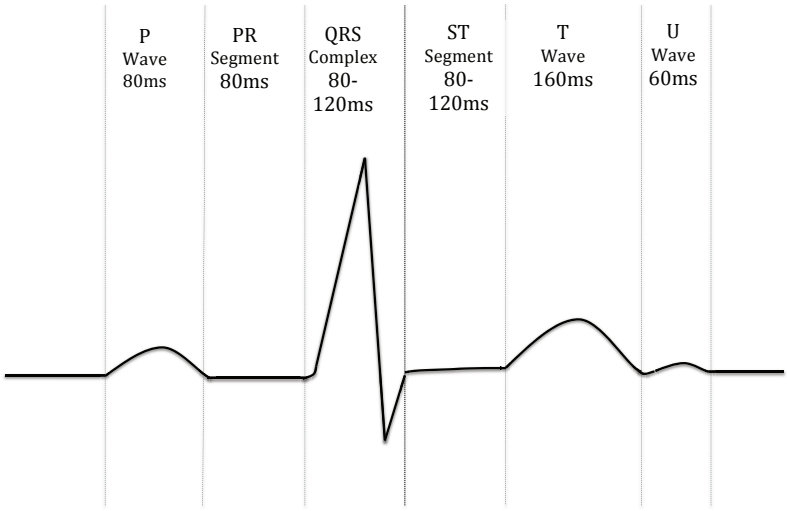

Figure 2.5: In the ECG signal, each heartbeat pulse has a 0.1 second QRS peak [46], which is caused by the ejection of blood from the ventricle. This peak stores most of the energy during a heartbeat and causes strong harmonics.

mattress. Lying down on the bed, the user does not feel the geophone at all, and her sleep won't be interfered in any way.

2.2.2 Unique Challenges of the HB-Phone System

HB-Phone is intended to detect heartbeats that propagate through a mattress, which poses serious challenges to the underlying system design. Below we explain the two major challenges that we have faced in designing the system.

Insensitive to Heartbeats at the Fundamental Frequency

A geophone is essentially a second-order high-pass filter, which is sensitive to movements whose frequency is above a certain threshold, referred to as T_{freq}, while it is insensitive to movements with frequencies lower than the threshold.

This can be explained as follows. As Figure 2.6 shows, the geophone response increases quadratically with frequency when the frequency varies within the range of 1-10Hz for a given speed. For example, let us consider a movement at 1m/s, the geophone generates a voltage about 20V when the frequency is at 10Hz, and a voltage of .2V when the frequency is 1Hz, resulting in a factor of 100 difference in the response

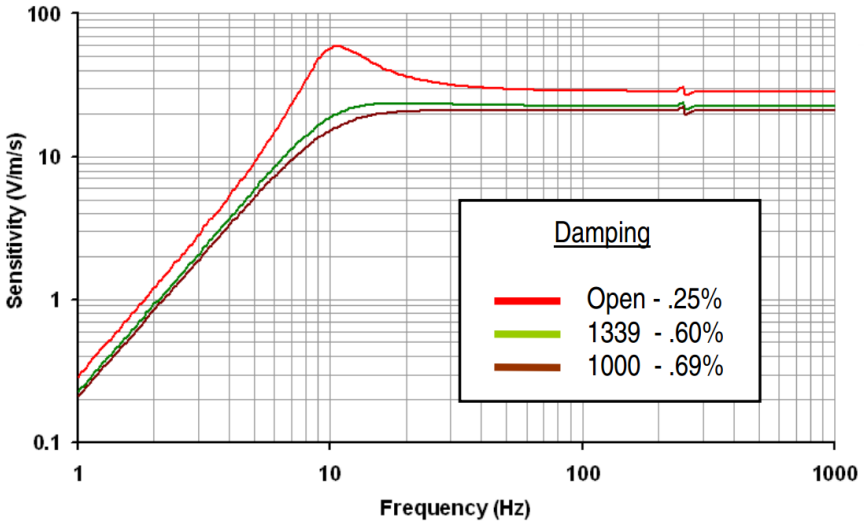

Figure 2.6: The response curve from the data sheet of Geophone SM-24 [47] that we use in our prototype.

between these frequencies. Hence, the geophone itself works as a high-pass filter, making it hard to detect responses to low-frequency movements. In the response curve shown in Figure 2.6, the value of T_{freq} is 10Hz.

Figure 2.5 illustrates an ECG heartbeat pulse, in which the QRS complex (caused by the ejection of blood from the ventricle) stores most of the heartbeat energy and has a frequency of 0.45 to 3.33Hz corresponding to the heartbeat rate of 27 bpm and 200 bpm. In general, we would directly detect vibrations caused by the QRS complex. However, considering the reduced response from the geophone in this frequency range and the noise from the environment, detecting heartbeat signals in this way would be infeasible. Instead, we would focus on the harmonics of the heartbeat signal as harmonics are at higher frequencies and have much stronger geophone responses.

Figure 2.7 shows the FFT results of a 30-second geophone signal when a subject lay still on the prototype bed. On the figure, we mark a few harmonic frequencies of the heartbeat signal with their corresponding harmonic numbers; we use number 1 to mark the fundamental frequency. Clearly, the geophone's response to the fundamental frequency is very weak, and its response to the next few harmonics (within the frequency range of 2-13Hz) is much stronger. In this study, we then aim to detect heartbeats' harmonic signals at these frequencies.

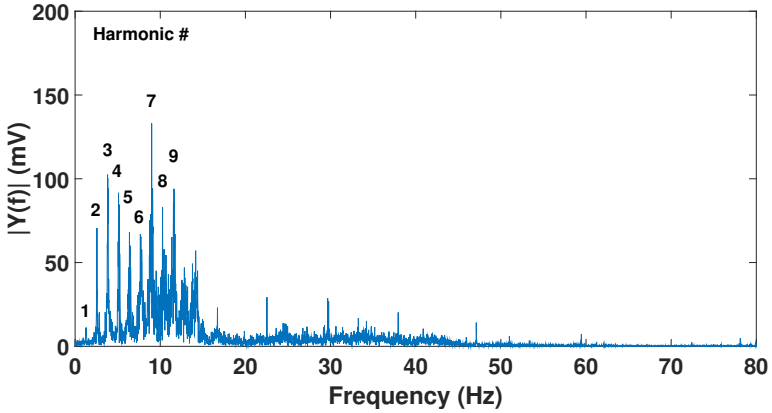

Figure 2.7: FFT results of a 30-second geophone signal when a subject, with an average heartbeat rate of 76.86 bmp, lay still on the bed. In the figure, we mark the heartbeat signal's fundamental frequency (with the number 1) and a few harmonic signals (2 means the second harmonic frequency). In order to clearly show the harmonic frequencies in this result, we adjusted the amplification circuit such that the resulting heartbeat amplitude is close to 3V. In the rest of this chapter, our amplifier circuit output for heartbeats is kept at 200mV.

Finally, we would like to point out that the geophone's response to respiration is much weaker than the response to heartbeats because respiration has even lower fundamental frequency. In this study, we focus on detecting heartbeats, and have not observed noise caused by respiration. In our future work, we will study how we can detect respiration activities using the geophone.

Highly Sensitive to Noise Caused by Motion

The geophone is very sensitive to motions if their frequency is above the threshold T_{freq}, which is also the very reason why we choose this type of sensor in the first place. It responds to tiny motions or vibrations in the environment – when placed under a mattress, its response signal shows fluctuation when someone walks in the room or someone closes the door. Thus, we need to differentiate heartbeats from other movements from the same user, movements from other users, or movements/vibrations in the environment. Examples include the subject's body movements during sleep, snoring, other people walking around while the subject is in sleep, fans in the room, pets moving on the bed, etc. Since many of these movements are more pronounced than heartbeats, detecting heartbeats in their presence is particularly challenging.

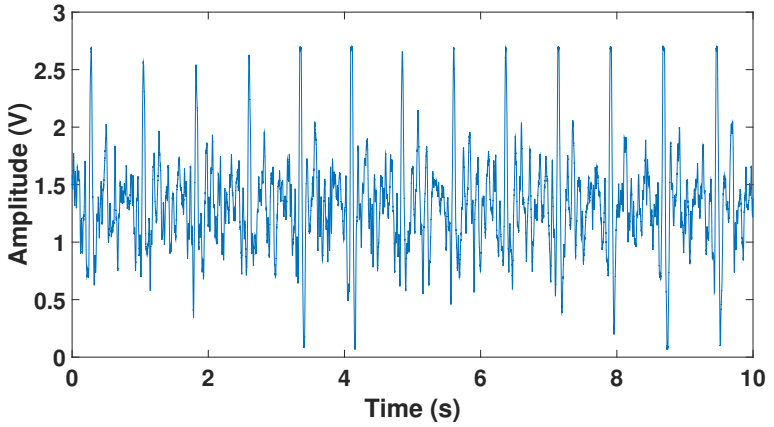

(a)

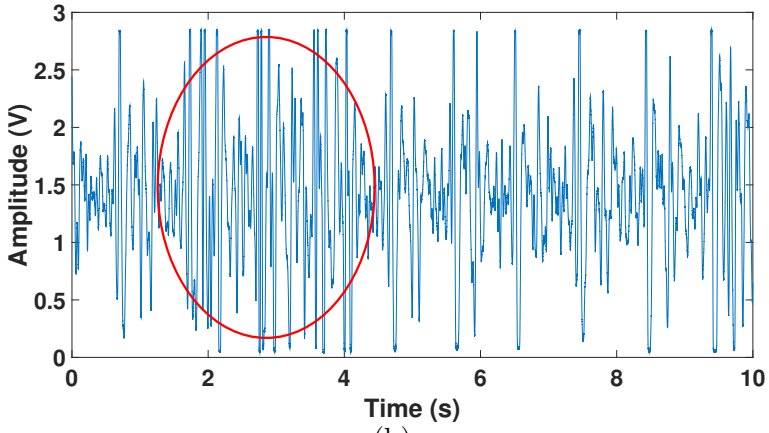

(b)

Figure 2.8: (a) A 10-second geophone response signal. In this experiment, the user was lying still on the experimental bed, without any movement in the environment. (b) A 10-second geophone response signal. In this experiment, the user was lying still on the experimental bed, while a second user was walking around 1 meter away from the bed.

Here, we use an example to illustrate the impact of movements in the environment. Figure 2.8(a) shows a 10-second geophone signal when a user was lying still on our experimental bed. During the data collection period, we made sure that there was no other movements near the bed. Next, we introduced movements around the bed by having a second subject walk 1 meter from the bed (on a concrete floor). We show the resulting geophone response in Figure 2.8(b), and mark the affected area using the red circle. This example shows that the geophone is very sensitive to noise in the environment, making heartbeat detection a challenging task.

2.3 Extracting Heartbeats from Geophone Signals

Next, we partition the geophone signal into equal-length windows (30 seconds in our case), and count how many heartbeats in each window. Our signal processing algorithm consists of the following steps: (1) applying a low-pass filter; (2) calculating sample auto-correlation function (ACF), (3) finding peaks in sample ACF data, and (4) detecting heartbeats. We choose this method because (i) we observe that it is possible to separate heartbeat signals from body movement signals by filtering, and (ii) heartbeats exhibit strong periodicity compared to most other body movements. Please note that geophone is very insensitive to respiration – another common periodic motion – due to its lower frequency.

2.3.1 FFT and Low-pass filtering

We first compute FFT on geophone signals from various body movement patterns (we only focus on body movements whose amplitude is at most 14 times of the heartbeat amplitude in this study as explained in Section 2.2) to find out whether there is a clear separation between heartbeats and body movements in the frequency domain.

We collected geophone signals when a subject performed three different types of body movements while standing half a meter from the bed. In this way, we can separate the signals caused by heartbeats and those caused by body movements, and only focus on geophone responses to body movements. We show a few such FFT results in Figures 2.9(a)-(c). In these results, we shifted the signal mean to zero to remove the DC component. In Figure 2.9(a), we show the FFT results when a subject tapped the mattress a single time during a 30-second window, representing impulse or one-time body movements whose signal only shows a narrow peak in the time domain. In Figure 2.9(b), we show the FFT results when a subject tapped the mattress once a second for the entire 30-second window, representing long-term body motions that last for many seconds or even minutes, whose signal will show up in the entire signal window. In Figure 2.9(c), we show the FFT results when a subject scratched the bed sheet for a few seconds, representing body movements that last for a relatively short period whose

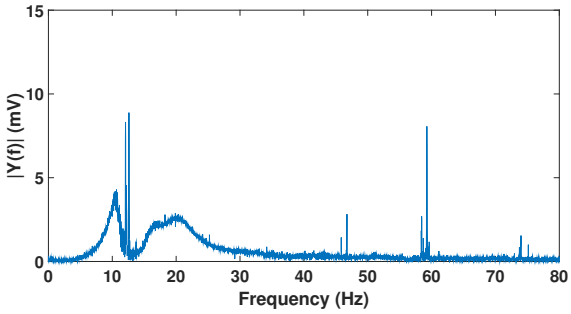

(a) Subject tapped the mattress once during the 30-second experiment

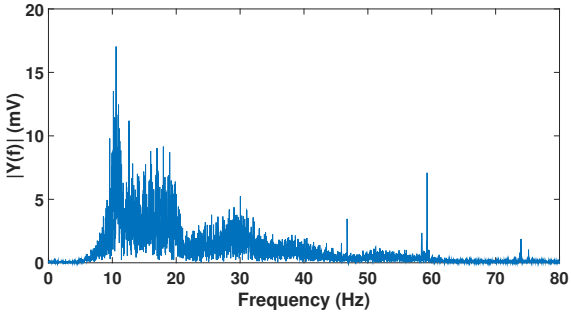

(b) Subject tapped the mattress once a second for 30 seconds

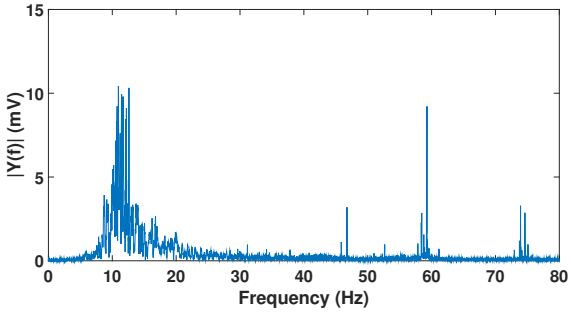

(c) Subject rubbed bed sheet for a few seconds

Figure 2.9: FFT results for geophone signals with different body movement patterns. According to the results, the majority of frequency components for different body movements are above 6Hz, and rise significantly after 8Hz.

signal covers a portion of the signal window.

The FFT results suggest that most geophone signals caused by body movements have frequencies 6Hz and above, with a sudden rise after 8Hz. Considering this, as well as the heartbeat FFT results shown in Figure 2.7, we hypothesize that a low-pass filter with a cutoff frequency between 6 and 10Hz would be able to effectively separate heart beats and body movements.

2.3.2 Calculating Sample ACF

Sample ACF [35] is often used to extract periodicity from a time series. For this purpose, we need to shift the signal mean to zero and square the voltage signal to produce a power signal proportional to the instantaneous mechanical power in the system.

Next, we calculate the sample ACF of the geophone signal power. For a time series signal $x(t)$, we have the following normalized sample ACF:

$$\bar{f}_{A\hat{C}F}(h) = \frac{f_{A\hat{C}F}(h)}{f_{A\hat{C}F}(0)} \qquad 0 \leq h < n, \tag{2.1}$$

where n is the number of sampling points, h is the time lag. The Sample ACF function is defined as

$$f_{A\hat{C}F}(h) = \frac{1}{n}\sum_{t=1}^{n-h}(x_{t+h} - \overline{x})(x_t - \overline{x}) \qquad 0 \leq h < n, \tag{2.2}$$

with the sample mean

$$\overline{x} = \frac{1}{n}\sum_{t=1}^{n} x_t. \tag{2.3}$$

When the time lag is 0, the heartbeat power signal aligns perfectly with itself and the autocorrelation reaches the maximum value. When the time lag starts to increase, the first signal stays the same while the second signal shifts right. The mismatch between two signals results in a decreased sample ACF value. However, when we have the time lag equal to a multiple of the heartbeat interval, heartbeat pulses in the first signal match nicely with pulses in the second signal, yielding a large sample ACF value. Thus, by detecting the peaks in the sample ACF results, we can infer the periodicity of heartbeats.

2.3.3 Sample ACF Peak Finding and Measurement

In this study, we adopt the peak finding and measure algorithm developed by Thomas C. O'Haver from University of Maryland [36] to locate peaks in the sample ACF results. Specifically, the algorithm detects the location and value of peaks using the following steps:

1. We denote the first derivative of the sample ACF $\bar{f}_{A\hat{C}F}(t)$ as $\bar{f}'_{A\hat{C}F}(t)$. We have $\bar{f}'_{A\hat{C}F}(t_p) = 0$ at any peak maximum with time lag t_p and a downside going trend.

2. To prevent finding peaks caused by noise, we smooth the signal using two passes of multi-point triangular smoothing with a proper window width.

3. We find peak maximums by checking whether the difference between the derivative of $\bar{f}'_{A\hat{C}F}(t)$ and $\bar{f}'_{A\hat{C}F}(t+1)$ exceeds the pre-determined threshold. If it does, then the peak lies in the vicinity of this location.

4. Since the smoothing step (step 2) could have distorted the original signal, we need to go back to the original signal and pick points that are near the peak location identified in step 3. Then we apply Least Square Curve-Fitting over these points to refine the peak location.

2.3.4 Extracting Heartbeats from Original Geophone Signals

Ideally, the number of peaks found from the sample ACF results is equal to the number of heartbeats within the time period. However, in practice, it is often the case that after the first few peaks, the remaining peaks found using the above algorithm may drift because human heartbeats have slight variations from one heartbeat to another, leading to incorrect peak numbers and locations if one assumes heartbeats are perfectly periodic. As an optimization technique, we only take the first 20% of the peaks from the sample ACF results to calculate average heartbeat interval. Suppose there are n peaks that belong to the first 20% of the established peaks. Further suppose the interval between the first peak and the n-th peak is T, then the average heartbeat interval I_{HB} is calculated as $\frac{T}{n-1}$. Based on the estimated I_{HB} value, we can go back to the original geophone signal and extract each individual heartbeat as follows:

1. We locate the geophone response to the first heartbeat[3] in the range of $[0, I_{HB}]$ by finding the maximum amplitude value. We use t_1 to denote its time.

2. Assuming that we have already detected h heartbeats, and that the h-th heartbeat occurs at t_h, then we intend to search for the $(h+1)$-th heartbeat within the time

[3]Here, we do not distinguish a heartbeat and the geophone's response to this heartbeat.

range of $[t_h + \frac{I_{HB}}{2}, t_h + \frac{3I_{HB}}{2})$. We locate the $(h+1)$-th heartbeat by finding the maximum amplitude value. in this range.

3. We repeat step 2 until we find all the heartbeats.

2.4 Evaluation Results

In this section, we describe our evaluation effort and present detailed experimental results. In the first phase of evaluation, we focused on testing HB-Phone's heartbeat rate estimation accuracy in a laboratory environment through controlled experiments, and considered noise caused by different body movements in the experiments. Our evaluation in this phase involved 34 subjects, and collected over 400 minutes of heartbeat signals. Then in the second phase, we investigated how HB-Phone performs in real-world settings through long-term field trials that involved 9 subjects for 25 nights. In total, we collected over 181 hours of data in the second phase[4].

In both phases, we obtained the ground-truth heartbeat rates, $\bar{H}$, by running a similar signal processing method (as described in Section 2.3) on signals collected by a pulse oximeter. Assuming the estimated heartbeat rate in the HB-Phone system is H, then we report the estimation error rate as $|H - \bar{H}|/\bar{H}$.

2.4.1 Evaluation Phase I: Controlled Experiments

In the first phase of evaluation, we conducted a series of controlled experiments in a laboratory environment emulating a wide range of noise caused by human body movements that are possible during sleep, and report the average estimation accuracy of HB-Phone in these experiments.

Participants: We had a total of 34 healthy volunteer participants for this experiment, including a total of 26 males and 8 females. The mean age of the participants was 28.0 years with a standard deviation of 7.7 years. The youngest participant was 22 years old while the eldest was 65 years old.

[4]Our studies were approved by the Institutional Review Board (IRB) of our institution.

Experiment Procedure: The controlled experiments in the first phase aimed to study the accuracy of HB-Phone by comparing the estimated heartbeat rate against the ground truth – the heartbeat rate measured by a pulse oximeter.

During the experiments, all participants were asked to lie on the prototype bed in our lab for the duration of a trial (30 seconds), during which we recorded the geophone signal and transported the data to a PC for subsequent signal processing. Meanwhile, we placed a pulse oximeter on the participant's index finger, whose data is transferred to a PC in real time for subsequent processing. We then obtained the number of heartbeats in both signals, and calculated the error rate for each trial. Each participant went through multiple trials, and we had more than 800 trials in total.

Here, we emulated two groups of scenarios; in the first group, the subjects were asked to lie still on bed, and in the second group, the subjects were asked to perform body movements with varying durations while lying on bed. The participants were engaged in different activities before the trails. For example, some subjects just finished running before a trial; some subjects fell asleep during the trial (and sometimes these subjects just ran before the trial). Hence, subjects' heartbeat rates varied considerably across all trials.

In addition, we note that our prototype bed is located in a very noisy university lab. There are more than four hundred computers in the same room, which were on and off during our experiments. The bed is close to the entrance to the room, and often people were walking in/out of the lab during experiments. Our results show that the HB-Phone prototype is resistant against the noise.

When the Subject Has No Body Movements: In the first group of experiments, the subjects did not make any body movements during a trial. As a result, the geophone signal was dominated by geophone responses to heartbeats.

Despite the environmental noise, HB-Phone delivers very accurate results in this scenario. We report the average error rate of HB-Phone over 502 samples/trials in Figure 2.10. These data were collected over a period of 7 months, covering different environmental noise in the laboratory. Here, we group the samples into 6 groups, based

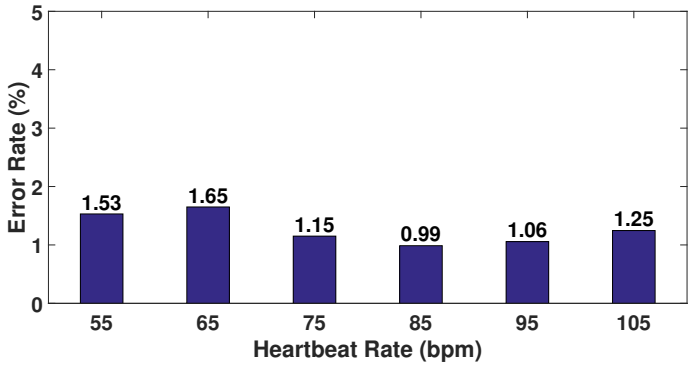

Figure 2.10: Average error rates in the following heartbeat rate ranges: [50, 60), [60, 70), [70, 80), [80, 90), [90, 100), [100, 110]. The average error rate across all the ranges is 1.30%. The subjects were lying still on bed in these experiments.

upon the heartbeat rate reported by the pulse oximeter, namely, [50, 60), [60, 70), [70, 80), [80, 90), [90, 100), [100, 110]. Then we report the average error rate of each group. The total average rate across all 502 samples is 1.30%. In this scenario, the cutoff frequency value for the low pass filter does not have a noticeable impact on the average estimation accuracy; any value above 6Hz yields a comparable performance. These results demonstrate that geophones are able to detect heartbeats through a mattress.

When the Subject Has Body Movements: It becomes much more challenging to accurately extract heartbeats while the subject has body movements while lying on bed because their signals overlap with heartbeat signals in the frequency domain and their amplitude is usually much larger. In HB-Phone, we carefully design the low-pass filter to minimize the impact of body movements on the geophone signal, as discussed in Section 2.3.1. Our results show that while challenging, HB-Phone is able to detect heartbeats with an average error rate around 3.87%.

In order to separate geophone responses caused by heartbeats and those caused by body movements, our signal processing method takes the following two measures: (1) applying a low pass filter to filter out frequency components above a certain threshold (since we observe that there are several heartbeat harmonic frequencies that are lower than body movement signals), and (2) finding the periodicity within the signal (since heartbeats have stronger periodicity than other movements). As a result, the cutoff frequency's value is the key to HB-Phone's estimation accuracy. We varied the cutoff

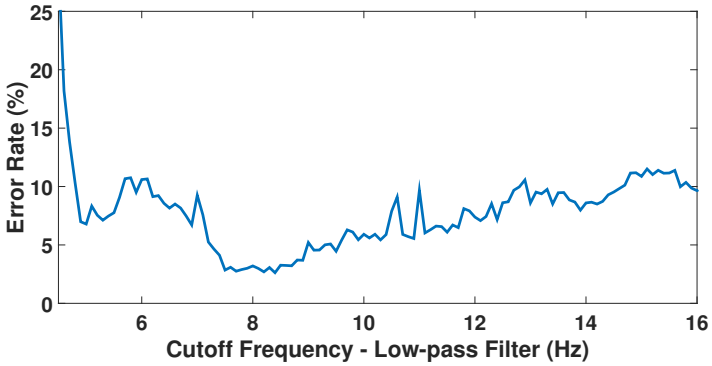

Figure 2.11: The average estimation error rate with different cut off frequency values for the low-pass filter. Results show that a frequency value around 8Hz gives the best results, which also agrees with the observation in Figure 2.9.

frequency from 4.5 to 16Hz and reported the resulting average estimation error rate in Figure 2.11. We find that when the cutoff frequency is around 8.4Hz, HB-Phone has the best estimation accuracy, with an average estimation error rate of 3.87%. This also agrees with our observation in Section 2.3.1 from the FFT results shown in Figure 2.9 – the majority of body movements' frequency components have a sudden rise around 8Hz.

As in Section 2.3.1, we categorize usual body movements into the following three groups: (i) impulse movements that include one-time movements; (ii) movements that last for seconds or even minutes, thus longer than an experiment window (30 seconds); and (iii) movements that last for a few seconds, thus occupying a portion of an experiment window. Fixing the cutoff frequency at 8.4Hz, we show the detailed estimation error rate for the three types of body movement patterns in Table 2.1. We find that the average error rate is the highest for long-duration movements, and the lowest for impulse motions.

	Impulse Motion	Long Motion	Short Motion	Overall
Error Rate (%)	3.34	4.07	3.89	3.87

Table 2.1: The average error rate for three types of body movement patterns. The error rate is the highest for long periods of movements and lowest for impulse motions.

2.4.2 Evaluation Phase II: Long-Term At-Home Deployment for Heartbeat Monitoring During Sleep

In the second phase of evaluation, we deployed the HB-Phone system in 9 subject's homes for a total of 25 nights. We also deployed a pulse oximeter and a video camera to obtain ground truth for heartbeat rates and body movements[5]. In total, we collected 181.1 hours' data. Our results show that HB-Phone is easy to use and robust against many different types of events that occurred during sleep.

Participants: We had a total of 9 volunteer participants for these experiments, including a total of 8 males and 1 female. The mean age of the participants was 26.3 years with a standard deviation of 3.9 years. The youngest participant was 22 years old while the eldest was 34 years old.

Experiment Procedure: Table 2.2 summarizes the 9 subjects' house, floor, and bed information, among whom 7 subjects had experiments for multiple nights, and 2 subjects had experiments for a single night each. In total, we conducted experiments for 25 nights.

For each experiment, we arrived at the subjects' home 30-60 minutes before their bed time and it took about 20 minutes to install a HB-Phone prototype, a pulse oximeter, and a video camera. Among these three devices, the latter two usually took more time to install – we had to make sure the pulse oximeter was secured on the subject's index finger, and the video camera could capture the view of an entire bed. The actual installation of the HB-Phone hardware was very straightforward; we just inserted the wood board (to which the geophone and amplifier are attached) between the bed frame and the mattress.

Right before the subject turned off lights, we turned on the system and started with a simple synchronization process: the subject uses the hand that has the pulse oximeter on to tap the mattress 20 times. We could capture this motion from all three devices, thus synchronizing their data. During our experiments, all participants slept through

[5]We obtained the consent from all the participants before deployment.

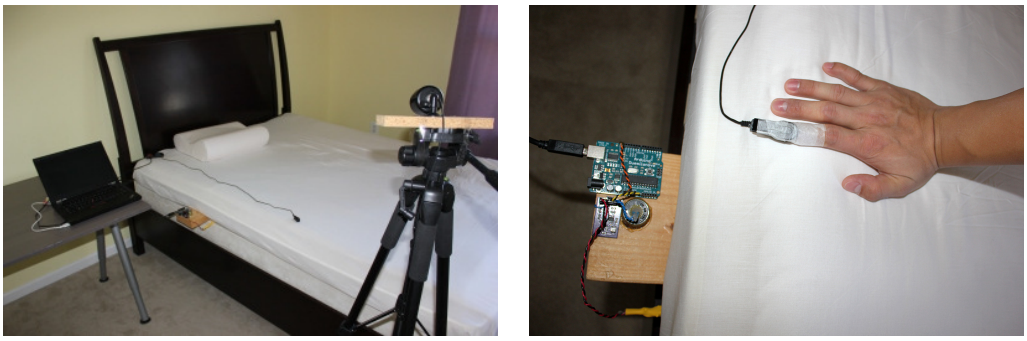

(a) (b)

Figure 2.12: Our deployment setting. (a) The HB-Phone prototype was easily installed on the bed. A video camera was used to collect ground-truth data for the subjects' movements. (b) A pulse oximeter was used to collect ground-truth data for the subjects' heartbeat rate.

Subject	**House Type**	**Floor Type**	**Bed Size**	**Bed Frame /Box**	**Mattress**
S_1	Condo mini	Thick carpet over wood	Queen	Hardwood box	Thin sheet
S_2	Condo mini	Thick carpet over wood	Queen	Hardwood box	Thin sheet
S_3	Single family	Thin carpet over wood	Queen	Hardwood box	Spring mattress
S_4	Apt	Thin carpet over concrete	Queen	Hardwood box	Spring mattress
S_5	Single family	Thin carpet over wood	Queen	Steel platform	Spring mattress
S_6	Single family	Thin carpet over concrete	Queen	Box spring	Memory foam
S_7	Condo mini	Thick carpet over wood	Queen	Hardwood box	Thin sheet
S_8	Dorm	Wood	Twin	Hardwood frame	Futon
S_9	Apt	Thin carpet over concrete	Full	Steel platform	Memory foam

Table 2.2: We have deployed HB-Phone in 9 subject's homes. This table summarizes the house type and bed information of these deployments.

the night until the next morning. Upon waking up, they turned off all three devices. All the data collected were transferred to a PC for offline processing.

The average system "on" time per night was 7.2 hours. When processing the data, we removed the first few minutes data as well as the last few minutes data.

Cutoff Frequency for the Low-Pass Filter: In real-world deployment, the cutoff frequency value plays a very important role in determining the overall performance of HB-Phone. We first report the average estimation error rate with different cutoff frequency values in Figure 2.13. The results show that when the cutoff frequency is above 6Hz, the average error rate decreases significantly, which agrees with the observation

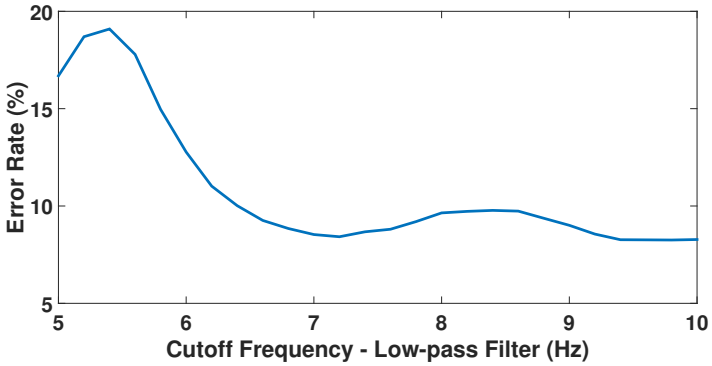

Figure 2.13: The average estimation error rate with different cut off frequency values for the low-pass filter for the 25 nights' deployment data. The error rate drops significantly when the cutoff frequency is above 6Hz. In this study, we choose the cutoff frequency of 9.8Hz which gives us an error rate of 8.25%.

presented in Figure 2.9. Our observation through empirical studies is that a cutoff frequency between 7 and 10 Hz usually leads to accurate heartbeat detection results. In the rest of this study, we choose the cutoff frequency value of 9.8Hz, which leads to an average error rate of 8.25%.

Heartbeat Rate Estimation Accuracy: Next we discuss the details involved in processing the long-term deployment data. We have collected data for a total of 25 nights. For each night, we partition the data sets into 30-second windows, and apply our signal processing algorithm to each window to count the number of heartbeats contained in that window. We compare this number against the number calculated from the pulse oximeter data, and compute the error rate in each window. The detailed results are summarized in Table 2.3. We note that there are windows during which we were unable to detect heartbeats, and thus we categorize each window into one of the following four groups:

- Ground Truth Missing. On average, for 13.83% of the total number of windows, the pulse oximeter data was missing. We checked the video data during these windows and found out that the missing ground truth happened when the finger that had the pulse oximeter on moved. For these windows, we did not attempt to extract heartbeats from the geophone signal.

- Amplifier Range Exceeded. On average, for 5.22% of the total number of windows,

Subject	% of windows ground truth missing	% of windows amplifier range exceeded	% of windows heartbeats undetectable	% of windows heartbeats detected	Average error rate (%)
S_1	5.87	6.73	2.58	84.82	14.08
S_2	9.86	3.14	1.94	85.06	6.64
S_3	28.16	6.22	3.62	62.00	13.53
S_4	19.34	6.97	3.48	70.21	8.43
S_5	10.18	0.60	1.20	88.02	3.05
S_6	12.93	0.49	2.20	84.38	5.31
S_7	10.18	4.38	2.19	83.25	5.41
S_8	23.66	1.10	4.88	70.36	7.22
S_9	8.69	0.36	0.84	90.11	4.45
Overall (25 nights)	13.83	5.22	2.87	78.08	8.25

Table 2.3: We deployed the HB-Phone prototype in 9 subjects' homes. For each subject's data, we report the percentage of windows (30 seconds) during which the ground truth data was missing (P_m), the percentage of windows during which the amplification maximum range was reached (P_r), and the percentage of windows during which our signal processing algorithm failed to detect heartbeats (P_f). Then the percentage of windows during which we detected heartbeats is calculated as $1 - (P_m + P_r + P_f)$. For these windows, we report the average estimation error rate. On average, we could detect heartbeats for 78.08% of the windows, with an average error rate of 8.25%. The results strongly suggest that HB-Phone provides a compelling solution for heartbeat monitoring during sleep.

the geophone signal amplitude reached the amplifier range (3.0V in our case) and no useful information could be extracted from these signals. We checked the video data and found out that during these windows, the subject had large body movements; for example, we observed turning, and leg/arm twitches. For these windows, we did not attempt to extract heartbeats from the geophone signal.

- Heartbeats Undetectable. On average, for 2.87% of the total number of windows, our signal processing algorithm failed to detect heartbeats – the number of detected heartbeats was either too small or too large to be reasonable. We checked the video data and found that there were usually moderate movements during these windows, such as rubbing the face, changing the lying position, moving the arm position, etc.

  To identify those windows that fall into this group, we searched all the ground truth results, and found the minimum heartbeat rate value (r_{min} = 41.6bmp) and maximum heartbeat rate value (r_{max} = 91.4bmp). Then assuming a 20% estimation error rate, we set the normal heartbeat rate range as $[.8 \times r_{min}, 1.2 \times r_{max}] = [33, 109]$. If the calculated heartbeat rate from our signal processing

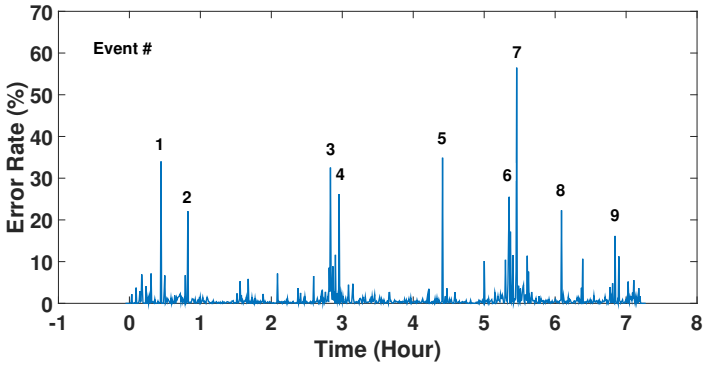

Figure 2.14: In this figure, we calculate the error rate every 30 seconds for 7.3 hours on the night of Sep. 30, 2015 from 11:57 PM to 7:16 AM. Here, we mark 9 events on the figure whose error rate is above 15%.

algorithm is outside of this range, we declare heartbeats are undetected during this window.

- Heartbeats Detected. On average, for 78.08% of the windows, we were able to detect heartbeats and compare the results from HB-Phone against the ground truth. The overall estimation error rate is 8.25%.

  We further broke down these windows into the following two groups: (1) windows without motions, and (2) windows with motions. Specifically, we look at the geophone signal during each window; if the difference between the maximum and minimum voltages in a window is less than 200mV, then we categorize this window as without motions (it could still contain minor motions such as finger movements). By looking at the data collected in 25 nights with an average error rate of 8.25%, we find that 45.70% of the windows are no-motion windows, which have an average error rate of 5.23% , while 54.30% of the windows have motions and their average error rate is 10.28%.

Motions During Sleep: Finally, we take the geophone signal collected in the night of Sep. 30, 2015 (which has the lowest average error rate, 3.05%), and plot the error rate in every 30-second window in Figure 2.14. In the figure, we mark the 9 windows whose error rates are above 15%, and figure out the movements in these windows by looking at the video data.

In the first marked window, the subject stretched his leg and then scratched the face with his right hand. In the second marked window, the subject's chest twitched. In the third marked window, the subject scratched his chest. In the fourth marked window, the subject scratched his face and then placed the hand back to the chest. In the fifth marked window, the subject scratched his face and then changed his facing direction. In the sixth and seventh marked windows, the subject scratched his nose. In the eighth window, the subject had an twitch in his left arm and then moved his left hand. In the ninth marked window, the subject scratched his face and placed the hand back to the chest. Then, he stretched his leg.

We note that these windows had high error rates mainly because the subject had a combination of multiple body movements – each single movement alone usually could be effectively filtered out by HB-Phone as observed in other windows. In our ongoing research, we will continue to improve the effectiveness of HB-Phone and lower the overall error rates.

2.5 Related Work

2.5.1 Overview of Existing Bed-Mounted Heartbeat Sensors

Quite a few bed-mounted heartbeat sensing systems have been developed. We can broadly categorize existing bed-mounted heartbeat monitoring sensors into the following categories (based upon the sensor modality): air/water pressure sensors, e.g., those in [16–22], or piezoelectric sensor [23–25]; force sensors, e.g., those in [26–28]; optical sensor, e.g., those in [29]; radar sensor, i.e., those in [12]; ultrasound sensors, e.g., those in [13], and foil pressure sensor, e.g., those in [30, 31].

We note that, among these systems, few satisfies the following requirements – i.e., accuracy, low cost and ease to use – at the same time.

Sensors that Require Special Mattress/Cushion: Some systems require specialized mattresses to monitor heartbeats, which is cumbersome and may curb their wide adoption. For example, Watanabe et al. [16] proposed to use a pneumatic system that

consists of an air cushion, a pressure sensor, and electric filters for heartbeat monitoring. The air cushion is placed under the mattress, and the sensor detects the change of pressure due to human vital functions. Similarly, the air mattress sensor system proposed in [17] requires an air-cell mattress. By measuring the air pressure difference between two air cells during heartbeats, the system can monitor a user's heartbeats. In [18], Tanaka et al. proposed to place a phonocardiographic sensor on the edge of a water-mat. The sensor detects the acceleration of vibration caused by heartbeats. Kortelainen et al. [30] proposed to measure heartbeat intervals using a foil pressure sensor (piezoelectric or ferroelectric) with electronic casing boxes placed inside of the mattress. Hansen et al. [48] proposed to build a mattress embedded with a sensitive motion detector. The sensor has two sheets of different dielectric constants which generate an electric charge while rubbing against each other, where the charge is picked up by a capacitor-like antenna. Heartbeats are thus detected by observing the charge variation.

Sensors that Require Special Handling of Bedding: Some systems need to place sensors (usually film sensors) in specific locations (usually near the heart) under the sheet, which entails a great deal of manual overhead as it requires adjustment every time when the user changes sleeping position/pose, or changes the sheet. For example, Bu et al. [23] proposed to use a piezoelectric film sensor under ones back, near the heart. The sensor measures pressure fluctuation due to heartbeats. Wang et al. [24] proposed to use a polyvinylidene fluoride piezopolymer film sensor in the thorax area under the sheet. The sensor picks up pressure fluctuation on the bed caused by the heartbeats. In [31], a foil pressure sensor is placed in the thorax region under a thin mattress. Then a specially designed mattress is placed on top of the existing mattress and bed frame. Similarly, Zhu et al. [49] proposed to place two pressure sensors under a pillow, assuming that the user will always use the pillow during sleep.

Some systems assume users always sleep on the same spot. Mack et al. [50] proposed to place two pressure pads on the bed surface assuming the user always sleeps in the same location. Bruser et al. [29] proposed to monitor heartbeats by placing four optical ballistocardiography (BCG) sensors in a diamond configuration in the thorax

area underneath a regular bed mattress. The sensor generates light and measures the intensity of light which is reflected or scattered back from the mattress. Bruser et al. [27] proposed to place a slat of four strain gauges under the thorax area in the bed slatted frame. Rosales et al. [19] proposed to use four water transducers that are placed vertically between mattress and bed frame, close to the subject's back area.

Custom-Built Sensors: Some systems require custom-built sensors. Heise et al. [21] proposed to use a hydraulic bed sensor that consists of a self-built hydraulic transducer and an integrated pressure sensor. Choi and Kim [12] proposed to build RF circuits to capture human heartbeats. The transmitter continuously emits a sinusoidal signal and the receiver captures the signal reflected from human body. Heartbeats and respiration are captured by detecting the phase shift between the original signal and the reflected signal.

Costly Commercially Off-the-Shelf (COTS) Sensors: Some systems use expensive COTS sensors. For example, sensitive load-cell sensors placed underneath bed legs can measure the vibration of heartbeats as discussed in [26]. Nukaya et al. [25] proposed to use a piezoceramic system to detect heartbeats. The sensor is bonded to the stainless steel plate sandwiched between floor and bed legs.

Sensors That are Hard to Install: Some systems require a considerable amount of manual installation effort. For example, Yamana et al. [13] proposed a system that has a 40-kHz ultrasound transmitter and receiver pair, a plywood board, aluminum support under the board, and aluminum guide rail on the bed surface. The wood board and aluminum guide rail are used to hold transmitter and receiver in place while the aluminum support is used to prevent the board from bending. The ultrasound signal is transmitted toward the head side, and the receiver obtains the ultrasound reflected at the below-surface of the mattress.

2.5.2 Overview of Signal Processing for Heartbeat Detection

One of the main challenges faced by many heartbeat sensors is to differentiate heartbeats from respiration. Most of studies address this challenge through the fact that these two

activities have very different frequencies. Below we summarize popular signal processing methods for heartbeat detection:

- Filtering. In [18], bandpass filters are applied to differentiate these two. In [21], a low pass filter and windowed peak-to-peak deviation is computed for heartbeat detection. In [29], highpass and lowpass filters are applied and continuous local interval estimation algorithm is used to extract the beat-to-beat intervals. In [13], envelope detector and bandpass filter are applied for different detection purposes.

- Decomposition. In [23], Empirical Mode Decomposition (EMD) is applied to the signal, and respiration and heartbeat waves are reconstructed by summing up waves from EMD at different frequency ranges. In [24], wavelet multi-resolution decomposition analysis is used for the detection of respiration and heartbeats.

- Peak Finding Algorithm. In [12], the peak finding with power spectral density is utilized to extract heartbeats. In [28], the signal is first low-pass filtered, and then heartbeats and respiration are detected by a peak finding algorithm within a moving window.

- Machine Learning. In [27], an unsupervised learning technique with three indicators (cross correlation, euclidean distance, HV signal) is used to extract the shape of a single heart beat from the recorded signal. In [19], a k-means clustering method is used to extract heartbeats from the input signal.

- Discrete Fourier Transform Analysis. In [30], sliding Discrete Fourier Transform is applied on heartbeat signal and principal component analysis on respiration signal.

The problem we face in this study is more challenging than merely differentiating heartbeats and respiration. Firstly, geophone is insensitive to low-frequency movements such as respiration. Secondly, in this study, we seek to extract heartbeats in the presence of other types of body movements, which are often within the same frequency range as heartbeats. Finally, in addition to controlled experiments within the laboratory

environment, we also installed our system in 9 subjects' homes and measured their heartbeats for 25 nights.

2.6 Concluding Remarks and Future Direction

In this chapter, we have developed HB-Phone, a bed-mounted heartbeat monitoring system that uses a geophone sensor to capture and extract heartbeats during sleep. The geophone is highly sensitive to movements whose frequency is above a certain threshold, while insensitive to lower-frequency motions such as respiration. This characteristic lends itself to heartbeat detection since each heartbeat pulse contains a high-frequency component that can generate harmonic frequencies that geophones can easily detect. Compared to other existing solutions, HB-Phone uses affordable off-the-shelf hardware, making it is very easy to deploy with an individuals existing bed, while also providing accurate and robust heartbeat detection.

We have built a HB-Phone prototype and conducted extensive experiments that involved 43 subjects. We compared the heartbeat rate estimated by our prototype with that reported by a pulse oximeter. From a sample of 34 subjects, we collected 502 30-second heartbeat data during a time when the subject was lying still, and found that the average estimation error rate was 1.30%. We also collected 301 30-second heartbeat data from a time when the subject was lying on bed and making a variety of different movements. During this scenario, we found that the average estimation error rate was 3.87%. We have also installed our prototype in the homes of 9 different subjects for a period of 25 nights, and found that HB-Phone can detect heartbeats with an average error rate of 8.25%. These results demonstrate that HB-Phone provides a viable solution to at-home heartbeat monitoring during sleep. In particular, this study provides the first, strong evidence that geophones can be used as a low-cost solution for at-home sleep monitoring. Looking forward, there are several challenges that remain before such a technology can be deployed as a long-running solution to sleep monitoring. Notably, our future work will focus on developing detailed signal processing algorithms that focus on detecting and classifying the heartbeat shape and other detailed information about heartbeats.

Chapter 3

Monitoring a Person's Heart Rate and Respiratory Rate on a Shared Bed Using Geophones

3.1 Introduction

Monitoring a person's vital signs during sleep, especially heart rate and respiratory rate, has received a great deal of attention in the last few years. Many systems [9–11, 13–15, 19, 21, 25, 27, 30, 32, 51–53] have been proposed in both industry and academia, promising to potentially serve as a proxy to various health/medical applications, such as monitoring sleep quality [4], detecting obstructive sleep apnea [5], evaluating the risk of heart failure under certain situations [6, 7], and even monitoring patients with Parkinson's diseases [8], etc.

Most of these systems monitor vital signs by measuring one or more aspects of the ballistic force during a heartbeat pulse, ranging from force magnitude [25, 27], pressure [19, 21], to the resulting position change [11, 13–15, 52, 53]. Even though they are able to perform accurate monitoring, most of them are quite cumbersome to install on a bed (e.g., requiring special mattress/sheets, requiring the user to keep the same sleeping position/posture, etc), or are inconvenient/invasive to the users.

Recent work [32] has shown that the geophone sensor [44], which measures the vibration velocity caused by ballistic force, provides a viable alternative in detecting heart rate during sleep without having the above problems of the existing systems. Thanks to being sensitive to even minute vibrations, geophones offer accurate monitoring, are easy to install, can be installed anywhere on the bed frame, and do not assume any sleeping patterns from the user.

Despite these nice features, a great deal of effort is still required to build a full-fledged vital sign monitoring system using the geophone sensor. First, we need to detect respiration using geophones, which is very difficult because the vibrations caused by respiration are weak and the frequency components are below the extremely low frequency (ELF) band (<1 Hz). Thus geophones don't capture those vibrations well. Second, we need to extract the target subject's heart rate from the mixed vibration signal when multiple people share a bed. The difficulty of this problem is mainly due to the fact that the heartbeat vibration signals are mixed together in the time domain and the frequency components from multiple people can be quite close to each other. In this chapter, we seek to develop VitalMon, an in-bed heart rate and respiratory rate monitoring system using geophones, and set out to address these two challenges.

Challenges of Respiration Monitoring: Detecting respiration using geophones is challenging. A geophone is naturally a velocity sensor and a second-order high-pass filter, thus insensitive to low-speed low-frequency vibrations. Unfortunately, the vibration speed of the thoracic cavity during each breath is slow compared to the ballistic movement of a heartbeat, and the respiration signal frequency is low.

In general, the vibration signal caused by each respiration event is so weak that the respiration signal is buried under noise from the environment. In this chapter, we propose an alternative approach by modeling the geophone signal as a signal after amplitude modulation (AM). Here, the heartbeat signal is our carrier signal and the respiration signal is our information signal. Then, we use a square-law amplitude demodulation (SLD) algorithm [37] combined with autocorrelation function (ACF) [35] to estimate the respiratory rate.

Challenges of Heart Rate Monitoring: Even though earlier work [32] has shown that geophones are suitable to monitor heart rate when the person occupies a bed alone, monitoring a person's heart rate when he/she shares the bed with others remains an unsolved challenge. The heartbeat vibration signals from the bed occupants are mixed together in the time domain during propagation, and the frequency of the heartbeat signals and respiration signals from multiple people can be very close in the frequency

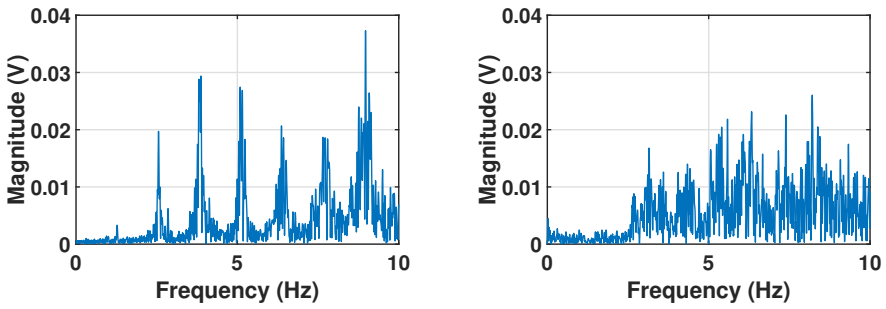

(a) (b)

Figure 3.1: (a) The geophone signal in the frequency domain, with a single subject on the bed, and (b) the geophone signal in the frequency domain, with two subjects on the bed. Peaks caused by heartbeats and harmonics are obvious in (a), making single-subject heart rate monitoring rather simple. When we have two subjects on one bed, however, heartbeat peaks are less obvious and hard to detect directly.

domain. Figures 3.1 (a) and (b) show two Fast Fourier Transform (FFT) examples of the vibration signals when we have (a) one person on a bed, with a heart rate of 76.7 BPM_{hr}[1] (about 1.28 Hz), and (b) two people on one bed, with heart rates of 62.8 (about 1.05 Hz) and 59.2 BPM_{hr} (about 0.99 Hz), respectively. It is hard to tell there are two heartbeats from the mixed signal. In fact, the amplitude at different frequencies is even smaller than when we had only one subject, mainly due to the relative phase delay between two heartbeat signals. Furthermore, heartbeats over time are not perfectly periodic. Therefore, it is hard to separate them in both time and frequency domains. In this study, we address this challenge by taking advantage of the spatial differences between two heartbeats. Suppose we have two geophones G_1 and G_2. As far as the source closer to G_1 is concerned, its vibration signal captured by G_1 has higher amplitude and less phase delay compared to the same source's signal captured by geophone G_2. Based upon this spatial difference, we can extract the target source's signal from the mixture.

Considering the similarity between heartbeat signals and human sound signals, and how they are similarly mixed together in real life, we turn to literature in the acoustic field for wisdom. Popular solutions include Independent Component Analysis (ICA) [54], Principal Component Analysis (PCA) [55], etc. Among the solutions that

[1]In this chapter, we use BPM_{hr} to denote 'beats per minutes' for heart rate and BPM_{rr} to denote 'breaths per minute' for respiratory rate.

have been proposed, Degenerate Unmixing Estimation Technique (DUET) [38, 39] is well-suited to address our needs because (1) unlike ICA, it can tolerate propagation delays; and (2) the sudden change in a heartbeat signal may make consecutive heartbeat pulses look uncorrelated, which may trick some methods into treating those signals as independent, but has less impact on the DUET because it does not rely solely on such correlation.

Applying DUET to our heartbeat separation problem is not straightforward, due to the unique characteristics of heartbeat signals that propagate through a bed. Firstly, the fundamental frequency of a heartbeat is significantly lower than that of the audio signal. Its average range is from 0.33 Hz to 4 Hz, corresponding to 20 BPM_{hr} (e.g., the heart rate for patients with heart block disease) to 240 BPM_{hr} (the maximum heartbeat rate estimated based on the minimum cardiac refractory period of a human being), respectively. As a result, we need high frequency resolution when we extract individual heartbeats from a mixture, which is particularly challenging for us because heartbeats are not perfectly periodic and stable.

Secondly, the bed and mattress have much more complex propagation properties than air. The grouping velocity of any vibration through a bed is around 1 km/s, whose form is a complex mechanical resonance depending on the details of the entire system – e.g., the human body, the bed, the geophone, and the floor, etc.

In addition, the structure of a modern bed often allows vibrations to last for at least a few cycles, and for a heartbeat signal, the preceding heartbeat may affect the subsequent ones. Because of these complex propagation properties, each heartbeat source's spatial signatures become less separable than audio signals, making heartbeat separation a much harder problem.

Our Contributions: In this study, we carefully design the VitalMon system to solve these challenges. For heart rate estimation, we take advantage of the high frequency components of the heartbeat signals, such as the harmonics, so that we have larger frequency differences between different heartbeat signals to enable smaller window sizes. For respiratory rate estimation, we model the signal as AM and use the modulated

signal itself to achieve demodulation, which allows us to apply demodulation without knowing the frequency of the carrier signal (heartbeats in our case). Through detailed experimentation, we show that VitalMon can successfully monitor the target person's respiration and heart rate, even when he/she shares the bed with others. We measured a total of 5084 data sets and collected vital sign signals over 56 hours[2]. The overall absolute estimation error for heart rate and respiratory rate is at 1.90 BPM_{hr} and 2.62 BPM_{rr}, respectively, and the median is 0.72 BPM_{hr} and 1.95 BPM_{rr}.

In summary, our work has made the following contributions:

1. We have developed a respiration detection technique based on square-law amplitude demodulation that can estimate the respiratory rate from the vibration signals. To our best knowledge, this is the first paper which shows that the overall amplitude of a heartbeat signal is modulated to carry the respiration signal and we show our technique can successfully demodulate the respiratory rate information.

2. We have developed a heartbeat separation technique that can accurately track the heartbeat of a specific person when there are multiple people on one bed. In developing our technique, we have taken into consideration the unique properties of heartbeat signals as well as the complex propagation properties of the bed and mattress.

3. We have developed a testbed with multiple vibration sensors (geophones in our case). In developing the testbed, we have taken into consideration the features of geophone sensors and their placement.

3.2 Background and Overview

In this section, we first provide the background on ballistocardiograph (BCG) based heart rate and respiratory rate monitoring. Then we present an overview of our geophone-based BCG measurement system.

[2]Our studies were approved by the Institutional Review Board (IRB) of our institution.

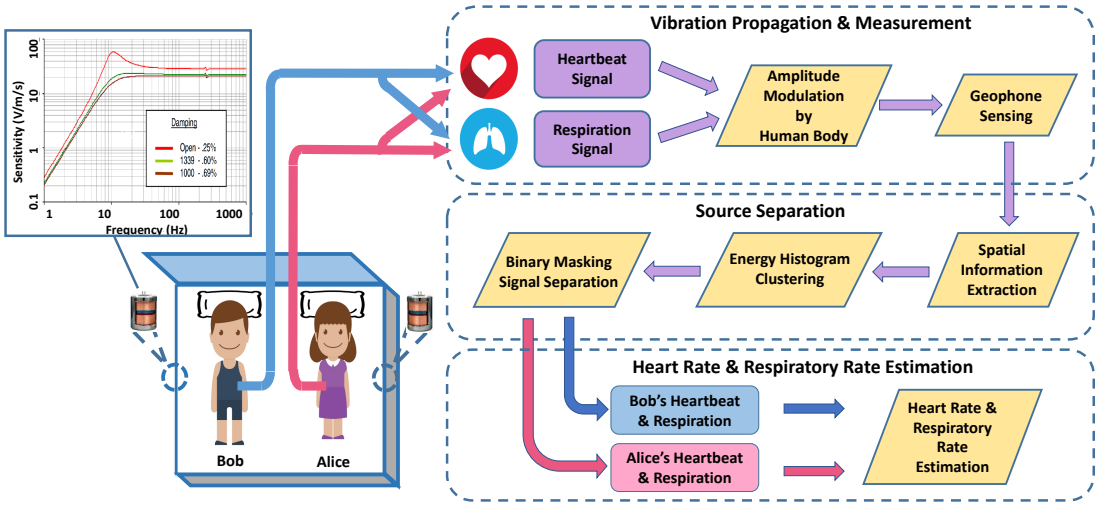

Figure 3.2: The overview of VitalMon. When two persons (Alice and Bob) share a bed, we use two geophones to capture the mixed vibration signals, and then perform a sequence of signal processing steps to monitor the heart rate and breathing rate of our target user (say, Alice).

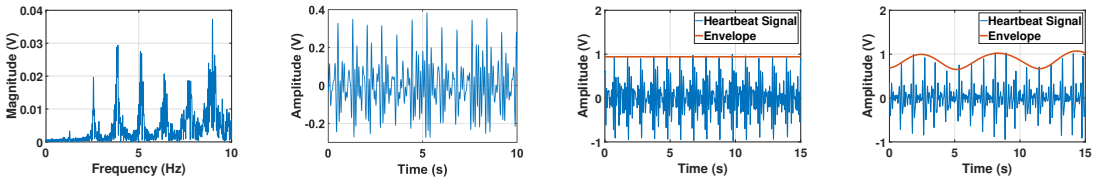

(a) (b) (c) (d)

Figure 3.3: (a) The geophone signal in the frequency domain, with a single person on the bed, (b) the same geophone signal as in (a), but in the time domain, (c) the geophone signal with a single person holding his breath, and (d) the geophone signal with a single person breathing normally. In (b) and (d), the subject's breathing rate is embedded in the heartbeat signal amplitude fluctuation, or the envelope.

3.2.1 BCG Based Heart Rate and Respiratory Rate Monitoring

Many BCG based systems have been developed to monitor a person's physiological signs by sensing the ballistic force on the heart. The earliest work we can find was done by J. W. Gordon in 1877 [56]. He designed an analog BCG system which consists of (1) a special designed mattress that is small but stiff, (2) four ropes to hang the mattress to the ceiling in a room, (3) a bunch of levers to amplify the analog vibration signal, and (4) a weighing machine to record the signal on paper. Despite of the cumbersome nature of such a system, it successfully captured the weak vibrations from each heartbeat. Later, many BCG-based systems have been proposed and we categorize them below based on

the sensor types:

1. Force sensors [25, 27], commonly installed under bed posts, measure the force change due to the ballistic force. The idea is straightforward, but it requires a fairly high sensitivity since it tries to detect a weak force change under the influence of the gravity of the bed and people.

2. Air/water pressure sensors [19, 21, 50], usually sandwiched between mattress and bed frame, measure the pressure exerted by the ballistic force. Due to the limitation of the sensitivity, the sensor should be installed under the thorax area of the human body, which requires prior knowledge of the person's location on the bed.

3. Position sensors measure the position change due to the ballistic force. Position change can be detected by a variety of means. For example, an optical sensor can detect position change when it is embedded in a mattress and placed in the thorax area [52, 53]; an ultrasound-based sensor can detect position change [13], but requires mounting a plywood board and an aluminum guide rail on the bed frame; a wireless-based system can also detect position change [14], but requires additional wireless infrastructure and could be easily interfered by other wireless signals in the environment.

4. Accelerometer sensors can detect the vibration acceleration caused by the ballistic force, such as a chest belt [57] or the commercial system in [58]. However, such a system is invasive and uncomfortable.

5. Velocity sensors, such as geophones [32], measure the speed of vibrations caused by the ballistic force. They can be attached anywhere on a bed, and are unobtrusive and convenient.

3.2.2 VitalMon Overview

Among the above BCG monitoring systems, the velocity sensing approach offers accurate, unobtrusive, low-cost, and robust monitoring, as shown in a recent study [32]. In

this study, we use a commercial off-the-shelf geophone, which is a moving coil based velocity sensor.

Geophones, traditionally used to measure seismic waves in geology, have been widely used in measuring vibrations from different sources. Recently, geophones have been used in several applications: building occupancy estimation by monitoring ambient vibration [59], indoor person localization via floor vibration [60], interaction tracking via surface vibration [61], heart rate estimation by monitoring bed vibration during sleep [32], etc. A geophone consists of a spring-mounted magnetic mass moving within a coil. It converts the physical vibration from the environment into an electrical voltage. The geophone we use, SM-24 Geophone Elements [44], is naturally a second-order high-pass filter and its natural frequency is 10 Hz.

The overview of VitalMon is illustrated in Figure 3.2. In VitalMon, our objective is to continuously monitor the heart rate and breathing rate of our user (say, Alice), whether Alice occupies a bed alone or shares a bed with Bob. For monitoring purposes, we use the same number of geophones as the number of persons on a bed. When both Alice and Bob are present, we use two geophones to measure the vibrations caused by their heartbeats and breathing. Since heartbeats lead to much more pronounced vibrations than breathing, we first extract Alice's heartbeat signals (the amplitude and frequency) from the geophone signals. Then we further extract the respiration signal from her heartbeat signals. Both steps introduce serious challenges, and we have devised efficient techniques to address them. In the following two sections, we present our proposed signal processing techniques – we first focus on how to extract respiration from heartbeat signals, and then focus on how to extract individual heartbeat signals from the mixture signal.

3.3 Monitoring Respiratory Rate Using Geophone

In this section, we discuss how we monitor the respiratory rate using geophones, assuming there is only one person on a bed. We first formulate the respiration signal

extraction problem as an amplitude modulation problem. We then explain the difference between our problem and the traditional amplitude problem in communications. Finally, we present our amplitude demodulation algorithm.

3.3.1 Formulating Respiration Signals as Amplitude Modulation

The most straightforward approach to extracting the respiration signal would involve directly performing FFT on the geophone signal and then looking for the frequency component corresponding to respiration. However, as shown in Figure 3.3 (a), we don't observe any obvious respiration frequency components (that should be below 1 Hz) from the geophone signal. This is because a geophone is a natural second-order high-pass filter, insensitive to motions whose frequencies are below a certain threshold (referred to as detection threshold, 8.4 Hz in our case). The frequency components of respiration are usually lower than this detection threshold. Also, the velocity of breathing is quite slow, which makes it even harder to detect by geophones. As a result, this direct approach fails to detect respiration signals.

On the other hand, a closer look at the geophone signal reveals an interesting phenomenon – the amplitude of the geophone signal fluctuates in a periodic fashion, and the fluctuation frequency is very close to the subject's breathing frequency. For example, in Figure 3.3(b), the subject's respiratory rate is 15.04 BPM_{rr}, which is very close to the amplitude fluctuation frequency of 0.251 Hz. To further investigate this observation, we conducted an experiment and compared the geophone signals when the subject held his breath with the signals when the subject breathed normally. Figure 3.3(c) shows the geophone signal when a subject lies on a bed while holding his breath for at least 15 seconds, while Figure 3.3(d) shows the geophone signal when the subject breathes at a rate of 10 BPM_{rr}. In both figures, we plot the estimated envelope of the signals. It is clear that there is a direct relationship between breathing and the amplitude fluctuation.

After deliberation, we conclude that respiration causes the amplitude fluctuation of the geophone signal. It can be explained as follows. Breathing changes the amount of air in the chest, which in turn changes the effective 'stiffness' of the chest and the

amount of energy loss of the heartbeat signal after propagation through the chest. As such, the relationship between the respiration signal and the heartbeat signal can be modeled as amplitude modulation (AM) in communications [62]. Here, the heartbeat signal, including its fundamental frequency and the associated harmonics, is the carrier signal, the respiration signal is the information signal, and the geophone signal is the signal after amplitude modulation.

Following amplitude modulation, we can model the three signals as follows:

$$\begin{aligned} s(t) &= s_r(t) \sum_{j=1}^{N} s_{h_j}(t), \\ s_r(t) &= a_r \times cos(2\pi f_r t + \theta_i), \\ s_{h_j}(t) &= a_{h_j} \times cos(2\pi f_{h_j} t + \theta_{h_j}), j = 1, 2, ..., N, \end{aligned} \tag{3.1}$$

where $s(t)$ denotes the source signal for single person case, s_r denotes the respiration signal and s_{h_j} denotes the j-th harmonics of the heartbeat signal. Note, s_{h_1} means the fundamental frequency of the heartbeat signal.

Next, we devise a suitable amplitude demodulation algorithm to extract the respiratory rate information from the geophone signal. However, our problem significantly differs from the conventional RF amplitude modulation problem in that the RF signal's carrier frequencies are known beforehand, while the frequency of our carrier signal – the heartbeat signal – remains unknown. To make matters worse, unlike the RF signal which has a single carrier frequency, the heartbeat signal includes a fundamental frequency and multiple higher frequency components.

Due to these differences, typical detectors for demodulating AM signals that were proposed for RF signals are ill suited for our problem. For example, an envelope detector, such as the Moving Root-Mean-Square (RMS) envelopes approach [63] or the analytic signal approach [64], is sensitive to the choice of the window size; window size depends on the frequency of the information signal, which is unknown in our case. The RMS envelopes approach also doesn't work well with an impulse-like signal such as the ballistic force within each heartbeat. Meanwhile, a product detector [65] usually requires knowledge of the carrier frequency, which is again unknown in our case. Finally, neither of these detectors work well when carrier signals are quasi-periodic, like

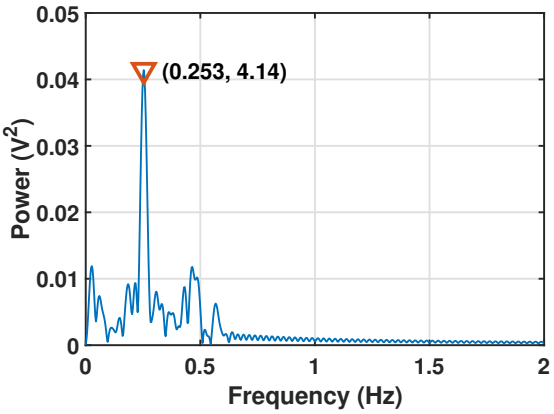

Figure 3.4: FFT of the power signal after our amplitude demodulation. We observe a peak at 0.253 Hz (marked with a red inverted triangle), which corresponds to a respiratory rate of 15.18 BPM_{rr} and agrees with the ground truth measured by a Zephyr strip [66].

heartbeats in our system.

Therefore, we choose the square-law demodulation approach in this study, using the geophone signal as the carrier signal which can demodulate itself to extract the information signal (the respiration signal in our case). AM during propagation shifts the respiration frequency components to a higher frequency range (around the heartbeat frequency range). By squaring the signal, we reverse the frequency shift and can separate the respiration signal by applying a low-pass filter.

3.3.2 Respiratory Rate Estimation

Next, we present our respiratory rate estimation algorithm based on the square-law demodulation.

Before presenting our algorithm, we first discuss how we estimate the environmental noise and eliminate its impact. We do so by recording the geophone signal when the bed is empty and computing the FFT. The FFT results show that the majority of the noise is above 11 Hz. We note that our lab environment has a considerably greater noise level than an average bedroom environment as we have a few hundred computers sharing the same lab space, most of which are equipped with powerful fans. Next, we collect the geophone signal when a single subject is lying on a bed. The corresponding FFT results show the frequency components of our target signals (heartbeat signals and

respiration signals) are below 15 Hz. Therefore, we believe a high-order low-pass filter with a cutoff frequency at 10 Hz can effectively minimize the impact of environmental noise.

Next, we perform amplitude demodulation by multiplying the geophone signal with itself. That is, we treat the geophone signal as its own carrier signal. For our objective of estimating heart rate and respiratory rate, we only need to recover their frequency components, but not phase information. As such, we can simply set both signals' phases to be 0. Then, based on Equation 3.1, we have

$$\begin{aligned} s^2(t) &= (s_r * \sum_{j=1}^{N} s_{h_j})^2 \\ &= a'_i * cos(4\pi f_r t) + \sum_{j=1}^{2N} (a'_{h_j} * cos(2\pi f_{h_j} t)) \\ &\quad + \sum_{j=1}^{2N} (a'_{h-_j} * cos(2\pi (f_{h_j} - 2f_r)t)) \\ &\quad + \sum_{j=1}^{2N} (a'_{h+_j} * cos(2\pi (f_{h_j} + 2f_r)t)) \end{aligned} \tag{3.2}$$

The multiplication result consists of several low frequency components that are less than $1Hz$ and many frequency components that are greater than or equal to $1Hz$. As we observe from Equation 3.2, the lowest frequency component, $a_1 * cos(4\pi f_r t)$, has twice the frequency of the respiration signal. If we can identify this particular component, we can derive the respiration frequency.

Figure 3.4 shows an example of the demodulation result. After applying a low-pass filter with a cutoff frequency of 0.6 Hz, we successfully remove the high frequency energy. Then, we compute the square root of the filtered signal in time domain and obtain the low frequency signal in frequency domain at 0.253 Hz (about 15.2 BPM_{rr}) which is the respiratory rate.

3.4 Monitoring Target Heart Rate When Multiple Subjects are Present

In this section, we discuss how we monitor the heart rate for the target person – say, Alice – when she shares a bed with Bob. In order to achieve this objective, we need

to be able to extract Alice's heartbeat signal from the geophone signal in which both heartbeat signals are lumped together. In this study, we aim to separate the two heartbeat signals (their frequency components) so that we can extract either if needed. That way we can monitor the physiological signs for both people on the bed.

3.4.1 Modeling Mixture Signals

We first formulate the heartbeat separation problem by formally defining the mixed signal [67]. Suppose we have 2 signal sources s_1 and s_2, with signals $s_1(t)$ and $s_2(t)$, respectively. Suppose we have 2 geophone receivers x_1 and x_2, which receive mixed signals $x_1(t)$ and $x_2(t)$ such that

$$x_k(t) = \sum_{j=1}^{2} a_{k,j} s_j(t - \delta_{k,j}), k = 1, 2, \tag{3.3}$$

where $a_{k,j}$ and $\delta_{k,j}$ are the attenuation coefficients and time delay parameters associated with the path from s_j to x_k. Since we don't have prior knowledge of the true signal attenuation and delay in our system, we rely on relative signal attenuation and delay. Here, we consider $x_1(t)$ as reference signal (with $a_{1,1} = a_{1,2} = 1$ and $\delta_{1,1} = \delta_{1,2} = 0$), and compare $x_2(t)$ to it to obtain the corresponding relative attenuation and delay coefficients.

After calculating the short-time Fourier transform (STFT) of $x_1(t)$ and $x_2(t)$, we obtain their time-frequency representation:

$$\begin{bmatrix} \hat{x}_1(\tau, \omega) \\ \hat{x}_2(\tau, \omega) \end{bmatrix} = P_{2\times 2} \begin{bmatrix} \hat{s}_1(\tau, \omega) \\ \hat{s}_2(\tau, \omega) \end{bmatrix}, \tag{3.4}$$

where the propagation matrix $P_{2\times 2}$ is defined as

$$P_{2\times 2} = \begin{bmatrix} 1 & 1 \\ a_{2,1} e^{-i\omega\delta_{2,1}} & a_{2,2} e^{-i\omega\delta_{2,2}} \end{bmatrix}. \tag{3.5}$$

In Figure 3.5, We illustrate our experiment setting which includes two subjects (s_1 and s_2) and two geophone sensors (x_1 and x_2). The direct propagation paths from s_1 to both geophone sensors are marked in green, and the paths from s_2 to both geophone sensors are marked in brown. Using the same color, we also mark the corresponding attenuation coefficients and time delay parameters.

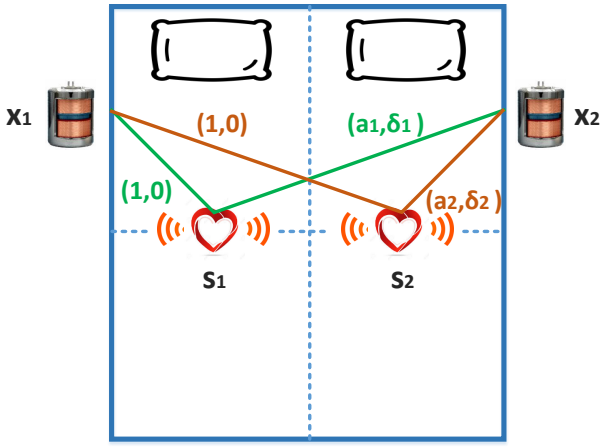

Figure 3.5: We illustrate our experiment setting, which includes two subjects (s_1 and s_2) and two geophone sensors (x_1 and x_2). We mark the corresponding attenuation coefficients and time delay parameters on the figure, using green for one source and brown for the other source.

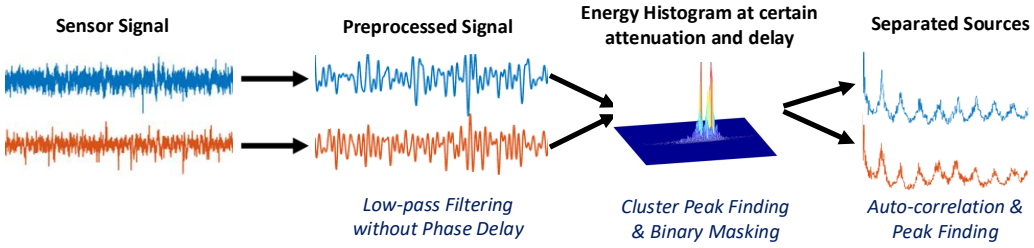

Figure 3.6: Overview of our heartbeat separation algorithm.

3.4.2 Background on Blind Source Separation and the DUET Algorithm

Our heartbeat separation problem is similar to the cocktail party problem [68] where an arbitrary number of people are talking simultaneously at a cocktail party and a listener is trying to identify and follow one particular discussion. DUET [38, 39] has proven to be a good solution to the cocktail party problem. It computes the symmetric attenuation and relative delay of the signals, calculates the energy histogram within different ranges of attenuation-delay values, and finally identifies each energy peak as a signal source.

This is suitable for the cocktail party problem because it cleverly leverages the

unique properties of audio signals. Audio signals have spatial signatures as the attenuation and delay parameters between an audio source and the receiver are unique. In addition, mixture audio signals usually have sparse frequency components because it is rare to have two people talking at the same frequency at the same time.

In this study, we choose to adopt DUET due to the similarity between audio signals and heartbeat signals. Firstly, both heartbeat signals and audio signals have a fundamental frequency component and high frequency components (harmonics). Secondly, we have no control of, nor a priori knowledge of, the frequencies of heartbeat signals or audio signals. Thirdly, the paths between different sources and receivers have diversity, making it possible to establish spatial features for each source.

Heartbeat signals, however, have their own characteristics. For examples, heartbeat signals have much narrower frequency ranges than audio signals; heartbeats from multiple people have less frequency difference than audio signals; the frequency of heartbeat signals fluctuates from beat to beat while audio signals are consistent for at least a few cycles. These characteristics may not satisfy the implicit assumptions made by DUET and impose challenges in our system design. We will explain how we tackle these challenges in the rest of this section.

3.4.3 Heartbeat Signal Separation and Heart Rate Estimation

Next, we present our algorithm that separates individual heartbeat signals and estimates each person's heart rate.

Here we assume we have two synchronized geophone receivers that continuously collect mixed signals from two subjects. We partition the signals into processing windows of equal length (40 seconds) and apply the following signal processing steps on both signals within the same window:

1. Filtering. We apply a suitable low-pass filter to filter out environmental noise (discussed in Section 3.4.3), and then remove the direct current (DC) component from the filtered signal;

2. STFT. We compute the STFT results of the two filtered signals (discussed in

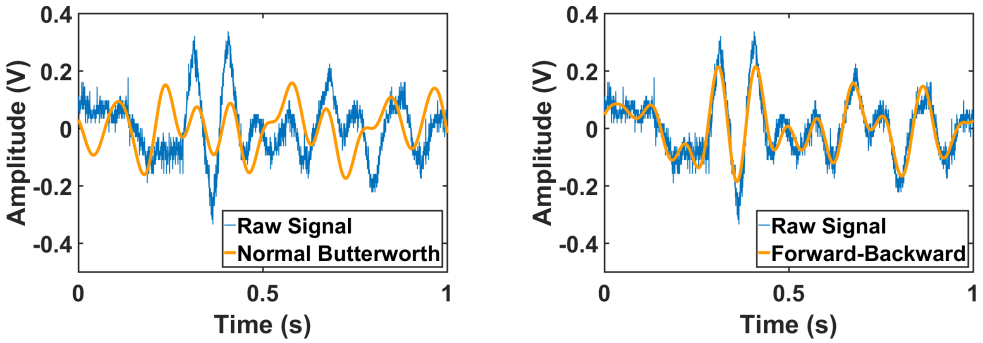

(a) (b)

Figure 3.7: (a) A normal Butterworth filter introduces phase delays, while (b) a forward-backward filter can leave the filtered signal in perfect alignment with the original signal.

Section 3.4.3);

3. Spatial Signatures. We calculate symmetric attenuation and relative delay between the two STFT results (discussed in Section 3.4.3);

4. Energy Clustering. We calculate the energy of each frequency bin (we partition the entire frequency range into discrete bins) and sum the energy values for different ranges of symmetric attenuation and relative delay. We then rebuild the signals in the new coordinate system with the relative delay on x-axis, symmetric attenuation on y-axis and the energy histogram on z-axis (discussed in Section 3.4.3);

5. Binary Masking. We identify the coordinates of the peaks in this new three-dimensional space and apply a binary mask to separate peaks that represent different heartbeats (discussed in Section 3.4.3);

6. Heart Rate Estimation. We convert the signal from the frequency domain back to the time domain, and then estimate the heart rate using the method discussed in [31,32]. We also estimate the respiratory rate using the algorithm in Section 3.3.

Figure 3.6 pictorially shows these steps involved in our algorithm.

FFT and Low-pass Filtering for Noise Reduction

Geophone signals are usually highly noisy because the sensor is quite sensitive, and therefore efficient noise reduction becomes an essential step. We note that, as mentioned in Section 3.3, most of the noise is above 11 Hz while the target signals are mainly below 15 Hz. Therefore, a high-order Butterworth low-pass filter with cut-off frequency at 10 Hz can effectively reduce the noise.

Since DUET separates signals from different sources using their spatial signatures, we want to make sure the filtering step does not cause any signal distortions that may change the signal signature. For this purpose, we perform a high-order low-pass Butterworth filter, followed with a forward-backward digital filtering technique [69]. By applying this forward-backward digital filter technique in both directions, the phase distortions caused by the two filters cancel out each other. Eventually, we introduce no phase distortion at all.

Shown in Figure 3.7(b), the signal after the forward-backward digital filter aligns perfectly with the original signal, while a normal high-order low-pass Butterworth filter introduces delay between the original signal and the resulting signal (Figure 3.7(a)). In addition, the forward-backward filter also squares the amplitude response. Finally, after applying the low-pass filter, we remove the DC component since it contains no heartbeat related information.

Time-Frequency Representation for Locating Spatial Information

In this step, we obtain the time-frequency representation of the filtered signals. We choose STFT for this purpose.

Lack of Short-Term Frequency Stability: Audio signals usually have stable frequency components within a short time window. Rabiner [70] pointed out that audio signal frequencies within a 45 ms time window can be considered stable. However, this is not true for heartbeats. As shown in Figure 3.8, the instantaneous heart rate fluctuates considerably around the average heart rate. Hence, compared to the audio signal, the heartbeat signal's frequency varies a lot more from cycle to cycle. As a result, when

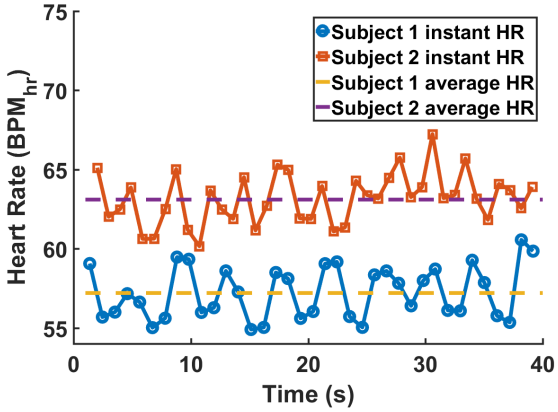

Figure 3.8: The instantaneous heart rates of two participates at a calm state, fluctuate around their average heart rates, 57.2 and 63.1 BPM_{hr}.

we compute STFT, we have to further partition the signals within a processing window of 40 seconds into smaller segments.

Insufficient Frequency Difference: For any pair of signals that have the same length, $s_1(t)$ and $s_2(t)$, they are W-disjoint orthogonal when they satisfy:

$$\hat{s}_1(\tau,\omega)\hat{s}_2(\tau,\omega) = 0, \forall\tau,\omega, \tag{3.6}$$

where $\hat{s}_1(\tau,\omega)$ and $\hat{s}_2(\tau,\omega)$ are the time-frequency representation of signal $s_1(t)$ and $s_2(t)$, respectively. It means that the energy from one source is much larger than the other source.

This assumption doesn't hold true for signals at the same frequency. The sum of any two signals at the same frequency, regardless of their amplitude and phase values, constitutes a single signal at that frequency. As a result, if we don't have additional information about the two signals' amplitude and phase information, we can't separate them since there are an infinite number of ways of decomposing the mixed signal. As such, heartbeat separation does not work if the individual heartbeats are at the same frequency.

Though it is rare for two people to have exactly the same heartbeats, it is quite often that their heartbeat frequencies are close to each other due to the small heartbeat frequency range. For example, let us consider two heartbeat signals whose frequencies are 1 Hz and 1.1 Hz respectively. In order to discriminate the two signals, we actually need at least a 10-second signal to see the difference: one has 10 beats within 10s, while

the other one has 11 beats. However, it is very hard, if not impossible, for a heartbeat signal to hold steady at a the same frequency for a duration of 10 seconds.

Our Solution: In VitalMon, we deal with these challenges by the following tricks. First, we focus on the heartbeat signal's high frequency components for more sparsity. For example, for heartbeat signals at 1 Hz and 1.1 Hz, their eighth harmonics – 8 Hz and 8.8 Hz respectively – have greater frequency difference. Second, we partition each processing window (40 seconds) into much smaller slots to ensure the two signals are W-disjoint orthogonal during each slot. Figure 3.9 plots the heart rate estimation error with different slot durations. Generally, a slot duration less than 1.7 seconds leads to much lower estimation error. In particular, we find the slot duration around 0.7 second yields the lowest estimation error, 1.90 BPM_{hr}. In our evaluation, we then adopt a slot duration of 0.7 second for our heartbeat separation and extraction.

Calculating Symmetric Attenuation and Relative Delay

From the STFT results, we are able to compute the relative attenuation and relative delay as in [38]:

$$\hat{a}(\tau,\omega) = \left|\frac{\hat{x}_2(\tau,\omega)}{\hat{x}_1(\tau,\omega)}\right|, \tag{3.7}$$

$$\hat{\theta}(\tau,\omega) = -\frac{1}{\omega}\angle\frac{\hat{x}_2(\tau,\omega)}{\hat{x}_1(\tau,\omega)}, \tag{3.8}$$

where $\hat{x}_1(\tau,\omega)$, $\hat{x}_2(\tau,\omega)$ are the time-frequency representation from the STFT results, and ω is the frequency vector. Considering that symmetric attenuation yields higher resolutions when signals from the same source get different attenuation at different receivers, we further compute the estimated symmetric attenuation:

$$\tilde{\alpha}(\tau,\omega) = \hat{a}(\tau,\omega) - \frac{1}{\hat{a}(\tau,\omega)}. \tag{3.9}$$

Combining symmetric attenuation and relative delay, we are able to separate signals from the two sources. The next step is to compute the energy histogram based on the attenuation-delay values. For any given frequency that falls into the range that has the same symmetric attenuation and relative delay, we compute the energy histogram by

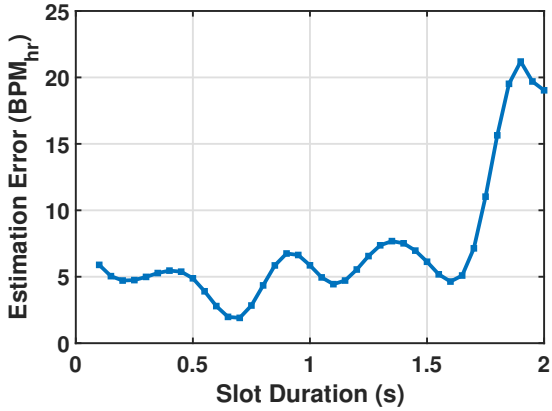

Figure 3.9: The mean absolute estimation error (in BPM_{hr}) with different slot durations. The slot duration of 0.7 second gives the best estimation, with an error of 1.90 BPM_{hr}.

summing up the estimated energy in those frequency ranges. Following this process, we eventually cluster the frequencies that are from the same source and have similar symmetric attenuation and relative delay values.

Finding Cluster Peaks and Applying Binary Masking in 3D Space

Next, we explain how we find cluster peaks, which each correspond to a separate signal. In our problem, symmetric attenuation and delay values from different sources overlap with each other, leading to poorly formed clusters that are hard to identify. As a result, we cannot rely on normal peak finding algorithms or machine learning algorithms such as K-Means Clustering [71], or CLIQUE [72] to identify the peaks.

Instead, we take advantage of the spatial diversity in our system. If we place geophone x_2 close to Alice, and x_1 close to Bob, and use $x_1(t)$ as the reference, then symmetric attenuation of Alice's heartbeat signal is positive while symmetric attenuation of Bob's heartbeat signal is negative. Then, we can use a simple binary mask to assign each attenuation-delay pair to either Alice or Bob.

Estimating Target Heart Rate

Once signals from different sources are properly separated, we perform inverse STFT to return them to the time domain. We then apply the heartbeat detection algorithm discussed in [32] to extract the heartbeats. Namely, we compute the signal power,

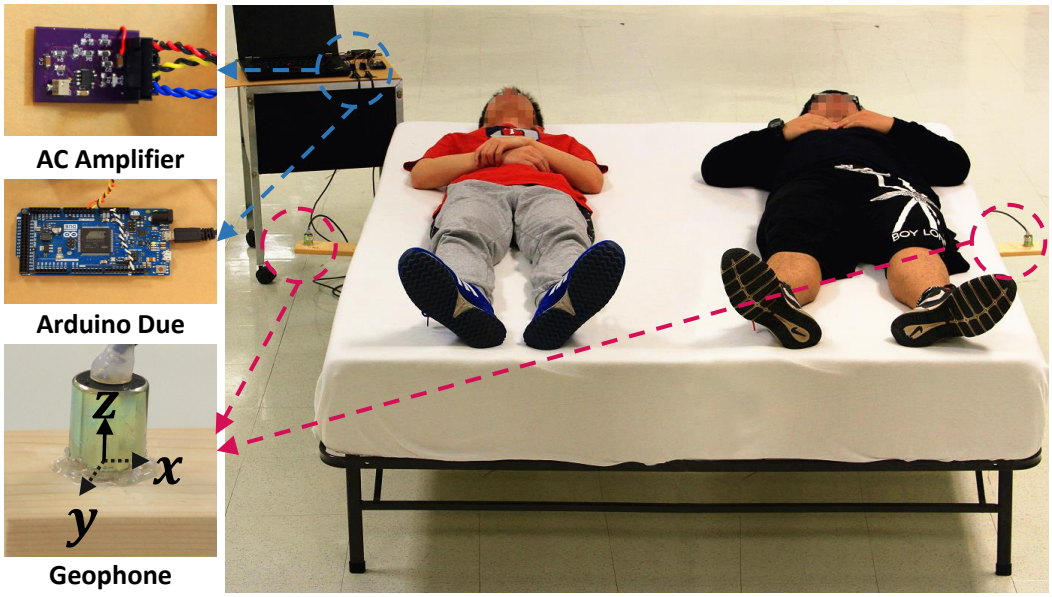

Figure 3.10: Our prototype bed. We install two geophone boards that are sandwiched between the mattress and the frame, one on each side of the bed.

calculate the sample auto-correlation function (ACF), find peaks in the sample ACF results [36], and finally convert the peak locations to corresponding heartbeat pulses. Once we obtain the heart rates, we associate each heart rate to the correct person on the bed, based on the location information. Meanwhile, we also apply our respiratory rate estimation algorithm in Section 3.3.2 on each heartbeat signal to estimate each subject's breathing rate.

3.5 VitalMon Testbed

Amplifier and ADC: In our testbed, we use two SM-24 geophones [44] to track the heart rate and respiratory rate. The raw analog signal from each geophone is first amplified through its own amplifier circuit whose amplification is 200. Then, the amplified signals are fed into a 12-bit analog-to-digital converter (ADC) on an Arduino Due [73] whose range is 0 to 3.3 V and sampling frequency is 2.5 kHz. Meanwhile, the two geophone signals are synced through the internal clock of the Arduino Due. Figure 3.10 shows the experiment setting with two participants on our prototype bed. The bed has a memory foam mattress and a steel frame.

Vertical vs Horizontal Geophones: Many geophones respond to vibrations in a

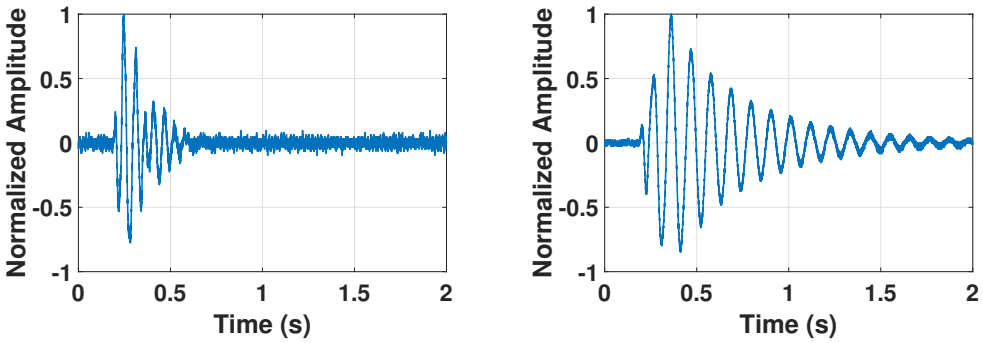

(a) (b)

Figure 3.11: When we gently tap the prototype bed, response from a vertical geophone (a) is much more crisp (shorter oscillation) than the response from a horizontal geophone (b).

single direction, although more complex geophones that can sense vibrations in multiple directions are available. In our experiments, we have tried vertical geophones (responding to vibrations in the z direction in Figure 3.10) and horizontal geophones (responding to vibrations in the $x-y$ plane in Figure 3.10). Through experimentation, we choose vertical geophones in our testbed. We explain the reason below.

Our first intuition was to choose horizontal geophones. Each heartbeat is mainly caused by the sudden ejection of blood during the ventricle systole. The direction of such momentary ejection first goes from the ventricle to the aorta and then gets split to different blood vessels of a human body. Due to such directionality, the strongest vibration is along the head-foot direction (in the $x-y$ plane). Intuitively, we would like to capture the strongest vibration by using multiple horizontal geophones.

However, when we consider the human body, the bed, the floor and our system as a whole piece, we find horizontal geophones a poor choice because beds are designed to allow the joints to be underdamped on the $x-y$ plane, yielding more horizontal oscillations. Such oscillations usually last for more than 1 second, which is one heartbeat cycle, such that a heartbeat may last long enough to affect the following heartbeat(s). On the other hand, we find vertical geophones experience much smaller and shorter oscillations because oscillations in the z direction are damped against the floor.As a result, horizontal geophones and multi-dimension geophones that can measure horizontal vibrations are not suitable for our system.

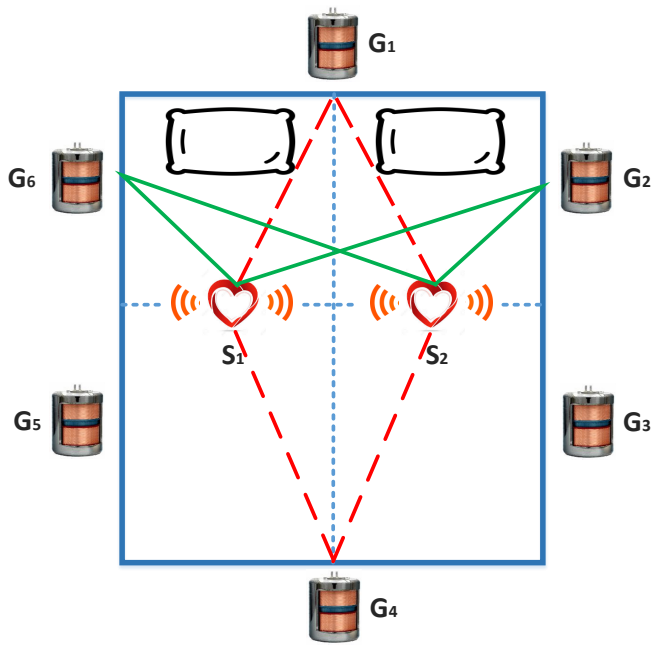

Figure 3.12: This figure shows the top view of a bed, that has two sources s_1 and s_2. Here we show two example installation plans. The plan marked by red dashed lines represents a poor installation where two sources have same symmetric attenuation and relative delay. The plan marked by green solid lines is a good installation.

Figures 3.11 (a) and (b) show the responses from a vertical geophone and a horizontal geophone when we lightly tap the bed just once. For each signal, we normalized the amplitude to observe how long the oscillation lasts. The tapping motion occurred at time 0.2 second. The vertical oscillation lasted for roughly 0.3 second, while the horizontal oscillation lasted for more than 1.8 seconds.

Geophone Placement: Next, we carefully consider how the two geophones should be placed on the bed. Our heartbeat separation algorithm involves inferring the symmetric attenuation and relative delay information from the amplitude and phase of frequencies in the signal STFT. To avoid any ambiguity of phase delay caused by phase wrap [74], we should not separate the two geophone sensors by more than half of the wavelength of the signal. Fortunately, in our case, this requirement is easy to satisfy because the wavelength of the heartbeat signal is usually much larger than the length of a regular bed. For example, for a heartbeat signal whose rate is 60 bpm, its wavelength roughly is 1 km.

Our technique separates signals from different sources by their unique spatial signatures. As a result, when we install geophone sensors, we need to make sure there is difference between the sources' spatial signatures. Suppose the two hearts' positions are s_1 and s_2, and the two geophones' positions are x_1 and x_2. Then we need to the following inequality is satisfied

$$\frac{||x_1 s_1||}{||x_1 s_2||} \neq \frac{||x_2 s_1||}{||x_2 s_2||},$$

where $||x_1 s_1||$ is the distance between x_1 and s_1. In Figure 3.12, we illustrate six possible geophone positions named G_1, ..., and G_6 in the clockwise sequence and the two heartbeat locations. In this example, we cannot place the following geophone pairs, (G_1, G_4), (G_2, G_3), and (G_5, G_6). Any of the rest of the combinations could work well for our purpose. In our testbed, we mount the two geophones according to $(G6, G2)$ in the diagram.

3.6 Evaluation

In this section, we use our testbed to evaluate VitalMon in the following aspects: (1) estimating the respiratory rate for a single subject, (2) estimating the target subject's heart rate when two subjects are present, and (3) estimating the target subject's respiratory rate when two subjects are present. Also, we have a discussion on the real world deployment.

3.6.1 Monitoring a Single Subject's Respiratory Rate

We conducted 525 experiments and recorded more than 350 minutes data from a total of 23 subjects. We report the respiratory rate estimation error as the absolute difference between the estimated BPM_{rr} and the ground truth $\overline{BPM}_{rr}$.

Participants: We had a total of 23 healthy volunteer participants for this experiment, including 14 males and 9 females. The mean age of the participants was 25.14 years with a standard deviation of 3.42 years. The youngest participant was 21 years old while the oldest was 34 years old.

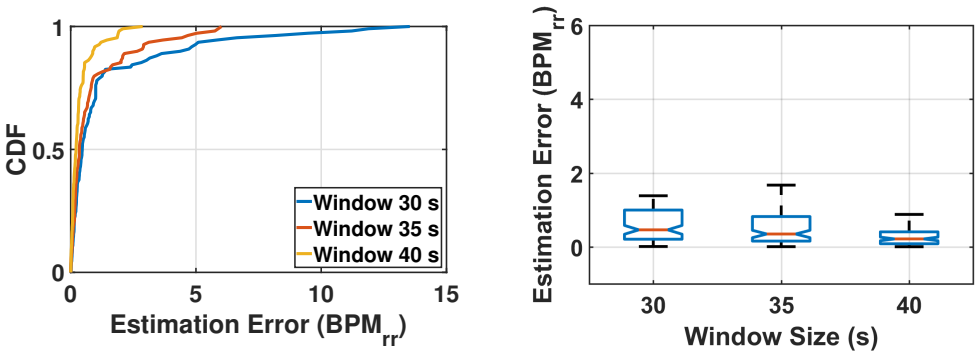

(a) (b)

Figure 3.13: CDF (a) and box plot (b) of the respiratory rate estimation error when we have a single subject, with the processing window of 30, 35, and 40 seconds. Window length of 40 seconds has the best results – mean estimation error of 0.38 BPM_{rr}, and median error of 0.22 BPM_{rr}, over 525 samples – which is then adopted in the rest of the evaluation.

During each experiment, subjects were asked to lie on the prototype bed and breathe at a certain rate for the duration of 40 seconds. Specifically, we played a metronome at 1 tick per second and asked the subjects to breathe in and out every 2, 3, 4, 5, or 6 ticks (the respiratory rate during each experiment was thus fixed). We manually monitored the participant's breathing rate by observing how his/her chest moved during the experiment. Each subject went through at least 20 experiments and in total we conducted 525 experiments.

Figures 3.13(a) and (b) show the cumulative distribution function (CDF) and a box plot of the estimation error with different processing window lengths. Both plots show that larger window sizes yield lower estimation errors: we have mean error of 0.38 BPM_{rr}, and median error of 0.22 BPM_{rr}, when the window length is 40 seconds. In the rest of the evaluation, we use the processing window of 40 seconds. We also note that a median estimation error of 0.22 BPM_{rr} and a mean estimation error of 0.38 BPM_{rr} are better than many other systems when estimating the breathing rate for a single subject. For example, the estimation error reported in [11,31] is 0.47 and above 2 BPM_{rr}, respectively.

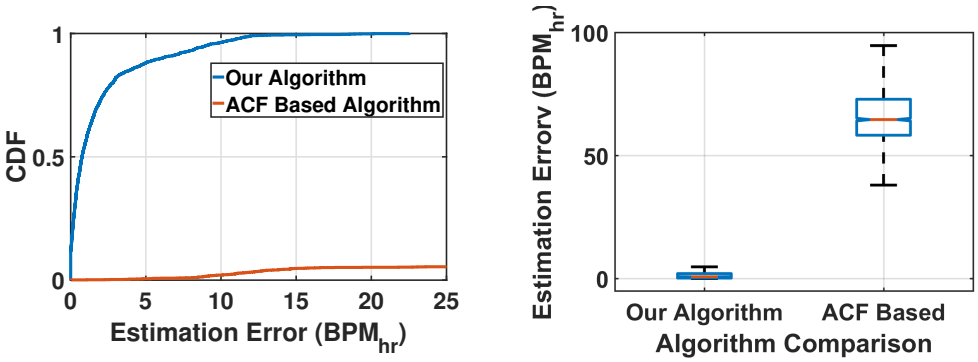

(a) (b)

Figure 3.14: We compare the heart rate estimation error of our algorithm with the ACF-based heartbeat separation algorithm: (a) CDF, and (b) box plot of the estimation error. Our algorithm yields much lower estimation error.

3.6.2 Monitoring Target Heart Rate when Multiple Subjects are Available

In this part of the evaluation, we conduct more than 3000 experiments and record more than 33 hours of geophone data from a total of 35 subjects. We compare the estimated BPM_{hr} against the ground truth $\overline{BPM}_{hr}$ measured by a medical grade pulse oximeter [75] and report the estimation error.

Participants: We had a total of 35 healthy volunteer participants for this experiment, including 19 males and 16 females. The mean age of the participants was 25.26 years with a standard deviation of 3.25 years. The youngest participant was 21 years old while the oldest was 35 years old.

Mean Heart Rate Estimation Error

We first conducted a series of experiments to evaluate how our algorithm performs over a large range of heart rates while two subjects share the prototype bed (without gross body motions). To ensure we evaluate our system over a large range of heart rates, we asked one of the two subjects to exercise (e.g. running outdoor, climbing stairs, etc.) for a few minutes before each experiment. The participants lay on their back in this set of experiments.

We collected 952 experiments in this part, including a large range of heart rates that range from 43 to 137 BPM_{hr}. Figure 3.15 shows the estimation error over different

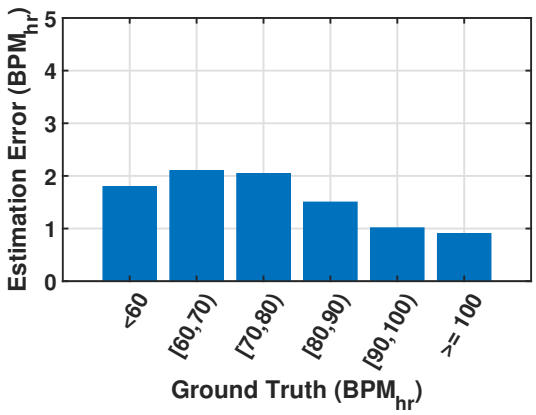

Figure 3.15: When two subjects share a bed, average heart rate estimation errors are shown for each of the following heartbeat rate ranges: < 60, [60, 70), [70, 80), [80, 90), [90, 100), ≥ 100. Over more than 1900 samples, our mean error is 1.90 BPM_{hr}, and median error is 0.72 BPM_{hr}.

heart rate ranges. Based on the ground truth heart rate collected by a pulse oximeter, we group the 4304 samples (we have two samples per experiment) into 6 groups: < 60, [60, 70), [70, 80), [80, 90), [90, 100), and ≥ 100. The median and the mean of overall estimation error over more than 4000 samples is 0.72 and 1.90 BPM_{hr}, respectively. We note that this result, which evaluates two subjects together, is in the range of other systems that detect a single person's heart rate (e.g., mean error of 1.17 BPM_{hr} in [31] and mean error around 2 BPM_{hr} in [15]).

Comparison with the ACF-based Approach: We next compare our algorithm with the direct ACF-based heartbeat detection algorithm (results shown in Figure 3.14), where we use our ACF-based heart rate estimation algorithm, but don't first separate the signal. Instead, we assume geophone x_1's signal is dominated by $s_1(t)$, and use the ACF-based heartbeat detection algorithm in [32] to directly count the heartbeats in $x_1(t)$ for s_1. Similarly, we run the same algorithm on $x_2(t)$ to count heartbeats for s_2. We show that our algorithm has a much lower estimation error, mean error of 1.90 BPM_{hr}, compared to the ACF based algorithm whose mean error is 66.53 BPM_{hr}. The ACF-based separation approach works poorly because it often captures both heartbeats from each geophone signal.

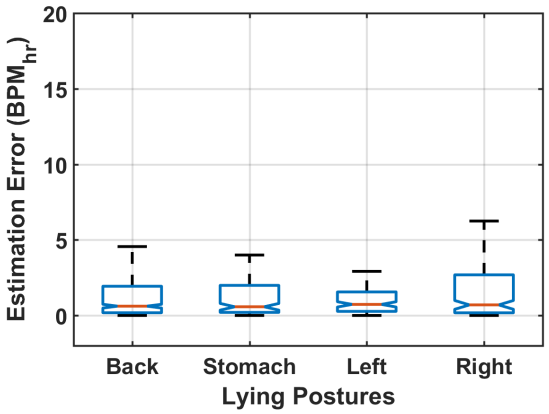

Figure 3.16: The box plot of the heart rate estimation error when two subjects share a bed and lie in different postures, including lying on back/stomach/left/right. Our mean estimation error is below 2.5 BPM_{hr} and median error is below 0.74 BPM_{hr} regardless of the posture, suggesting our system is robust against different lying postures.

The Impact of Lying Posture

In this part, we conducted 1203 experiments to evaluate the impact of lying posture on our performance. During each experiment, two subjects were asked to adopt one of the following postures: (1) lying on back, (2) lying on stomach, (3) lying on his/her left side, and (4) lying on his/her right side. The length of each experiment is again 40 seconds.

Figure 3.16 shows the box plot of the heart rate estimation error for different lying postures. The results show that our system is robust against different lying postures – the mean estimation error for lying on back, stomach, left, and right is 1.75, 1.62, 2.17, and 2.47 BPM_{hr}, respectively, while the median error is 0.61, 0.57, 0.73, and 0.70 BPM_{hr}. We note that the estimation error when the subject was lying on the right is slightly higher because the heart position is slightly further away from the mattress in this posture.

The Impact of Different Mattress Type

We also conducted 901 experiments to evaluate the impact of different mattress types, including a memory foam mattress (our default mattress), a spring mattress, and a hardwood mattress. Figure 3.17 shows that the mean estimation error for these three types of mattresses is 1.85, 2.44, and 1.53 BPM_{hr}, respectively, while the median

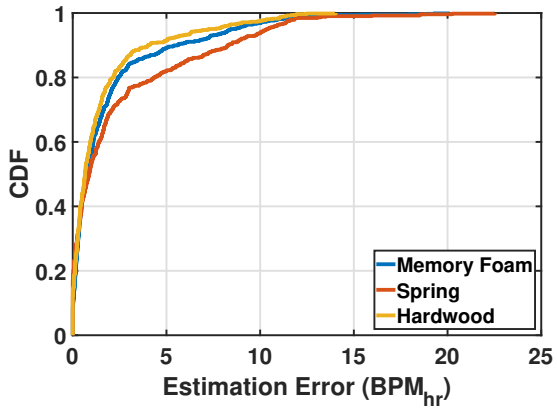

Figure 3.17: CDF of the heart rate estimation error when two subjects share a bed with different mattress types. A spring mattress has slightly higher estimation error than a hardwood or a memory foam mattress.

error is 0.73, 0.88, and 0.66 BPM_{hr}. The results are as expected – among these three mattress types, a hardwood one adds to the least oscillations to the geophone signal while a spring mattress has the most oscillation. However, we argue that even with the spring mattress which gives the highest estimation error, the estimation accuracy is still sufficient for most applications.

3.6.3 Monitoring Target Respiratory Rate When Multiple Subjects are Present

In this part of the evaluation, we conducted 1503 experiments on our prototype bed and recorded more than 16 hours of data. During each experiment, we didn't give any instructions on how the subjects should breathe. We evaluate the performance of our respiration detection algorithm by comparing the estimated respiratory rate against the ground truth measured by a Zephyr bioharness belt [66] and report the estimation error.

Participants: We had a total of 28 healthy volunteer participants for this experiment, including 15 males and 13 females. The mean age of the participants was 24.79 years with a standard deviation of 2.99 years. The youngest participant was 21 years old while the oldest was 34 years old.

Experiment Procedure: We conducted more than 1500 experiments and evaluated

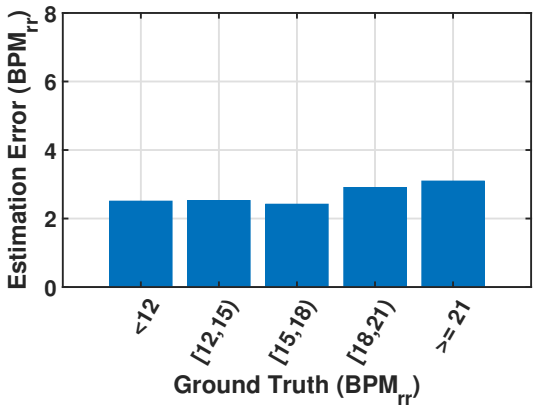

Figure 3.18: When two subjects share a bed, mean breathing rate estimation errors are shown for each of the following breathing rate ranges: < 12, [12, 15), [15, 18), [18, 21), ≥ 21 – 2.51, 2.53, 2.42, 2.90, 3.09 BPM_{rr}, respectively. The average error rate across all the 2406 samples is 2.62 BPM_{rr}, while the median error is 1.95 BPM_{rr}.

our algorithm over a large range of respiratory rates, from 8.61 to 25.09 BPM_{rr}. Before experiments, some subjects were asked to exercise, including running, climbing stairs, etc.

Based on the respiratory rate measured by a Zephyr belt, we grouped the 3006 samples into 5 groups: $<$12, [12, 15), [15, 18), [18, 21), and $\geq$21 BPM_{rr}. Figure 3.18 shows that the overall mean estimation error across more than 3000 samples is 2.62 BPM_{rr}, while the median error is 1.95 BPM_{rr}. We note that this result is worse than our single-person breathing rate estimation because we have to go through two levels of indirection in estimate breathing rate when multiple people share a bed. In our on-going work, we are developing techniques to improve our performance in this case.

Next, we evaluate how different types of sleep postures affect our estimation error. Figure 3.19 shows that lying postures have little impact on estimating respiratory rate – the average estimation error for these different postures (lying on back/stomach/left/right) is 2.77, 2.36, 2.68, and 2.40 BPM_{rr}, respectively while the median error is 2.15, 1.66, 2.09, and 1.67 BPM_{rr}.

3.6.4 Discussion on Real World Deployment

Real world deployment of our system could potentially enable quite a few interesting applications. So far, we have shown our system can monitor heart rate and respiratory

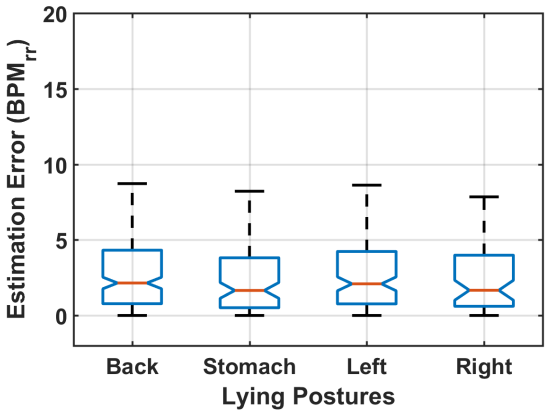

Figure 3.19: Box plot of the breathing rate estimation error when two subjects share a bed and lie in different postures, including lying on back/stomach/left/right. The average estimation errors for these different postures are very close to each other.

rate for one or two people on a bed. We have found our system is also able to detect a user's gross body motions, or smaller activities such as snores during sleep. These functions combined , we could build a more sophisticated sleep monitoring system that can accurately detect a person's sleep stage and evaluate the sleep quality. To achieve this objective, we need to carefully tune several system parameters to detect and classify these fine-grained information. One possible solution is to add more geophone sensors at different locations to form a small-scale sensor network that facilitates more accurate separation of various target signals.

3.7 Related Work

In this section, we categorize different vital sign monitoring systems in two ways: (1) systems which detect the heart rate and respiratory rate of a single person, e.g. [15, 23, 25, 27–32, 53, 76]; (2) systems which detect heart rate and respiratory rate of two people simultaneously, such as the system shown in [14, 15]. Also, we summarize their signal processing methods for heart rate and respiratory rate estimation.

3.7.1 Vital Sign Monitoring of a Single Person

There are diverse systems proposed to detect heartbeats and respiration of a single person. So far, it is the most commonly studied field.

Sensors installed under the thorax area: Bu et al. [23] inserted a piezoelectric sensor which measures the pressure fluctuation due to heartbeats and respiration. The detected signal is processed by Empirical Mode Decomposition and the vital sign signals are reconstructed by summing up the signal within the predefined frequency range. Bruser et al. [27] packaged a Wheatstone bridge of four sensitive load cells onto one slat from the slatted frame and measured the vibration caused by heartbeats. An unsupervised learning technique is used to extract the shape of a single heart beat from the signal. In [29], an array of photodetectors under the mattress are used to detect the change of reflected and scattered light caused by vibration. The heartbeat and respiration signals can be separated by applying a simple low-order high-pass filter. Šprager et al. [53] used an optical sensor which transmitted and received interferometric signal to capture optical variation caused by vibrations from heartbeat and respiration. Later a wavelet-based decomposition technique was applied to extract heartbeats and respiration signal from the received signal. Kortelainen et al. [30] deployed several pressure sensitive foils under the mattress. The heartbeats were extracted from the channel averaged cepstrum based on Fourier transformation, while respiration is calculated by an adaptive principal component analysis. Aubert et al. [31] put a foil pressure sensor in the thorax area under a thin mattress to detect vital signs during sleep. The heart rate and respiratory rate are obtained from analyzing the autocorrelation function after applying appropriate bandpass filters.

Sensors that requires special cushion: Heise et al. [76] deployed four hydraulic-transducer tubes under the mattress and showed three possible signal processing strategies (a Window-based Peak-to-Peak Deviation algorithm, a K-means clustering algorithm, and a Hilbert transform algorithm) to extract the heartbeats. Yamana [13] designed an ultrasound transmitter and receiver system mounted under a plywood support. The system is placed under the mattress and measures the shape change of the plywood support. A simple bandpass filter is applied to separate the heartbeat signal.

Sensors installed under the bed post: Nukaya et al. [25] proposed to use a piezoceramic system to detect heartbeats. Four sensors were bonded to two metal plates

on top and bottom, then sandwiched between floor and bed posts. A simple bandpass filter was applied to get the heartbeat signal. Brink et al. [28] built a set of four optical load cells which were installed under each bed post and directly find the heartbeats as the local maximums after low-pass filtration.

Wearable Sensors: Phan et al. [57] uses a chest belt with a built-in biaxial accelerometer to measure the vibrations on the surface of the chest cavity. A bandpass filter is applied to extract the respiration signal, and a combination of envelope detection and peak finding algorithm is used for estimating the heart rate.

Mobile Sensors: Nandakumar et al. [77] detects sleep apnea events within a meter by turning a smartphone into a sonar system. The system emits frequency-modulated sound signals and detects the frequency shifts of the reflections due to chest movements.

Sensors that can be attached to anywhere on the bed frame: Jia et al. [32] proposed a heartbeat monitoring system based on an on-the-shelf geophone which could be inserted anywhere between a mattress and a bed frame. A combination of low-pass filter, sample auto-correlation function and peak finding algorithm are used to extract the periodicity of heartbeats. An evaluation of real world data varying different types of bed and house environment shows the possibility of using the system in daily heartbeat monitoring.

3.7.2 Vital Sign Monitoring of Multiple People

Only a few papers addressed detecting multiple people's vital signs simultaneously. Adib et al. [14] use a wireless radar to measure the distance change of a human chest, due to heartbeats and respiration. The device can send Frequency Modulated Carrier Waves (FMCW) which can isolate signals from different distances, and then estimate the heart rate and respiratory rate of multiple people via FFT. Liu et al. [15] use WiFi to measure the Channel State Information (CSI) of the reflections off the human body. The system takes the advantages of Received Signal Strength (RSS) from multiple subcarriers and estimates the heart rate and respiratory rate by using a power spectral density based algorithm. RSS values are sensitive to the multipath situation in the

environment, and therefore wireless systems that are based on RSS readings may be affected by the changes in the environment.

3.8 Concluding Remarks and Future Direction

In this chapter, we discuss and evaluate an unobtrusive, vibration-based vital sign monitoring system during sleep. Our system centers around a geophone sensor that can sense the vibration velocity caused by ballistic force. Compared to earlier geophone-based in-bed vital sign monitoring systems that could only detect heartbeats from a subject lying in bed, our system is significantly improved. First, it can monitor the subject's breathing rate, even though geophones cannot directly detect breathing. Second, it can track the subject's heart rate and breathing rate when he/she shares the bed with another person. In this case, vibrations caused by multiple heartbeats are mixed together and need to be separated. After involving 86 participants and collecting 56 hours of geophone data, we show that our system is accurate and can work in different scenarios (e.g., lying postures, mattress types).

Going forward, there are several important directions we plan to investigate, including (1) obtaining better signal-to-noise ratio for more accurate heart rate and respiratory rate monitoring; (2) understanding the physical respiration phenomenon better and adjusting our respiration model accordingly; (3) investigating the time and frequency characteristics of gross body motions and updating our model accordingly.

Chapter 4

Touch-Chair: Learning a User's respiratory rate and identity through Capacitive Sensing

4.1 Introduction

Passively learning a person's behavior and activities has become increasingly popular in the ubiquitous computing area, for example, knowing when a person is commuting, working, relaxing and sleeping, and how well he or she is. In one's everyday life, a person spends a large portion of time sitting on a chair, especially when working or studying. According to the data collected from the 2003-2004 National Health and Nutrition Examination Survey, people spend 7.7 hours in sedentary behaviors [78]. An article from The Washington Post mentions office workers sit for about 10 hours on average in 2015 [79].

Several aspects of sitting behaviors, especially irregular breathing behavior, is considered important problems in the medical field. As a result, quite a few studies [80,81] have been conducted to help people monitor their breathing behavior. However, few of them can achieve ease of use, unobtrusiveness, robustness, accuracy, and low power at the same time. Furthermore, most of the systems need to plug into the wall, which obviously undermines the mobility nature of a chair and brings inconvenience to users.

In this study, we present a smart chair system, which can identify the person sitting on it and measure the respiratory rate, at the same time. Shown in Figure 4.1, our prototype has 16 wireless capacitive sensors that are mounted on the surface of the chair, one receiver and one Raspberry Pi. Each capacitive sensor mainly consists of a resistor-capacitor (RC) circuit that is connected to a properly sealed low power active tag. After collecting sensor samples from our prototype, we apply machine learning techniques including Extreme Gradient Boosting (XGBoost) [82] and Random Forests

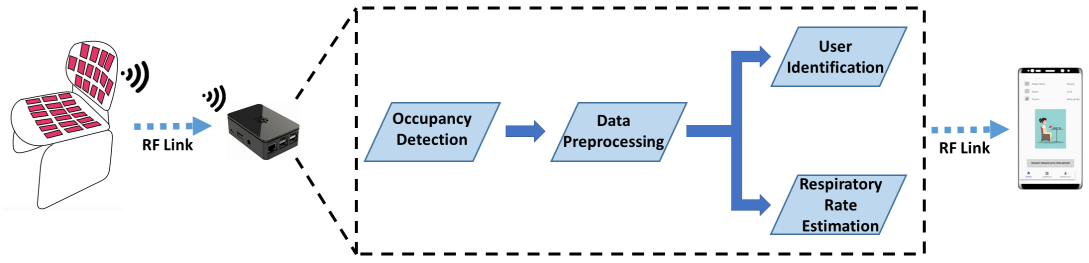

Figure 4.1: The system overview of our Touch-Chair system. We mount 16 capacitive sensors on the surface of a chair to capture the capacitance change caused by any user activity. We use low-power wireless tags to measure the sensor signals and transmit the data wirelessly to a tag receiver. A Raspberry Pi reads data from the tag receiver, detects the occupancy event, applies signal processing and machine learning techniques to identify the user and monitoring the respiratory rate. Eventually, a mobile app queries the processed results from the Raspberry Pi via WiFi and displays the user's name and the respiratory rate.

(RF) [83] to infer the user identify, and apply signal processing techniques to estimate the user's breathing rate. Capacitive sensors are very sensitive to distance changes between the chair and the human body, thus yielding accurate results in all the three intended use cases.

As far as unobtrusive respiration detection is concerned, our system offers several advantages. It provides more privacy than computer vision based systems [84], has higher accuracy than pressure based [85]and inertial sensor based systems [86], and is much more robust than wireless signal based systems [87]. Meanwhile, our system also improves the state of the art for on-chair respiration detection. Earlier on-chair breathing monitoring mainly relies on sensors that are placed on the back of a chair [80, 81] and requires the user to lean back on the chair. Our system, however, does not have this constraint and can conveniently monitor respiration regardless of user posture.

We conducted 5,001 experiments involving 29 subjects for user identification and 889 experiments involving 19 subjects for respiratory rate monitoring. In total, we collected 77.3 hours of data over a period of 7 months[1]. We have a group of subjects of different age, height, and weight. In order to be more realistic, we collect at least 10-day data from most of the subjects, considering that their sitting habits and clothes may vary over time. The results show that our system is robust and can serve users with

[1]Our studies were approved by the Institutional Review Board (IRB) of our institution.

different physical shapes and clothing. Furthermore, we demonstrate that our system can recognize the person with an accuracy of 98.77% and monitor the respiratory rate with the error of 1.05 *breaths per minute* (*bpm*). Also, thanks to the low-power design, our system can run for at least 306 days for user identification on a 3-volt coin cell battery.

This work has the following contributions:

- We designed a smart chair system that can identify the user and monitor the respiratory rate, at the same time. In particular, this is the first work that shows it's possible to monitor a person's respiration rate using a single unobtrusive contact-based sensor on a chair without requiring the user to be in a specific posture.
- Our system is very accurate. It can identify the person with 98.77% accuracy for 29 subjects. Also, the average error of respiratory rate monitoring is 1.05 *bpm*.

4.2 Motivation: Chair Occupancy Detection Using a Single Capacitive Sensor

Before presenting the details of our system, we first study whether we can detect when the user sits on/leaves the chair using a single capacitive sensor. This simple task can help design our prototype as well as user identification algorithms. In this section, we also show the way of capacitance measurement in our system and its robustness to the aging impact of any chemical batteries.

4.2.1 Chair Occupancy Detection

Figure 4.2 shows the measured capacitance values in the following three situations: (1) chair is empty, (2) chair becomes occupied, and (3) chair becomes empty again. Initially, the chair was empty and the measured signal only consists of the capacitance of the sensor (plus some noise). When the user sat on the chair, the capacitance experiences a sudden increase due to the presence of the human body. Note that over time, the capacitance slowly increases with some fluctuation, as shown in the zoomed-in plot in

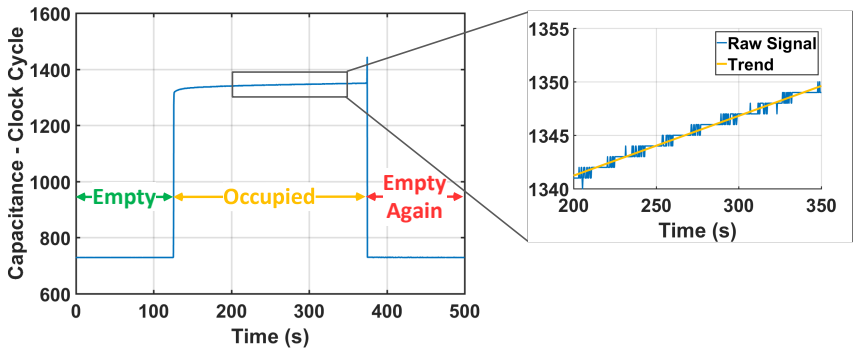

Figure 4.2: We show an example experiment that a chair is at first empty, then occupied by a subject and empty after the subject leaves. From the transitions between the empty chair and the occupied chair, we observe a sharp rising/falling edge and can easily detect the occupancy events by simple thresholding. Also, the details of the capacitance change of the occupied chair reveal the respiration and the skin moisture of the subject: the fluctuation is mainly caused by respiration and the trend is the consequence of the moisture built up in the air gap between the hip and the sensor. Note the average discharge time for 1 pF is 34.74 clock cycles in our case.

Figure 4.2. This slow increase in capacitance is caused by the moisture that builds up between human skin and the capacitive sensor. When the imbalance between the humidity in the air and the moisture of the skin surface occurs, the water diffusion and evaporation process within the gap tries to reach an equilibrium state. Eventually, the increasing humidity in the air changes the dielectric constant of the air itself and shows up in the measured signal as a slow increase of capacitance. Meanwhile, the fluctuation of the measured capacitance is caused by mostly respiration plus some noise. Our Touch-Chair system is sensitive enough to capture the tiny distance changes between the human hip and the sensors, which is caused by respiration. Once the user leaves the chair, the capacitance drops again. As such, it's rather straightforward to detect whether the chair is occupied or not.

4.2.2 Capacitance Measurement

In this work, we choose to measure the capacitance value by simply measuring the time that elapses while discharging a resistor-capacitor (RC) circuit. We form an RC circuit by grouping a capacitive sensor (a pair of copper mesh screens mounted on the chair) and a resistor on a general-purpose embedded sensor platform (called PIP tags) [88]).

The discharge can be modeled as:

$$V(t) = V_0 e^{-\frac{t}{RC}}, \tag{4.1}$$

where $V(t)$ is the voltage across the capacitor at time t, V_0 is the initial voltage across the capacitor C, and R is a fixed resistor (2 $M\Omega$ in our case). Solving this equation for C, we have

$$C = -\frac{t}{R}\left(\ln\frac{V(t)}{V_0}\right)^{-1}. \tag{4.2}$$

The capacitance value is proportional to the discharge time, when R, $V(t)$, and V_0 are fixed. As such, we can measure the discharge time and infer the capacitance accordingly.

In practice, V_0 may drift over time for any mobile DC/AC power supply, thus leading to measurement drifts. We solve this challenge by: (1) fully charging the capacitor so V_0 reaches the voltage directly from the DC power supply V_{cc} (the $3V$ coin cell battery in our case), and (2) having a comparator in the PIP tag compare $V(t)$ against $\frac{1}{2}V_{cc}$ and counting how much time has elapsed till $V(t) = \frac{1}{2}V_{cc}$. Since every capacitive measurement lasts less than 10 ms in our experiment, we can reliably assume that V_{cc} from a coin cell battery stays constant within each measurement. As a result, according to Equation 4.2, we can keep each measurement independent of the battery voltage drift over time. By applying linear least square estimation on various capacitance values, we calculate the average discharge time (to $\frac{1}{2}V_{cc}$) for 1 pF is 5.79 μs.

4.3 Touch-Chair Prototype

When designing the Touch-Chair prototype, we have the following two main design objectives: (1) sensor placement should be unobtrusive and bring no discomfort to users, (2) the shape and the mounting position of the sensors should be designed to maximize its sensitivity.

Our prototype chair has 16 capacitive sensors, among which 9 are mounted on the surface of the seat pad and 7 more on the surface of the backrest, shown in Figure 4.3. Each capacitor consists of two pieces of copper mesh screen (as terminal plates) side by side. The size of each piece is 8.50 cm (length) by 4.50 cm (width) by 0.04 cm (thickness) and the distance between two adjacent pieces is 2.00 cm. We empirically

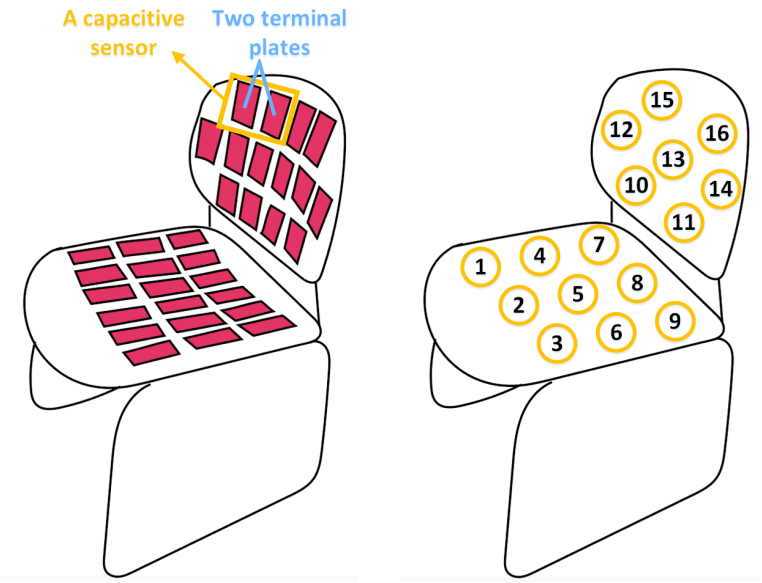

(a) (b)

Figure 4.3: (a) A chair prototype has 16 capacitive sensors. Each sensor has two terminal plates adhered on the surface of the chair. Further, we label each sensor in (b) and refer each sensor using its index number in the rest of the paper. Further study shows that we can possibly reduce the number of sensors but keep about the same performance.

chose the current design considering our design objectives and the following factors: (1) the size of the chair surface is limited, (2) larger and farther-apart terminal plates lead to better resolution, (3) sensors should be spread out for better spatial coverage, and (4) the number of sensors needs to be minimized to conserve energy. In our prototype, the sampling rate for most of the capacitive sensors are 1 Hz, but 4 Hz for sensor ⑤ (to meet the sampling rate requirement for respiration monitoring).

We use PIP tags to measure capacitance and wirelessly transmit measurements to a PIP tag receiver on a Raspberry Pi. PIP tags are carefully designed low-power tags, including a Texas Instrument (TI) MSP430G2553 microcontroller and a Texas Instrument CC1100 radio transceiver module. PIP tags run at 6 MHz on a $3V$ coin cell lithium (CR2032) battery, as shown in Figure 4.4.

Power Consumption Profile: Touch-Chair consists of four parts of hardware: 16 PIP tags, 1 PIP tag receiver, 1 Raspberry Pi, and 1 smartphone. The Raspberry Pi takes most of the computation and is powered by a power outlet, while the mobile application is mainly used as a user interface and doesn't have much computation

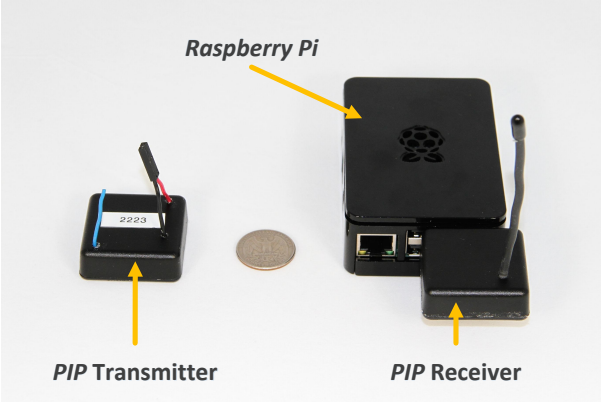

Figure 4.4: A capacitive PIP tag transmitter and a Raspberry Pi with a PIP tag receiver, compared to a United States quarter. The transmitter connects to the copper mesh screen by wire, measures the capacitance and broadcast the measurement packets. The receiver read the wireless packets and send them to Raspberry Pi which processes the data and pushes the results to the mobile app end.

requirement. As such, we only focus on the power consumption of the PIP tag part. We profile the power consumption of a PIP tag in three stages: the sleep stage, the measurement stage[2] , and the radio transmission stage. For this purpose, we mount a resistor in series with a DC Power Supply and the PIP tag, and then accurately measure the current drawn through the tag by converting voltage drop across the resistor, shown in Figure 4.5. Next, we calculate the power consumption based on the given voltage of the power supply and the measured current. From the results shown in Table 4.1, we observe that the measurement stage and the transmission stage consume much more power but last for a much shorter time, while the sleep stage costs much less power and lasts longer. Also, the power consumption is dependent on the chair status – the overall power consumption for a 1-Hz tag is 56.40 μW and 136.50 μW, when the chair is empty and occupied, respectively. If we assume a user occupies a chair for 10 hours per day, then the 1-Hz tag can last for at least 306 days with one CR2032 coin cell battery (3 V with a nominal capacity of 220 mAh) and more than 9 years with one AA Tadiran lithium battery (3.6 V with a capacity of 2400 mAh) [89].

[2]In this study, we consider the microprocessor wake-up configuration and the capacitor charging as part of the measurement stage.

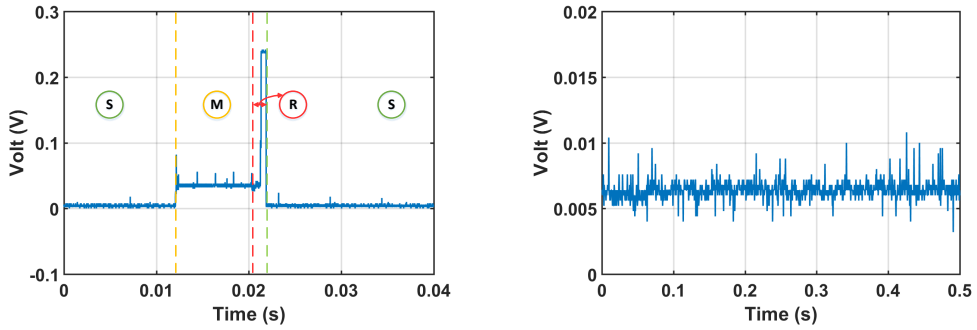

(a) (b)

Figure 4.5: The power consumption profile of a 1-Hz capacitive tag (a) consists of three parts: sleep stage Ⓢ, measurement stage Ⓜ, and radio transmit stage Ⓡ. We use a large capacitor to mimic the largest capacitance occurred in our experiment and compute the overall power consumption of the tag by measuring the voltage drop across 10 Ω resistor (a) in series with the tag. In order to accurately measure the power consumption of the sleep stage, we use a 10 $k\Omega$ resistor (b) instead of 10 Ω resistor, because the power consumption of the sleep stage is extremely low. Overall, the average power consumption of the 1-Hz tag on an occupied chair is at most 136.50 μW.

4.4 User Identification

Capacitive sensors are very sensitive to sitting posture changes. When a user sits still on the chair, the gap between the body and the sensor is roughly around 1 mm, which is the thickness of the pants. Even a tiny adjustment of the posture will sufficiently change the capacitive value because any adjustment will likely change the gap by at least a few mm. Thus, our Touch-Chair system can capture the details about these posture changes and yield accurate user identification.

It is often the case that we want to monitor a particular user's respiratory behavior, but that user may share a chair with other people. As a result, we envision that our Touch-Chair can correctly identify the target user and focus on his/her behavior. In fact, according to the survey reported in [80] that involved 550 people in the U.S., 31% of people share their chairs with at least one other person. Let us assume a smart home scenario where we have 1 to 5 primary users[3] and occasionally a few guests. Thus, having a way of identifying the person on the smart chair is the important first step before focusing on their respiration.

[3]According to the U.S. Census Bureau, the average number of people per household between 2011 to 2015 is 2.64.

Sampling Frequency	1 Hz			
Occupancy	Empty		Occupied	
	Power (μW)	Time (ms)	Power (μW)	Time (ms)
Sleep	1.91	997.95	1.91	990.24
Measurement	11,600	0.52	10,400	8.28
Transmission	31,700	1.53	31,700	1.53
Overall Power Consumption (μW)	56.40		136.50	

Table 4.1: The power consumption profile of a single PIP tag sampling at 1 Hz on a chair. The tag only consumes 56.40 μW on an empty chair and 136.50 μW on an occupied chair. Assume a chair is occupied 10 hours per day, the tag can last for 306 days with a single coin cell battery and more than 9 years for one AA Tadiran lithium battery.

We try to identify users by recognizing his/her transitional behavior between the first moment that a user sits on a chair and the moment that the posture is stable. Each person's transitional behavior generates unique sensor readings due to different body size, weight, initial sitting posture, micro adjustment, etc.

4.4.1 Classification Algorithms

Using wireless PIP tags to measure capacitance, we received 16 streams of non-synchronized sensor data, a small fraction of which will be missing or polluted due to packet collisions. We address this problem by applying the spline interpolation technique [90] on each sensor data stream. After applying the interpolation step, we have one sample per second from each data stream (the ultra-low sampling rate is an advantage of our system).

To correctly recognize users, we first need to identify the occupancy event in a timely fashion by detecting the corresponding rising edge of the sensor signal. An example of the rising edge is shown in Figure 4.2. Then, we interpolate the sensor data within a preset window size, 11 seconds in our case, in order to synchronize the data and prevent any potential missing packets due to the wireless collision.

	Age ($year$)	Height (cm)	Weight (kg)	BMI (kg/m^2)
Min	22	161	47	16.9
Max	36	182	91	30.4
Mean	25.7	172.8	69.4	23.1
Std	3.5	5.9	12.8	3.6

Table 4.2: 29 participants are recruited for user identification study. The table shows the minimum, maximum, mean and standard deviation of the participants' age, height, weight and BMI.

For the identification purposes, we treat the resulting samples as features and classify people's identity by using two popular tree-based machine learning algorithms, Extreme Gradient Boosting (XGBoost) [82] and Random Forests (RF) [83]. These two algorithms focus on reducing a different part of the error during the learning process, with XGBoost focusing on reducing the bias while Random Forests focusing on the variance part. Specifically, XGBoost takes advantages of weak learners and reduces bias in the dataset by adjusting the weight of certain data, while Random Forests decreases the variance by having many uncorrelated trees.

In general, having more primary users introduces an extra challenge to classification. In the rest of this paper, we assume there are 5 primary users in a house. One exception is that we vary the number of users from 1 to 5 and report the performance in Section 4.4.3.

4.4.2 Experiment Design

In this experiment, we focus on evaluating the performance of our Touch-Chair on accurately identifying the users.

Participants: We had a total of 29 healthy volunteer participants for this experiment, including 22 males and 7 females. The mean age of the participants was 25.7 years with a standard deviation of 3.5 years. The youngest participant was 22 years while the oldest is 36 years old. More details about the participants' biographies are shown in Table 4.2.

Experiment procedure: For each data collection session, in order to mimic the typical daily sitting behavior, we asked a participant to walk towards a chair from a

distance of 2–3 meters and sit comfortably but freely on a chair for about 15 seconds. We conducted all the sessions in an indoor academic laboratory environment and at least one of our members oversaw the sessions. During the session, we allowed the participant to move the chair around, adjust his/her posture, and watch a video of his/her own choice. Also, we helped the participant to track time using a time counter on the PC and we labeled each participant with a unique index as the ground truth.

The participants were allowed to take a 30-second break between any two data collection sessions and withdraw from the data collection session at any time. In order to ensure the diversity of the data, we asked most of the participants to repeat the experiments for at least 5 different working days. We observed that the majority of the participants performed similar sitting patterns as they did previously and 4 participants changed several sitting patterns during the experiments. Most participants went through at least 100 experiments and at most 200 experiments in a period of 12 to 60 days, and 2 more participants finished at least 80 experiments within 3 days. In total, we conducted 5001 experiments under varies conditions (summer/winter, high/low moisture, thin/thick clothes, etc.) and collected more than 41.6 hours data in 7 months.

4.4.3 User Identification Evaluation Results

In this part, we first tune three important parameters – the depth of the trees in Random Forest and XGBoost, the time window and the number of capacitive sensors required. Then, we evaluate the performance of user identification. Here, we mainly focus on the situation that we have 1 to 5 primary users (the most common scenario in an office or home), while occasionally we have a few guests. We conducted more than 5,000 experiments from a total of 29 participants and recorded more than 20 hours data in 5 months. We report the user identification results (with 5 primary users) in a confusion matrix and compare the cases where the number of users varies from 1 to 5.

Depth of the tree: We tune the tree depth and report the user identification error in Figure 4.6. Figure 4.6(a) shows XGBoost is less sensitive to the tree depth and the depth of 3 is sufficient. Figure 4.6(b) shows Random Forests is more sensitive to the

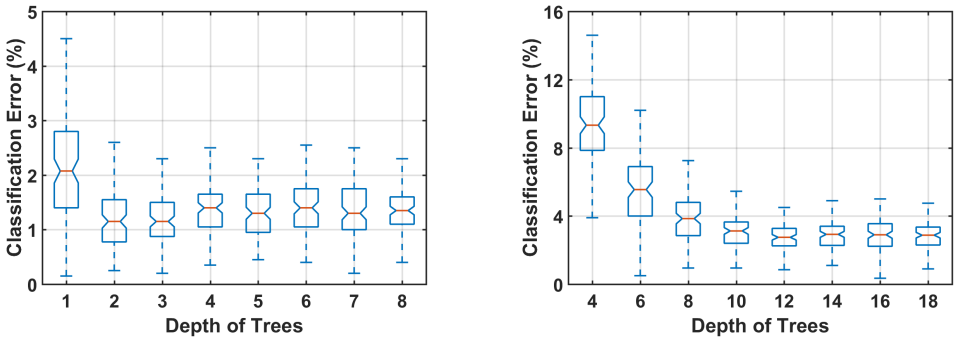

(a) XGBoost (b) Random Forests

Figure 4.6: The depth of the trees vs user identification classification error. (a) XGBoost performs well even the depth of the trees is as shallow as 3. Meanwhile, (b) Random Forests is more sensitive to the depth of the trees, and depth above 12 gives the best performance. The average classification error of XGBoost and Random Forests over 100 cross-validation iterations is 1.23% and 2.82%, respectively. In the rest of the paper, we set the depth of the trees in XGBoost and Random Forests to be 3 and 12, respectively.

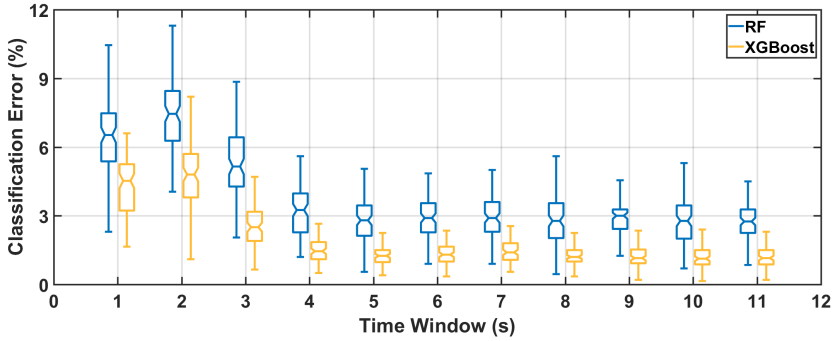

Figure 4.7: The box plot of the user identification error over the window size between 1 and 11 seconds. Having a longer window improves the accuracy gradually. The best average classification error of XGBoost and Random Forests over 100 cross-validation iterations is 1.23% and 2.82% at an 11-s window size.

tree depth. Increasing the number of trees from 4 to 12, we decrease the classification error from 9.27 to 2.82%. In the rest of the paper, we use the depth of the trees in XGBoost and Random Forests to be 3 and 12 for user identification, respectively.

Time window: We tune the window size and see how fast we can identify a person. Figure 4.7 shows the performance of XGBoost and Random Forests algorithms while varying the size from 1 to 11 seconds. It's obvious that the first 3 seconds of a sitting event contains rich information about the user identity, as the classification error is 2.50 and 5.15 % for XGBoost and Random Forests algorithms, respectively. Also, we notice that the error for 2-s window size is the highest for both algorithms, because people

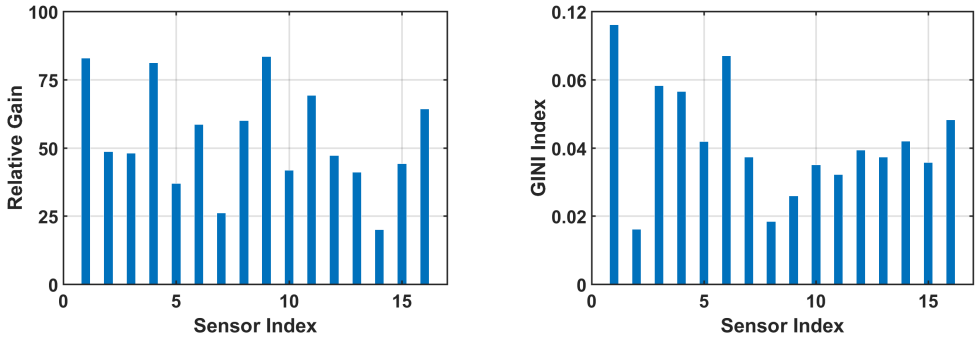

(a) XGBoost (b) Random Forests

Figure 4.8: We use (a) XGBoost and (b) Random Forests algorithms to evaluate the importance of sensors by summing up the importance of features from the same sensor. A higher value indicates a larger impact during the classification process.

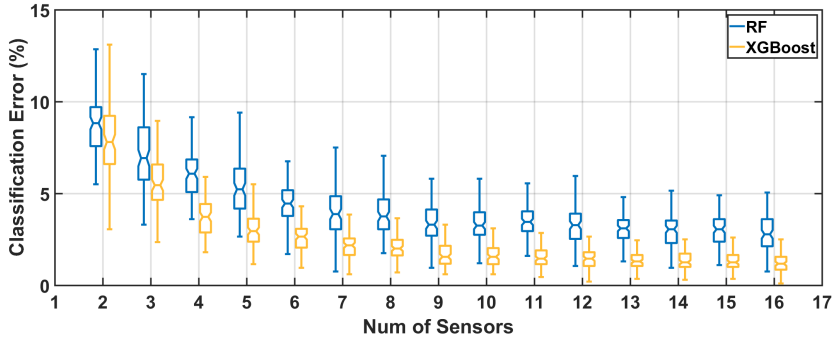

Figure 4.9: We increase the numbers of capacitive sensors from 2 to 16 and evaluate the performance of both algorithms. The sensors are selected by its importance calculated by summing up the importance of the features coming from the same sensor. The performance of both (a) XGBoost and (b) Random Forests increase when we increase the number of important capacitive sensors reported in Figure 4.8. Both XGBoost and Random Forests performs the best at 1.23% and 2.82%, respectively, while using all 16 capacitive sensors.

usually spend 2 to 3 seconds to fully settled on a chair and thus the samples measured around the 2nd second have large randomness.

Number of capacitive sensors: We tune the number of capacitive sensors used in user identification and evaluation the possibility of reducing the number of capacitive sensors required for user identification in the following steps: (1) ranking the importance of the features, (2) calculating the importance of a capacitive sensor by summing up the importance score of all features coming from the same sensor, (3) taking the features measured from the N most important capacitive sensors, and (4) evaluating the classification accuracy again using these features.

Feature importance: We hypothesize that among the 16 sensors we have, some sensors have correlated readings as they are rather close to each other in space and covered by the same user. We confirm our hypothesize in three steps: (1) ranking the importance of the sensors, (2) taking the N most important sensors, and (3) evaluating the classification accuracy using the N features. The importance of a specific sensor is calculated as the sum of the feature importance from the same sensor. The averaged importance of the capacitive sensors for both algorithms over 100 cross-validation iterations is shown in Figure 4.8. We observe that the two algorithms both agree that features from capacitive sensor ①, ④, ⑥, ⑯ are important. Also, there is some potential correlation among all the features. We take all the features from the $N(N = 2, ..., 16)$ most important capacitive sensors and evaluate the performance of both algorithms again. Both XGBoost or Random Forests, we use the N most important features from its own feature importance metric separately. Figure 4.9 shows the evaluation results. Both XGBoost and Random Forests start with high error rate and decreases rapidly while we increase the number of important capacitive sensors. In this evaluation, we do not observe any sign of performance decrease while increasing the number of important capacitive sensors. Using features from all 16 sensors, both XGBoost and Random Forests performs the best at 1.23% and 2.82%, respectively.

Comparison between two algorithms: We compare the classification performance over XGBoost and Random Forests algorithms. First, we evaluate how well our system performs when there are 5 primary users and 24 guests. The overall classification error of XGBoost and Random Forests over 100 cross-validation iterations is 1.23% and 2.82%, respectively. Table **??** shows an example of the confusion matrix of classifying 5 primary users vs 24 guests using XGBoost. The indices 1 through 5 means the index for each primary user and "Others" means the rest 24 guests. The classification error of this example is 0.20%.

Varying the number of users: We vary the number of users from 1 to 5 and evaluate the performance of both algorithms. Figure 4.10 shows the average error of XGBoost and Random Forests algorithms. As the number of primary users increases, the average

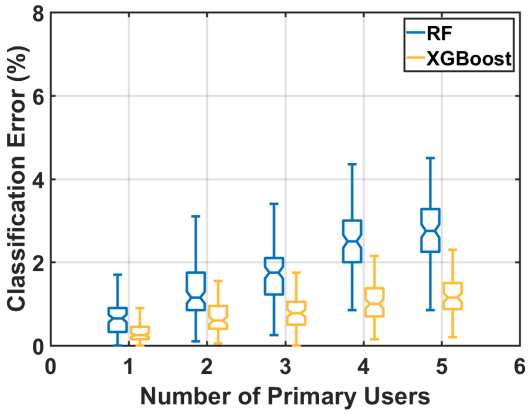

Figure 4.10: The box plot of the user identification error while varying the number of users. The average classification error of XGBoost and Random Forests over 100 cross-validation iterations increases while we have more primary users. The detailed average error is shown in Table 4.3.

Error (%)	Number of Primary Users				
	1	2	3	4	5
XGBoost	0.34	0.66	0.82	1.05	1.23
Random Forests	0.67	1.32	1.78	2.54	2.82

Table 4.3: The table shows the average classification error of XGBoost and Random Forests algorithms. The average classification error of XGBoost and Random Forests for the 1-user case is 0.34% and 0.67%, respectively. Also, the average classification error of XGBoost and Random Forests for the 5-user case is 1.23% and 2.82%, respectively.

error also increases as we have a higher chance to get a primary user whose behavior is similar to guests. Table 4.3 shows the average classification error of XGBoost and Random Forests. is 0.34% and 0.67% for the 1-user case and 1.23% and 2.82% for the 5-user case. Also, XGBoost performs better than Random Forests.

Varying the number of guests: We vary the number of guests from 1 to 5 and evaluate the performance of both algorithms.

4.5 Respiratory Rate Monitoring

It has been shown that respiration can be unobtrusively detected through contact-based sensors placed on the backrest of a chair [80,81]. In this paper, we take one step further and demonstrate that it's possible to monitor the respiration from the seat pad as well.

We monitor the user's respiratory rate by detecting the micro movements from the hip, which are caused by the contraction and relaxation of the thoracic diaphragm

during breathing. When a person is inhaling, the thoracic diaphragm contracts and causes expansion across the bottom of the thoracic cavity. The expansion naturally forces air into both lungs to balance the pressure in and out of human body. The exhalation starts after the inhalation is complete. The thoracic diaphragm relaxes which in turn causes the contraction of the thoracic cavity and air forced out of both lungs. The muscle contraction of the thoracic diaphragm causes human body slightly vibrating up and down. Such micro vibrations are hardly visible to a human eye, but our sensors are sensitive to tiny distance changes and able to capture these vibrations.

4.5.1 Respiration Monitoring Algorithms

The respiratory monitoring starts with collecting a capacitance signal using a PIP tag which connects to sensor ⑤ in Figure 4.3(b), sampling at 4 Hz. In order to focus on the respiration signal, we compute the trend of the signal by applying a central moving average (CMA) filter. A CMA filter computes the mean within a window using data equally spaced on either side of a point in the time series. In order to keep as many respiration details as possible, the window size of our CMA filter should be larger than at least one period of a respiration cycle. In our case, we use a 10 s window which is sufficient for our application. The result signal (i.e., the trend) after applying the CMA filter includes the capacitance measurement whose period is longer than 10 s. In other words, it contains the base signal from the sensor itself, as well as the signal from the user activities (assuming no posture change during this short period of time). Next, we subtract the trend from the original data and get the residue signal which mostly constitutes the respiration. In the rest of this section, we assume the noise is negligible and use $s_r(t)$ to denote the residue signal.

Once we obtain $s_r(t)$, we can apply a Sample Autocorrelation function (Sample ACF) [32] to extract its periodicity. The Sample ACF of the respiration signal $s_r(t)$ is defined as

$$f_{\hat{ACF}}(k) = \frac{1}{n}\sum_{t=1}^{n-k}(s_r(t+k) - \overline{s}_r)(s_r(t) - \overline{s}_r) \qquad 0 \leq k < n, 0 \leq t < T, \tag{4.3}$$

where n is the number of samples in the given time window, k is the time lag, $\overline{s}_r$ is the

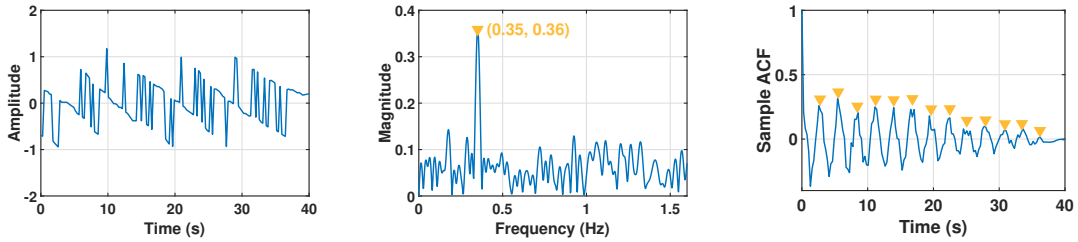

(a) (b) (c)

Figure 4.11: The participant's respiration rate is 21.13 *bpm*. (a) The capacitor sensor's residue after applying the CMA filter and removing the trend. The signal is messy with some repetitive pattern. However, it's difficult to tell what is the respiratory rate by eye. (b) The same capacitor signal as in (a), but in the frequency domain. We can see there is an obvious peak at 0.35 Hz, which correspond to the respiratory rate of 21.00 *bpm*. (c) The results after applying the Sample ACF and peak finding algorithm. We mark the identified peaks in yellow inverted triangles and we can easily tell the periodicity of the respiration which is the distance between any two adjacent peaks. The averaged interval among all the detected peaks is 2.84 s, which corresponds to 21.13 *bpm*.

mean of $s_r(t)$ over the window. Further, we normalize the Sample ACF as

$$\bar{f}_{A\hat{C}F}(k) = \frac{f_{A\hat{C}F}(k)}{f_{A\hat{C}F}(0)} \qquad 0 \leq k < n, \tag{4.4}$$

and apply a peak finding algorithm to extract the location of the peaks [36]. The main advantage of using ACF-based algorithm stems from its resistance to noise.

We show an example residue signal in the time domain, the same signal in the frequency domain and its Sample ACF results with peaks detected in Figures 4.11(a), (b), and (c), respectively. Figure 4.11(a) is the residue signal in the time domain which contains information about respiration and noise. The signal is quite weak. We can see some repetitive pattern, but can't tell the periodicity of the respiration. Figure 4.11(b) is the Fast Fourier Transform (FFT) of the same signal in Figure 4.11(a) but in the frequency domain. Clearly, we can see an obvious peak at 0.35 Hz, which matches the actual respiration rate of 21.13 breath per minute (bpm). Figure 4.11(c) shows the signal after applying Sample ACF and the peak finding algorithm. The interval between two adjacent peaks reveals the periodicity of the respiration. By averaging multiple peak intervals, we have better respiratory rate estimation than the basic FFT-based result shown in Figure 4.11(b).

	Age ($year$)	Height (cm)	Weight (kg)	BMI (kg/m^2)
Min	22	161	47	16.9
Max	36	182	91	30.1
Mean	26.3	172.3	67.2	22.5
Std	3.9	6.8	13.5	3.6

Table 4.4: 19 participants are recruited for respiration study. The table shows the minimum, maximum, mean and standard deviation of the participants' age, height, weight and body mass index (BMI).

4.5.2 Experiment Design

In this part, we conducted more than 800 experiments on our Touch-Chair system and collected more than 35 hours of data. During each experiment, we asked a participant to breathe normally and seat still on the chair. We evaluate the performance of our respiratory rate monitoring algorithm by comparing against the ground truth measured by a NeuLog respiration belt [91] and report the estimation error.

Participants: We had a total of 19 healthy volunteer participants for this experiment, including 13 males and 6 females. The mean age of the participants was 26.3 years with a standard deviation of 3.9 years. The youngest participant was 22 years while the oldest is 36 years old. More details about the participants are shown in Table 4.4.

Experiment Procedure: We asked a participant to wear a NeuLog respiration belt on top of the lower ribs and upper abdomen area before the session began. Also, we instructed the participant to breathe normally and sit comfortably on the chair throughout the session. We conducted all the sessions in an indoor academic laboratory environment and at least one of our members oversaw the sessions. Within the session, we allowed the participant to make micro posture adjustment, and watch a video of his/her own choice.

Participants were allowed to withdraw from the data collection session at any time. Each participant went through at least 5 sessions and each session lasted 2 to 30 minutes. In total, we conducted 889 experiments on our Touch-Chair system under varies conditions (summer/winter, high/low moisture, thin/thick clothes, etc.) and collected 35.6 hours data.

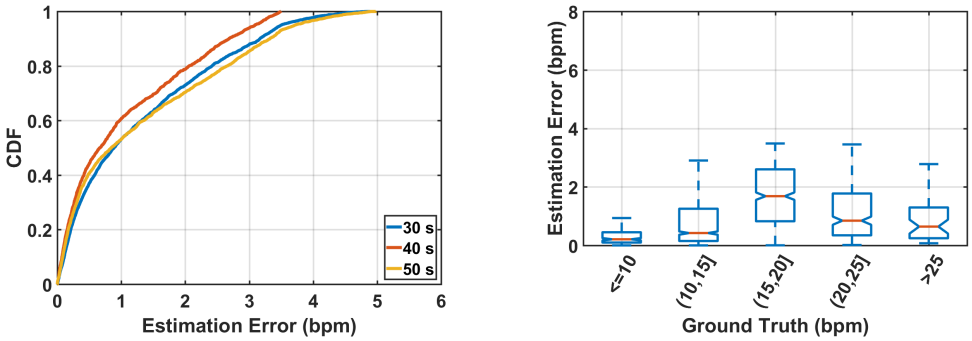

(a) (b)

Figure 4.12: (a) We evaluate the impact of different window size and plot the cumulative distribution function. The mean error is 1.29, 1.05 and 1.33 *bpm*, for a 30-second, 40-second and 50-second window, respectively. In the rest of the paper, we report the results using the 40-second window. (b) The box plot of the estimation error over a large range of respiratory rate. The median, mean, and standard deviation of the error are 0.67, 1.05, and 1.00 *bpm*, respectively.

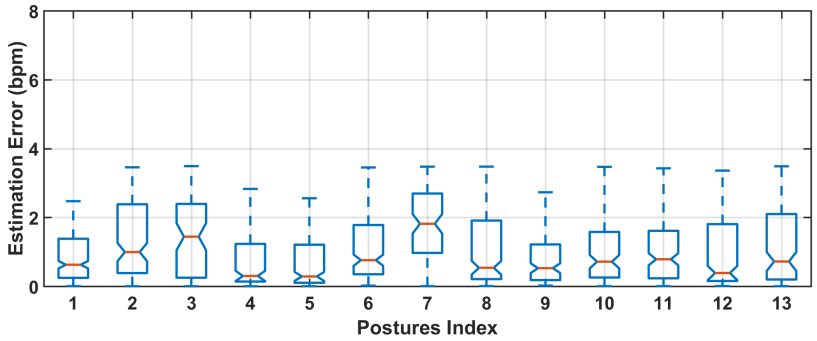

Figure 4.13: The box plot of the respiratory rate error while varying the sitting posture types. The overall estimated error is close. Posture (5), leaning backward, has the smallest average error at 0.74 *bpm*, while Posture (7), sitting on the edge, has the largest average error at 1.75 *bpm*.

Ground Truth: The ground truth of the respiratory rate is measured through a NeuLog respiration belt. The belt mainly consists of a flexible rubber tubing belt, a hand pump with a pressure release valve connected to the belt, and a resistor-based air pressure sensor embedded inside of the belt. While worn between the chest and the abdomen area, the device measures the pressure fluctuations due to the breathing activity. Also, the NeuLog respiration belt can be easily affected by other activities that involve upper limb motion, respiratory-related motion such as coughs and laughs. Thus, we dropped experiments affected by these unexpected motions and only report the results with accurate ground truth.

4.5.3 Respiration Evaluation Results

Within a total of 35.6 hours data, we found 9.1 hours data usable. The rest of the data is either corrupted ground truth or corrupted capacitive signal, due to varies body motions. Within 9.1 hours data, we apply a shifting window across the data. Figure 4.12(a) shows the cumulative distribution function (CDF) of the estimation error with different window size. A window size of 40 seconds gives the best performance: the mean error is 1.29 *bpm*, 1.05 *bpm* and 1.33 *bpm*, when the window size is 30, 40 and 50 seconds, respectively. In all cases, the hop size is 10 seconds. In the rest of the paper, we set the window size to be 40 seconds. Next, we evaluate the performance of our proposed system over a large range of respiratory rate and report the estimation error. Here, we category all 3201 experiments into 5 groups: ≤ 10, (10, 15], (15, 20], (20, 25], and > 25. In total, we have 3201 experiments. Figure 4.12(b) shows the distribution of ground truth, the distribution of the estimation error, and the box plot of the estimation error across a large respiratory rate range. We make further analysis and notice large errors are mainly caused by two reasons. First, some participants get excited while watching videos during the experiments and change their respiration rhythm dramatically. The ACF-based algorithm averages multiple periods of the respiration signal, thus responses to the sudden increase/decrease of respiratory rate with some delay. Second, some participants might have quite shallow respiration and the capacitive sensor could not capture signals with enough resolution for analysis.

The Impact of Sitting Posture: In this part, we evaluate the impact of sitting postures on our performance. Each participant was asked to perform 13 postures over time and the length of each experiment is at least 1 minute. Here, we adopt common postures reported in the literature, e.g. in [81, 85, 92–95], and consider the following 13 postures: (1) sitting upright, (2) leaning forward, (3) leaning left[4], (4) leaning right, (5) leaning backward, (6) hunched sitting, (7) sitting on the edge, (8) leaning towards the backrest with left leg crossed on top of right leg, (9) leaning towards left with left leg crossed on top of right leg, (10) leaning towards right with left leg crossed on top of

[4]In this paper, all the mentioned directions are with respect to the participants.

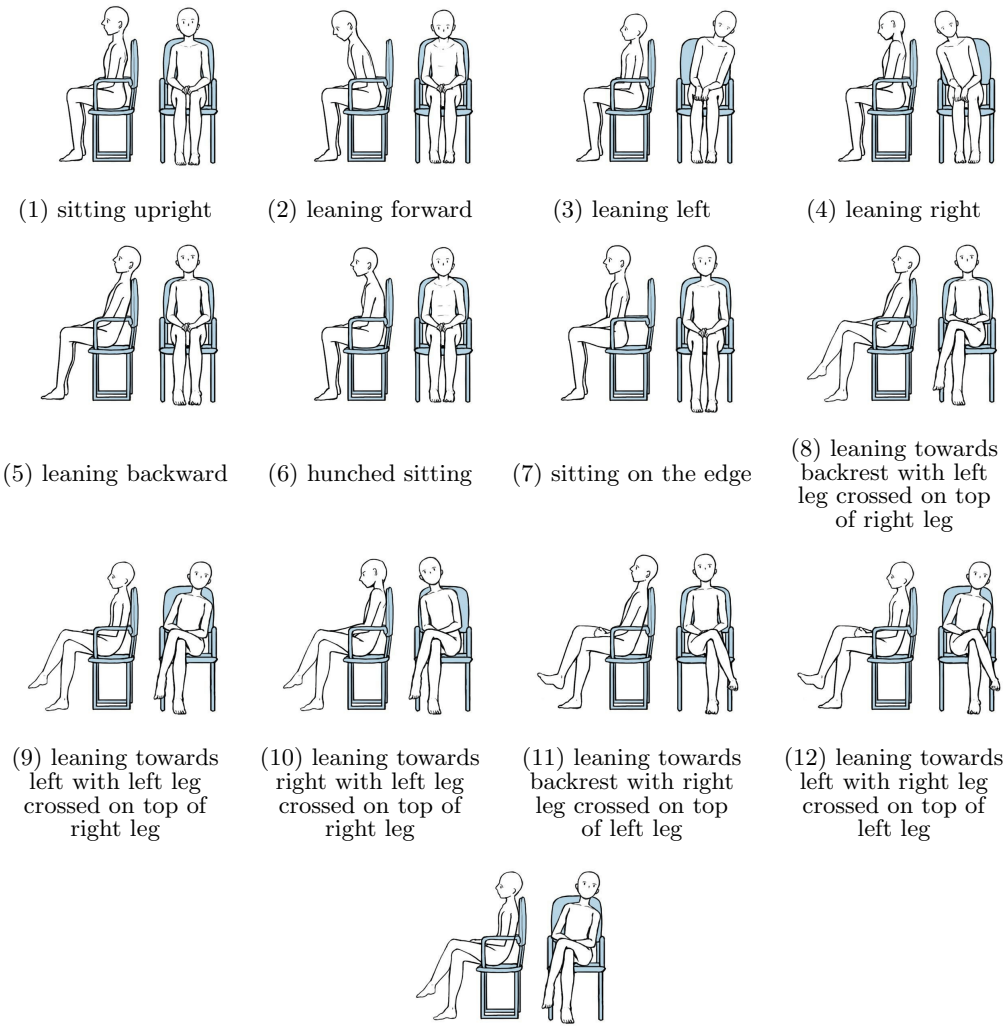

Figure 4.14: We consider 13 sitting postures and demonstrate each posture with two sketches – one front sketch and one left-side sketch.

right leg, (11) leaning towards the backrest with right leg crossed on top of left leg, (12) leaning towards left with right leg crossed on top of left leg, and (13) leaning towards right with right leg crossed on top of left leg. In Figure 4.14, we illustrate each posture with a pair of sketches – one illustrating the front view and the other the left side view. Figure 4.13 shows the box plot of the estimation error for different sitting postures. Posture (5), leaning backward, has the smallest average error at 0.74 *bpm*. Meanwhile, posture (7), sitting on the edge, has the largest average error at 1.75 *bpm*. In general, the error is negatively correlated with the area of sensor ⑤ (in Figure 4.3(b)) that a user covers. For example, sensor ⑤ is mostly covered for postures (1) sitting upright

and (5) leaning backward, but much less covered for posture (7) sitting on the edge.

4.6 Touch-Chair App Implementation

In this section, we show our Touch-Chair app implementation. We split the implementation into three parts. First, we have implemented an embedded program on the PIP tags and the PIP tag receiver using C++ and TI MSP430 native library. To achieve low power, we set the PIP tags to sleep mode most of the time and weak them up at 1 Hz. The only exception is that we set the wake-up frequency to 4 Hz on the tag which connects to sensor ⑤ for respiration monitoring purpose. Next, we have implemented signal processing and machine learning algorithms using Python on a Raspberry Pi. The processed results are periodically pushed to a mobile application implemented in Java on Android platform. Figure 4.15 shows an example of the mobile application interface.

4.7 Related Work

In this section, we categorize different systems in three ways: (1) systems which detect the user identity, e.g. [96–100]; (2) systems which detect user postures and gestures, such as systems shown in [81, 85, 92–95, 101]; (3) systems which monitor the user's vital signs focusing on respiratory rate [33, 80, 81].

4.7.1 User Identification

A few systems proposed to detect user identity [96,97] while sitting or walking, and more systems focused on user authentication [98–100]. Riener et al. [96] placed two 32 by 32 pressure sensor arrays on a driver's seat and backrest and detected the driver's identity using a machine learning algorithm based on pressure features. Pan et al. [97] proposed an indoor pedestrian identification system which takes advantages of the vibrations induced by pedestrian footsteps and propagated through building structures. Bo et al. [100] achieved continuous user identification on a smartphone by focusing on three screen-touch motions – finger tap, scroll and fling. They can silently verify a user by

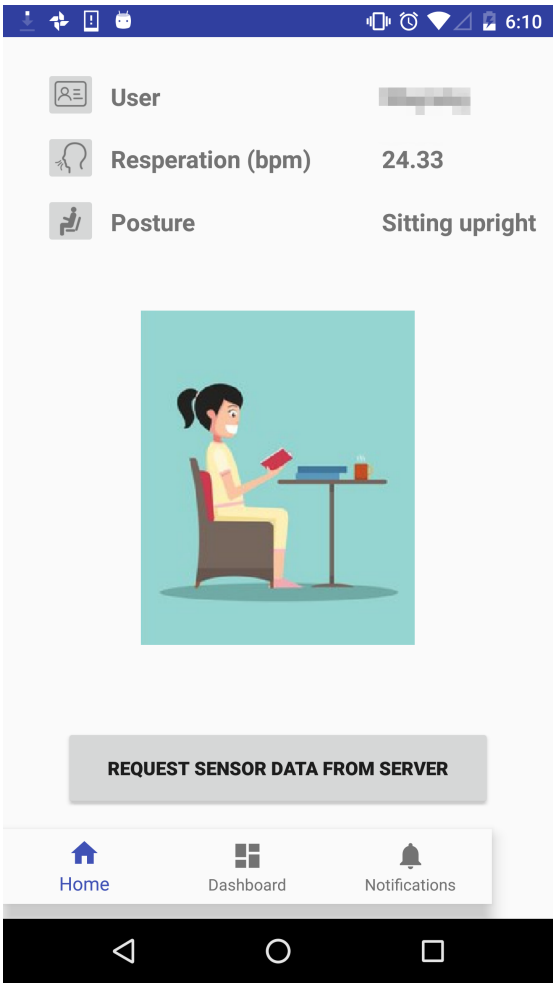

Figure 4.15: The mobile application of Touch-Chair periodically query from a Raspberry Pi and shows the occupancy states of a chair, the user's name, sitting posture, and respiratory rate. It also allows any user to query the data manually as well.

applying an SVM model on vibration features extracted from these finger motions. Holz et al. [99] take advantages of the existing capacitive screen on a smartphone to measure the capacitive images of user's ears, fists, or grips while pressing against the screen. By processing consecutive raw images from a single user and applying a multi-step voting approach, the proposed system can first classify the body part and then identify the user. Li et al. [98] proposed a user authentication system based on smart head-worn devices. The system recognizes a user through a set of unique user-defined head movements at a given rhythm.

4.7.2 Posture and Activity Detection

Detecting postures of a person is the most commonly studied in the research community and diverse systems have been proposed. We category these systems by the sensor types.

Force Sensors: Xu et al. [85] design a seat mat which has a 16 by 16 force sensor array and measures the force map when a person presents. To classify 7 different postures, dynamic time warping (DTW) is applied to the collected signals. Ma et al. [92] place 3 force sensors on a chair and apply decision tree algorithm to classify 5 sitting postures.

Pressure Sensors: Tan et al. [93] equip two 42 by 48 pressure sensor arrays on a chair to measure 10 sitting postures. They process the posture data through principal components analysis (PCA) and classify it based on the distance between the new posture data and the known posture clusters. Martins et al. [94] build an air cushion chair with 8 pressure sensors (4 in the seat pad and 4 in the backrest) to measure the pressure due to body weight. Later, Artificial Neural Networks (ANNs) is used for classifying 5 postures. Meyer et al. [101] develop a textile seat mat with 240 capacitive pressure sensors. They use the Preisach model of hysteresis to reduce the measurement error of those pressure sensors and apply a naïve Bayes classifier to classify 16 sitting postures. Bao et al. [95] place 5 pressure sensors on the seat pad and detect 7 common sitting postures via a density-based clustering method.

Capacitive Sensors: Braun et al. [81] design a layout pattern for 8 capacitive proximity sensors on an office chair. The system is trained through SVM and can recognize 4 postures. Grosse-Puppendahl et al. [102] embedded 8 capacitive proximity sensors in a couch and detect the sitting and lying postures using radial basis function (RBF) networks on extracted features.

Wearable Sensors: Sardini et al. [103] develop an impedance-based wireless wearable tee shirt and measure the impedance changes caused by a geometric deformation during different body postures. Li et al. [104] design a forearm-worn gesture-based mobile device based on one accelerometer and four surface electromyography sensors. They can recognize 19 gestures by combining a Bayes linear classifier and an improved dynamic

time-warping algorithm.

4.7.3 Respiratory Rate Measurement

A lot of work has shown it's possible to unobtrusively monitor a person's heart rate via sensors, mounted on a chair/bed or measured wirelessly, e.g. capacitive-coupled ECG, speed/acceleration-based vibration sensors [32, 105], microwave-based Doppler radar [14, 106], RGB camera [107, 108], etc. In this section, we mainly focus on monitoring respiratory rate monitoring.

Tarassenko et al. [108] use an RGB camera for respiratory rate monitoring. They first separate the face image from the background and then find the fluctuation of the green channel color intensity of the face reveals the periodicity of the respiration pattern. Griffiths et al. [80] show the possibility of using a capacitive proximity sensor mounted on the backrest surface of a chair to measure a person's respiratory rate. Jia et al. [33] find that the respiration signal is amplitude modulated with the heartbeat signal inside of a human body via physical vibration propagation. They extract the respiration signal from the mixture of heartbeat and respiration signals using a square-law demodulation algorithm and estimate the respiratory rate via an autocorrelation-based algorithm.

4.7.4 Comparison with Other Types of Sensors

The benefits of using the capacitive approach:

Compare to computer vision approach: Cameras can be used to classify different postures. Recently, many systems [84, 109] use the RGB-D camera since it offers additional information about the object, the depth. The idea is straightforward, but such systems can be easily affected by the environment changes (the ambient brightness, the camera location, the camera view angle, the potential obstacle between the camera and the target, etc.) and cause privacy concerns. Our system is robust against a variety of environment and preserves better privacy.

Compare to wearable approach: Wearables, mostly accelerometer-based, have been widely used in activity recognition. Many systems proposed to attach accelerometers

to the waist, the thigh [110, 111], and the ankle [86, 112]. However, managing multiple wearable devices at the same time is cumbersome. Furthermore, accelerometers, like other vibration sensors, are suitable for detecting motions, but are not very good at recognizing stationary postures.

Compare to force/pressure sensor approach: Force/pressure sensor approach, such as resistor-based sensors [85, 95] and capacitor-based pressure sensors [101], has been widely studied. Such systems rely on the weight distribution of the object on top. Compare to the existing systems, our system is much more sensitive to the micro distance change thus is able to capture the details of users' sitting behaviors (including the respiration events).

4.8 Concluding Remarks and Future Direction

In this chapter, we discuss and evaluate an unobtrusive, ultra-low-power Touch-Chair system that can recognize the user's identity and respiratory rate. The system is centered around capacitive sensors that can accurately measure micro details about a person's sitting behavior patterns such as posture adjustments, vibrations caused by respiration, and even humidity changes due to the moisture differences between the ambient environment and the user's skin. We have built a prototype and demonstrated that our Touch-Chair system is indeed very versatile. First, we achieve higher accuracy for user identification than existing solutions. Then, we improve the capacitive sensor based respiration monitoring in a more user-friendly manner: our Touch-Chair can monitor a user's respiratory rate as long as the user sits still on the chair, without requiring the user to be in any specific posture as required by existing approaches. As part of our future work, we will work on sensing the user's skin moisture level using the Touch-Chair system. To be more specific, we will carefully examine the diffusion and evaporation process caused by the imbalance between the humidity and the skin moisture and develop a practical model that maps the capacitive signal to the skin moisture level taking into consideration the temperature.

Chapter 5

Conclusion

In conclusion, this dissertation focuses on investigating whether we can build low-cost sensor systems which unobtrusively detect a person's vital signs by measuring ambient physical vibrations and is robust against environmental noise at the same time. A system built at an affordable price would allow large-scale deployment in real-world applications. With the help of long-term large-scale deployment, we can capture some rare but important vital-sign data, such as the regression from irregular breathing pattern to sleep apnea, the degeneration of abnormal heartbeats to heart failures, etc. We believe such valuable data can greatly improve the understanding of several types of medical diseases, which cannot be feasible by using expensive medical systems at hospitals. Towards this end, in this dissertation, we demonstrated three low-cost sensor systems which detect a person's vital signs during sleep on a bed and daytime on a chair.

First, we have shown our HB-Phone system, centered around a single geophone, can be easily mounted anywhere on a bed and accurately monitor a single user's heart rate with a cost of less than $100. Through detailed evaluation, we show that HB-Phone system is robust against noise of various types, different bed size, different mattress types. Potentially, the system can be used as an at-home heartbeat monitoring during sleep. Next, we have greatly extended our work and designed a VitalMon system. The system can monitor a user's respiratory rate even through geophones cannot directly detect vibrations caused by respiration. Also, the system can track a target user's heart rate and respiratory rate simultaneously even when he/she shares the bed with another user. Through more than 56 hours' experiments, we have shown that VitalMon is accurate and robust against different factors, such as lying posture and mattress types.

Last, we have demonstrated an unobtrusive chair-mounted system, called TouchChair, based on multiple capacitive sensors which can continuously monitor a person's respiratory rate and detect the person's identity as well. The capacitive sensors are sensitive to motions caused by users – weak vibration caused by respiration, occupancy, etc. The system measures the capacitance change through counting the time elapsed of discharging a resistor-capacitor (RC) circuit and costs about $180. We apply autocorrelation-based techniques to estimate breathing rate, and apply machine learning techniques to infer the user identification. Also, it can monitor a user's respiratory rate as long as the user sits on the chair, without requiring the user to be in any specific posture as required by existing approaches.

References

[1] B. M. Appelhans and L. J. Luecken, "Heart rate variability as an index of regulated emotional responding." *Review of general psychology*, vol. 10, no. 3, p. 229, 2006.

[2] R. D. Lane, K. McRae, E. M. Reiman, K. Chen, G. L. Ahern, and J. F. Thayer, "Neural correlates of heart rate variability during emotion," *Neuroimage*, vol. 44, no. 1, pp. 213–222, 2009.

[3] R. Lane, E. Reiman, G. Ahern, and J. Thayer, "21. activity in medial prefrontal cortex correlates with vagal component of heart rate variability during emotion," *Brain and cognition*, vol. 47, no. 1-2, pp. 97–100, 2001.

[4] T. Watanabe and K. Watanabe, "Noncontact method for sleep stage estimation," *IEEE Transactions on biomedical engineering*, vol. 51, no. 10, pp. 1735–1748, 2004.

[5] K. Narkiewicz, N. Montano, C. Cogliati, P. J. Van De Borne, M. E. Dyken, and V. K. Somers, "Altered cardiovascular variability in obstructive sleep apnea," *Circulation*, vol. 98, no. 11, pp. 1071–1077, 1998.

[6] R. E. Kleiger, J. P. Miller, J. T. Bigger, and A. J. Moss, "Decreased heart rate variability and its association with increased mortality after acute myocardial infarction," *The American journal of cardiology*, vol. 59, no. 4, pp. 256–262, 1987.

[7] J. Nolan, P. D. Batin, R. Andrews, S. J. Lindsay, P. Brooksby, M. Mullen, W. Baig, A. D. Flapan, A. Cowley, R. J. Prescott *et al.*, "Prospective study of heart rate variability and mortality in chronic heart failure," *Circulation*, vol. 98, no. 15, pp. 1510–1516, 1998.

[8] M. Apps, P. Sheaff, D. Ingram, C. Kennard, and D. Empey, "Respiration and sleep in parkinson's disease." *Journal of Neurology, Neurosurgery & Psychiatry*, vol. 48, no. 12, pp. 1240–1245, 1985.

[9] "Fitbit," https://www.fitbit.com/.

[10] "Gearfit2," http://www.samsung.com/global/galaxy/gear-fit2/.

[11] B. Fang, N. D. Lane, M. Zhang, A. Boran, and F. Kawsar, "Bodyscan: Enabling radio-based sensing on wearable devices for contactless activity and vital sign monitoring," in *Proceedings of the 14th Annual International Conference on Mobile Systems, Applications, and Services*. ACM, 2016, pp. 97–110.

[12] J. H. Choi and D. K. Kim, "A remote compact sensor for the real-time monitoring of human heartbeat and respiration rate," *Biomedical Circuits and Systems, IEEE Transactions on*, vol. 3, no. 3, pp. 181–188, 2009.

[13] Y. Yamana, S. Tsukamoto, K. Mukai, H. Maki, H. Ogawa, and Y. Yonezawa, "A sensor for monitoring pulse rate, respiration rhythm, and body movement in bed," in *Engineering in Medicine and Biology Society, EMBC, 2011 Annual International Conference of the IEEE*. IEEE, 2011, pp. 5323–5326.

[14] F. Adib, H. Mao, Z. Kabelac, D. Katabi, and R. C. Miller, "Smart homes that monitor breathing and heart rate," in *Proceedings of the 33rd annual ACM conference on human factors in computing systems*. ACM, 2015, pp. 837–846.

[15] J. Liu, Y. Wang, Y. Chen, J. Yang, X. Chen, and J. Cheng, "Tracking vital signs during sleep leveraging off-the-shelf wifi," in *Proceedings of the 16th ACM International Symposium on Mobile Ad Hoc Networking and Computing*. ACM, 2015, pp. 267–276.

[16] K. Watanabe, T. Watanabe, H. Watanabe, H. Ando, T. Ishikawa, and K. Kobayashi, "Noninvasive measurement of heartbeat, respiration, snoring and body movements of a subject in bed via a pneumatic method," *Biomedical Engineering, IEEE Transactions on*, vol. 52, no. 12, pp. 2100–2107, 2005.

[17] Y. Chee, J. Han, J. Youn, and K. Park, "Air mattress sensor system with balancing tube for unconstrained measurement of respiration and heart beat movements," *Physiological measurement*, vol. 26, no. 4, p. 413, 2005.

[18] S. Tanaka, Y. Matsumoto, and K. Wakimoto, "Unconstrained and non-invasive measurement of heart-beat and respiration periods using a phonocardiographic sensor," *Medical and Biological Engineering and Computing*, vol. 40, no. 2, pp. 246–252, 2002.

[19] L. Rosales, M. Skubic, D. Heise, M. J. Devaney, and M. Schaumburg, "Heartbeat detection from a hydraulic bed sensor using a clustering approach," in *Engineering in Medicine and Biology Society (EMBC), 2012 Annual International Conference of the IEEE*. IEEE, 2012, pp. 2383–2387.

[20] D. Heise and M. Skubic, "Monitoring pulse and respiration with a non-invasive hydraulic bed sensor," in *Engineering in Medicine and Biology Society (EMBC), 2010 Annual International Conference of the IEEE*. IEEE, 2010, pp. 2119–2123.

[21] D. Heise, L. Rosales, M. Skubic, and M. J. Devaney, "Refinement and evaluation of a hydraulic bed sensor," in *Engineering in Medicine and Biology Society, EMBC, 2011 Annual International Conference of the IEEE*. IEEE, 2011, pp. 4356–4360.

[22] Y. Hata, Y. Kamozaki, T. Sawayama, K. Taniguchi, and H. Nakajima, "A heart pulse monitoring system by air pressure and ultrasonic sensor systems," in *System of Systems Engineering, 2007. SoSE'07. IEEE International Conference on*. IEEE, 2007, pp. 1–5.

[23] N. Bu, N. Ueno, and O. Fukuda, "Monitoring of respiration and heartbeat during sleep using a flexible piezoelectric film sensor and empirical mode decomposition," in *Engineering in Medicine and Biology Society, 2007. EMBS 2007. 29th Annual International Conference of the IEEE*. IEEE, 2007, pp. 1362–1366.

[24] F. Wang, M. Tanaka, and S. Chonan, "Development of a pvdf piezopolymer sensor for unconstrained in-sleep cardiorespiratory monitoring," *Journal of intelligent material systems and structures*, vol. 14, no. 3, pp. 185–190, 2003.

[25] S. Nukaya, T. Shino, Y. Kurihara, K. Watanabe, and H. Tanaka, "Noninvasive bed sensing of human biosignals via piezoceramic devices sandwiched between the floor and bed," *Sensors Journal, IEEE*, vol. 12, no. 3, pp. 431–438, 2012.

[26] G. S. Chung, B. H. Choi, D.-U. Jeong, and K. S. Park, "Noninvasive heart rate variability analysis using loadcell-installed bed during sleep," in *Engineering in Medicine and Biology Society, 2007. EMBS 2007. 29th Annual International Conference of the IEEE*. IEEE, 2007, pp. 2357–2360.

[27] C. Bruser, K. Stadlthanner, S. de Waele, and S. Leonhardt, "Adaptive beat-to-beat heart rate estimation in ballistocardiograms," *Information Technology in Biomedicine, IEEE Transactions on*, vol. 15, no. 5, pp. 778–786, 2011.

[28] M. Brink, C. H. Müller, and C. Schierz, "Contact-free measurement of heart rate, respiration rate, and body movements during sleep," *Behavior research methods*, vol. 38, no. 3, pp. 511–521, 2006.

[29] C. Bruser, A. Kerekes, S. Winter, and S. Leonhardt, "Multi-channel optical sensor-array for measuring ballistocardiograms and respiratory activity in bed," in *Engineering in Medicine and Biology Society (EMBC), 2012 Annual International Conference of the IEEE*. IEEE, 2012, pp. 5042–5045.

[30] J. M. Kortelainen, M. van Gils, and J. Parkka, "Multichannel bed pressure sensor for sleep monitoring," *Computing in Cardiology*, vol. 39, pp. 313–316, 2012.

[31] X. L. Aubert and A. Brauers, "Estimation of vital signs in bed from a single unobtrusive mechanical sensor: Algorithms and real-life evaluation," in *Engineering in Medicine and Biology Society, 2008. EMBS 2008. 30th Annual International Conference of the IEEE*. IEEE, 2008, pp. 4744–4747.

[32] Z. Jia, M. Alaziz, X. Chi, R. E. Howard, Y. Zhang, P. Zhang, W. Trappe, A. Sivasubramaniam, and N. An, "Hb-phone: a bed-mounted geophone-based heartbeat monitoring system," in *Information Processing in Sensor Networks (IPSN), 2016 15th ACM/IEEE International Conference on*. IEEE, 2016, pp. 1–12.

[33] Z. Jia, A. Bonde, S. Li, C. Xu, J. Wang, Y. Zhang, R. E. Howard, and P. Zhang, "Monitoring a persons heart rate and respiratory rate on a shared bed using geophones," in *Proceedings of the 15th ACM Conference on Embedded Network Sensor Systems*, ser. SenSys '17. New York, NY, USA: ACM, 2017, pp. 6:1–6:14. [Online]. Available: http://doi.acm.org/10.1145/3131672.3131679

[34] "Arduino duemilanove," http://arduino.cc/en/MainarduinoBoardDuemilanove.

[35] J. Box and G. M. Jenkins, *Reinsel. Time Series Analysis, Forecasting and Control*. Prentice Hall, Englewood Cliffs, NJ, USA, 3rd edition edition, 1994.

[36] T. C. O'Haver, "Peak finding and measurement," 2008. [Online]. Available: http://terpconnect.umd.edu/~toh/spectrum/PeakFindingandMeasurement.htm

[37] *Analog Communication(Jntu).* McGraw-Hill Education (India) Pvt Limited, 2006. [Online]. Available: https://books.google.com/books?id=UbZgOTSnkg4C

[38] O. Yilmaz and S. Rickard, "Blind separation of speech mixtures via time-frequency masking," *IEEE Transactions on signal processing*, vol. 52, no. 7, pp. 1830–1847, 2004.

[39] S. Rickard, "The duet blind source separation algorithm," *Blind Speech Separation*, pp. 217–237, 2007.

[40] G. P. Succi, D. Clapp, R. Gampert, and G. Prado, "Footstep detection and tracking," in *Aerospace/Defense Sensing, Simulation, and Controls*, 2001.

[41] A. Pakhomov, A. Sicignano, M. Sandy, and E. T. Goldburt, "Single-and three-axis geophone: footstep detection with bearing estimation, localization, and tracking," in *AeroSense 2003*, 2003.

[42] "Intersec, heartbeat - human detection system," http://www.intelsec.comproduct_detail_heartbeat.html.

[43] R. D. Peters, "Mechanical cardiography using a geophone," 2005, http://physics.mercer.edu/petepag/cardio.html.

[44] "Geophone sm-24," https://www.sparkfun.com/products/11744.

[45] "Ti lmv358," http://www.ti.com/product/lmv358.

[46] "Medical decoded," http://lessons4medicos.blogspot.com/2008/06/basic-ecg-waveform-ecg-vitals.html.

[47] "Sparkfun," https://www.sparkfun.com/datasheets/BreakoutBoards/OpAmp_Breakout-v16.pdf.

[48] B. H. Jansen, B. H. Larson, and K. Shankar, "Monitoring of the ballistocardiogram with the static charge sensitive bed," *Biomedical Engineering, IEEE Transactions on*, vol. 38, no. 8, pp. 748–751, 1991.

[49] X. Zhu, W. Chen, T. Nemoto, Y. Kanemitsu, K. Kitamura, K.-i. Yamakoshi, and D. Wei, "Real-time monitoring of respiration rhythm and pulse rate during sleep," *Biomedical Engineering, IEEE Transactions on*, vol. 53, no. 12, pp. 2553–2563, 2006.

[50] D. C. Mack, J. T. Patrie, P. M. Suratt, R. A. Felder, and M. Alwan, "Development and preliminary validation of heart rate and breathing rate detection using a passive, ballistocardiography-based sleep monitoring system," *Information Technology in Biomedicine, IEEE Transactions on*, vol. 13, no. 1, pp. 111–120, 2009.

[51] R. Fletcher and J. Han, "Low-cost differential front-end for doppler radar vital sign monitoring," in *Microwave Symposium Digest, 2009. MTT'09. IEEE MTT-S International*. IEEE, 2009, pp. 1325–1328.

[52] S. Šprager and D. Zazula, "Heartbeat and respiration detection from optical interferometric signals by using a multimethod approach," *IEEE transactions on biomedical engineering*, vol. 59, no. 10, pp. 2922–2929, 2012.

[53] ——, "Detection of heartbeat and respiration from optical interferometric signal by using wavelet transform," *Computer methods and programs in biomedicine*, vol. 111, no. 1, pp. 41–51, 2013.

[54] A. Hyvärinen, J. Karhunen, and E. Oja, *Independent component analysis*. John Wiley & Sons, 2004, vol. 46.

[55] I. Jolliffe, *Principal component analysis*. Wiley Online Library, 2002.

[56] J. Gordon, "Certain molar movements of the human body produced by the circulation of the blood," *Journal of Anatomy and Physiology*, vol. 11, no. Pt 3, p. 533, 1877.

[57] D. Phan, S. Bonnet, R. Guillemaud, E. Castelli, and N. P. Thi, "Estimation of respiratory waveform and heart rate using an accelerometer," in *Engineering in Medicine and Biology Society, 2008. EMBS 2008. 30th Annual International Conference of the IEEE*. IEEE, 2008, pp. 4916–4919.

[58] "Murata contactless bed sensor," http://www.murata.com/en-us/products/sensor/accel/sca10h_11h.

[59] S. Pan, A. Bonde, J. Jing, L. Zhang, P. Zhang, and H. Y. Noh, "Boes: building occupancy estimation system using sparse ambient vibration monitoring," in *SPIE Smart Structures and Materials+ Nondestructive Evaluation and Health Monitoring*. International Society for Optics and Photonics, 2014, pp. 90 611O–90 611O.

[60] M. Mirshekari, S. Pan, P. Zhang, and H. Y. Noh, "Characterizing wave propagation to improve indoor step-level person localization using floor vibration," in *SPIE Smart Structures and Materials+ Nondestructive Evaluation and Health Monitoring*. International Society for Optics and Photonics, 2016, pp. 980 305–980 305.

[61] S. Pan, C. G. Ramirez, M. Mirshekari, J. Fagert, A. J. Chung, C. C. Hu, J. P. Shen, H. Y. Noh, and P. Zhang, "Surfacevibe: vibration-based tap & swipe tracking on ubiquitous surfaces." in *IPSN*, 2017, pp. 197–208.

[62] J. G. Proakis, "Digital communications." *McGraw-Hill, New York*, 1995.

[63] T. Park, *Introduction to Digital Signal Processing: Computer Musically Speaking*. World Scientific, 2010. [Online]. Available: https://books.google.com/books?id=10hpDQAAQBAJ

[64] C. Langton, "Hilbert transform, analytic signal, and the complex envelope," *Signal Processing and Simulation Newsletter*, 1999.

[65] D. O. Pederson and K. Mayaram, "Demodulators and detectors," *Analog Integrated Circuits for Communication*, pp. 457–484, 2008.

[66] "Zephyr performance systems," https://www.zephyranywhere.com/benefits/physiological-biomechanical.

[67] R. Mersereau and T. Seay, "Multiple access frequency hopping patterns with low ambiguity," *IEEE Transactions on Aerospace and Electronic Systems*, pp. 571–578, 1981.

[68] E. C. Cherry, "Some experiments on the recognition of speech, with one and with two ears," *The Journal of the acoustical society of America*, vol. 25, no. 5, pp. 975–979, 1953.

[69] J. O. Smith, *Introduction to digital filters: with audio applications*. Julius Smith, 2008, vol. 2.

[70] L. R. Rabiner, "A tutorial on hidden markov models and selected applications in speech recognition," *Proceedings of the IEEE*, vol. 77, no. 2, pp. 257–286, 1989.

[71] S. Lloyd, "Least squares quantization in pcm," *IEEE transactions on information theory*, vol. 28, no. 2, pp. 129–137, 1982.

[72] R. Agrawal, J. Gehrke, D. Gunopulos, and P. Raghavan, *Automatic subspace clustering of high dimensional data for data mining applications*. ACM, 1998, vol. 27.

[73] "Arduino due," https://www.arduino.cc/en/Main/arduinoBoardDue.

[74] J. M. Blackledge, *Digital signal processing: mathematical and computational methods, software development and applications*. Elsevier, 2006.

[75] "Neulog heart rate & pulse logger sensor," https://neulog.com/heart-rate-pulse/.

[76] D. Heise, L. Rosales, M. Sheahen, B.-Y. Su, and M. Skubic, "Non-invasive measurement of heartbeat with a hydraulic bed sensor progress, challenges, and opportunities," in *2013 IEEE International Instrumentation and Measurement Technology Conference (I2MTC)*. IEEE, 2013, pp. 397–402.

[77] R. Nandakumar, S. Gollakota, and N. Watson, "Contactless sleep apnea detection on smartphones," in *Proceedings of the 13th Annual International Conference on Mobile Systems, Applications, and Services*. ACM, 2015, pp. 45–57.

[78] C. E. Matthews, K. Y. Chen, P. S. Freedson, M. S. Buchowski, B. M. Beech, R. R. Pate, and R. P. Troiano, "Amount of time spent in sedentary behaviors in the united states, 2003–2004," *American journal of epidemiology*, vol. 167, no. 7, pp. 875–881, 2008.

[79] B. Schulte, "Health experts have figured out how much time you should sit each day," 2015, https://www.washingtonpost.com/news/wonk/wp/2015/06/02/medical-researchers-have-figured-out-how-much-time-is-okay-to-spend-sitting-each-day/?utm_term=.c0559a2ea424.

[80] E. Griffiths, T. S. Saponas, and A. Brush, "Health chair: implicitly sensing heart and respiratory rate," in *Proceedings of the 2014 ACM International Joint Conference on Pervasive and Ubiquitous Computing*. ACM, 2014, pp. 661–671.

[81] A. Braun, S. Frank, and R. Wichert, "The capacitive chair," in *International Conference on Distributed, Ambient, and Pervasive Interactions*. Springer, 2015, pp. 397–407.

[82] T. Chen and C. Guestrin, "Xgboost: A scalable tree boosting system," in *Proceedings of the 22nd acm sigkdd international conference on knowledge discovery and data mining*. ACM, 2016, pp. 785–794.

[83] L. Breiman, "Random forests," *Machine learning*, vol. 45, no. 1, pp. 5–32, 2001.

[84] E. S. Ho, J. C. Chan, D. C. Chan, H. P. Shum, Y.-m. Cheung, and P. C. Yuen, "Improving posture classification accuracy for depth sensor-based human activity monitoring in smart environments," *Computer Vision and Image Understanding*, vol. 148, pp. 97–110, 2016.

[85] W. Xu, M.-C. Huang, N. Amini, L. He, and M. Sarrafzadeh, "ecushion: A textile pressure sensor array design and calibration for sitting posture analysis," *IEEE Sensors Journal*, vol. 13, no. 10, pp. 3926–3934, 2013.

[86] E. Fortune, V. A. Lugade, and K. R. Kaufman, "Posture and movement classification: the comparison of tri-axial accelerometer numbers and anatomical placement," *Journal of biomechanical engineering*, vol. 136, no. 5, p. 051003, 2014.

[87] L. Yao, Q. Z. Sheng, W. Ruan, T. Gu, X. Li, N. Falkner, and Z. Yang, "Rf-care: Device-free posture recognition for elderly people using a passive rfid tag array," in *proceedings of the 12th EAI International Conference on Mobile and Ubiquitous Systems: Computing, Networking and Services on 12th EAI International Conference on Mobile and Ubiquitous Systems: Computing, Networking and Services*. ICST (Institute for Computer Sciences, Social-Informatics and Telecommunications Engineering), 2015, pp. 120–129.

[88] B. Firner, S. Medhekar, Y. Zhang, R. Howard, W. Trappe, P. Wolniansky, and E. Fenson, "Pip tags: Hardware design and power optimization," in *Proceedings of the Fifth Workshop on Embedded Networked Sensors (HotEmNets)*, 2008.

[89] T. Batteries, "Tadiran rapid response lithium batteries model tl-7903," 2018, http://www.tadiranbat.com/trr.html.

[90] H. Späth, *Two dimensional spline interpolation algorithms*. AK Peters, Ltd., 1995.

[91] NeuLog, "Respiration monitor belt logger sensor," 2018. [Online]. Available: https://neulog.com/respiration-monitor-belt/

[92] C. Ma, W. Li, R. Gravina, and G. Fortino, "Activity recognition and monitoring for smart wheelchair users," in *Computer Supported Cooperative Work in Design (CSCWD), 2016 IEEE 20th International Conference on*. IEEE, 2016, pp. 664–669.

[93] H. Z. Tan, L. A. Slivovsky, and A. Pentland, "A sensing chair using pressure distribution sensors," *IEEE/ASME Transactions On Mechatronics*, vol. 6, no. 3, pp. 261–268, 2001.

[94] L. Martins, R. Lucena, J. Belo, R. Almeida, C. Quaresma, A. Jesus, and P. Vieira, "Intelligent chair sensor–classification and correction of sitting posture," in *XIII Mediterranean Conference on Medical and Biological Engineering and Computing 2013*. Springer, 2014, pp. 1489–1492.

[95] J. Bao, W. Li, J. Li, Y. Ge, and C. Bao, "Sitting posture recognition based on data fusion on pressure cushion," *Indonesian Journal of Electrical Engineering and Computer Science*, vol. 11, no. 4, pp. 1769–1775, 2013.

[96] A. Riener and A. Ferscha, "Supporting implicit human-to-vehicle interaction: Driver identification from sitting postures," in *The First Annual International Symposium on Vehicular Computing Systems (ISVCS 2008)*, 2008, p. 10.

[97] S. Pan, T. Yu, M. Mirshekari, J. Fagert, A. Bonde, O. J. Mengshoel, H. Y. Noh, and P. Zhang, "Footprintid: Indoor pedestrian identification through ambient structural vibration sensing," *Proceedings of the ACM on Interactive, Mobile, Wearable and Ubiquitous Technologies*, vol. 1, no. 3, p. 89, 2017.

[98] S. Li, A. Ashok, Y. Zhang, C. Xu, J. Lindqvist, and M. Gruteser, "Whose move is it anyway? authenticating smart wearable devices using unique head movement patterns," in *Pervasive Computing and Communications (PerCom), 2016 IEEE International Conference on*. IEEE, 2016, pp. 1–9.

[99] C. Holz, S. Buthpitiya, and M. Knaust, "Bodyprint: Biometric user identification on mobile devices using the capacitive touchscreen to scan body parts," in *Proceedings of the 33rd Annual ACM Conference on Human Factors in Computing Systems*. ACM, 2015, pp. 3011–3014.

[100] C. Bo, L. Zhang, T. Jung, J. Han, X.-Y. Li, and Y. Wang, "Continuous user identification via touch and movement behavioral biometrics," in *Performance Computing and Communications Conference (IPCCC), 2014 IEEE International*. IEEE, 2014, pp. 1–8.

[101] J. Meyer, B. Arnrich, J. Schumm, and G. Troster, "Design and modeling of a textile pressure sensor for sitting posture classification," *IEEE Sensors Journal*, vol. 10, no. 8, pp. 1391–1398, 2010.

[102] T. Grosse-Puppendahl, A. Marinc, and A. Braun, "Classification of user postures with capacitive proximity sensors in aal-environments," *Ambient Intelligence*, pp. 314–323, 2011.

[103] E. Sardini, M. Serpelloni, and V. Pasqui, "Wireless wearable t-shirt for posture monitoring during rehabilitation exercises," *IEEE Transactions on Instrumentation and Measurement*, vol. 64, no. 2, pp. 439–448, 2015.

[104] Z. Lu, X. Chen, Q. Li, X. Zhang, and P. Zhou, "A hand gesture recognition framework and wearable gesture-based interaction prototype for mobile devices," *IEEE transactions on human-machine systems*, vol. 44, no. 2, pp. 293–299, 2014.

[105] A. Bonde, S. Pan, Z. Jia, Y. Zhang, H. Y. Noh, and P. Zhang, "Vvrrm: Vehicular vibration-based heart rr-interval monitoring system," in *Proceedings of the 19th International Workshop on Mobile Computing Systems & Applications*. ACM, 2018, pp. 37–42.

[106] D. Obeid, S. Sadek, G. Zaharia, and G. El Zein, "Multitunable microwave system for touchless heartbeat detection and heart rate variability extraction," *Microwave and optical technology letters*, vol. 52, no. 1, pp. 192–198, 2010.

[107] M.-Z. Poh, D. J. McDuff, and R. W. Picard, "Advancements in noncontact, multiparameter physiological measurements using a webcam," *IEEE transactions on biomedical engineering*, vol. 58, no. 1, pp. 7–11, 2011.

[108] L. Tarassenko, M. Villarroel, A. Guazzi, J. Jorge, D. Clifton, and C. Pugh, "Non-contact video-based vital sign monitoring using ambient light and auto-regressive models," *Physiological measurement*, vol. 35, no. 5, p. 807, 2014.

[109] A. Manzi, F. Cavallo, and P. Dario, "A neural network approach to human posture classification and fall detection using rgb-d camera," in *Italian Forum of Ambient Assisted Living*. Springer, 2016, pp. 127–139.

[110] V. Lugade, E. Fortune, M. Morrow, and K. Kaufman, "Validity of using triaxial accelerometers to measure human movementpart i: Posture and movement detection," *Medical engineering & physics*, vol. 36, no. 2, pp. 169–176, 2014.

[111] J. Skotte, M. Korshøj, J. Kristiansen, C. Hanisch, and A. Holtermann, "Detection of physical activity types using triaxial accelerometers," *Journal of physical activity and health*, vol. 11, no. 1, pp. 76–84, 2014.

[112] W. Tang and E. S. Sazonov, "Highly accurate recognition of human postures and activities through classification with rejection," *IEEE Journal of Biomedical and Health Informatics*, vol. 18, no. 1, pp. 309–315, 2014.